

Brane inflation and the WMAP data: a Bayesian analysis

Larissa Lorenz

E-mail: lorenz@iap.fr

Institut d'Astrophysique de Paris, UMR 7095-CNRS, Université Pierre et Marie Curie, 98bis boulevard Arago, 75014 Paris, France

Jérôme Martin

E-mail: jmartin@iap.fr

Institut d'Astrophysique de Paris, UMR 7095-CNRS, Université Pierre et Marie Curie, 98bis boulevard Arago, 75014 Paris, France

Christophe Ringeval

E-mail: ringeval@fyma.ucl.ac.be

Theoretical and Mathematical Physics Group, Center for Particle Physics and Phenomenology, Louvain University, 2 Chemin du Cyclotron, 1348 Louvain-la-Neuve, Belgium

Abstract. The Wilkinson Microwave Anisotropy Probe (WMAP) constraints on string inspired “brane inflation” are investigated. Here, the inflaton field is interpreted as the distance between two branes placed in a flux-enriched background geometry and has a Dirac-Born-Infeld (DBI) kinetic term. Our method relies on an exact numerical integration of the inflationary power spectra coupled to a Markov-Chain Monte-Carlo exploration of the parameter space. This analysis is valid for any perturbative value of the string coupling constant and of the string length, and includes a phenomenological modelling of the reheating era to describe the post-inflationary evolution. It is found that the data favour a scenario where inflation stops by violation of the slow-roll conditions well before brane annihilation, rather than by tachyonic instability. Concerning the background geometry, it is established that $\log v > -10$ at 95% confidence level (CL), where v is the dimensionless ratio of the five-dimensional sub-manifold at the base of the six-dimensional warped conifold geometry to the volume of the unit five-sphere. The reheating energy scale remains poorly constrained, $T_{\text{reh}} > 20 \text{ GeV}$ at 95% CL, for an extreme equation of state ($w_{\text{reh}} \gtrsim -1/3$) only. Assuming the string length is known, the favoured values of the string coupling and of the Ramond-Ramond total background charge appear to be correlated. Finally, the stochastic regime (without and with volume effects) is studied using a perturbative treatment of the Langevin equation. The validity of such an approximate scheme is discussed and shown to be too limited for a full characterisation of the quantum effects.

1. Introduction

Inflation is presently considered our best description of the early Universe, since it solves the puzzles of the Standard Hot Big Bang Model [1, 2, 3, 4, 5, 6] and, in addition, provides a very convincing mechanism for structure formation leading to an almost scale-invariant power spectrum [7, 8, 9, 10]. The small deviations from scale-invariance are connected to the micro-physics of inflation and are, therefore, of utmost importance when investigating the physical conditions in the very early Universe [11, 12, 13]. In practice, inflation is usually driven by a scalar field (or possibly several fields) and for this type of matter, the effective pressure can become negative, if the scalar field's potential is sufficiently flat. This condition is necessary to produce a phase of accelerated expansion (i.e. inflation) in General Relativity. In this context, one of the main open issues is the physical nature of the inflaton field. Since it is clear that this question should be addressed in the framework of extensions of the Standard Model of particle physics, String Theory seems to be a promising place to look for a physically well-motivated candidate field. In recent years, this issue has given rise to several studies, for reviews see references [14, 15, 16, 17, 18, 19]. In particular, string inspired brane world scenarios have turned out to be especially fruitful. In this context, the inflaton field is usually interpreted as the distance between two branes moving relative to each other in the extra dimensions [20, 21, 22]. The corresponding potential generically contains a Coulomb term of the form $\sim C - \phi^{-4}$, where C is a constant and ϕ the inflaton field [22, 23, 24, 25, 26, 27, 28, 29]. The end of inflation can then either occur by violation of the slow-roll conditions or by a mechanism of tachyonic instability, as in hybrid inflation. In either case, when the distance between the branes becomes of the order of the string length, the simple single field description breaks down and a more refined (fully stringy) treatment is necessary. The main goal of the present article is to carry out a detailed comparison of the inflationary predictions derived from one particular class of brane inflation scenarios, namely the Kachru-Kalosh-Linde-Maldacena-McAllister-Trivedi (KKLMMT) models, with the Cosmic Microwave Background (CMB) data presently available.

Analysing this class of potentials is further motivated by two rather different reasons. Firstly, although it is possible (for instance by using the slow-roll approximation) to span the space of (single field) inflationary models without relying on a specific form of the inflaton potential [30, 31, 32, 33], it is also interesting to not use any such approximation except, of course, the linear theory for the cosmological perturbations [34, 35, 36]. Let us also mention that with the incoming flow of more accurate data from the Planck satellite [37, 38] or from the future arc-minute resolution CMB experiments [39, 40, 41], the errors linked with the current approximation schemes may become a problem. The no-approximation approach often requires numerical computations. As a consequence, one has to pay the price of choosing a particular form for the inflaton potential, which implies some loss of generality. A possible way out and a systematic strategy to span the space of inflationary models is to choose

potentials that are representative examples of a whole class of scenarios. For instance, a scenario where inflation takes place in the regime of large (in Planck mass units) vacuum expectation value (vev) for the field, and where the potential goes to infinity as the vev of the field increases towards infinity, is illustrated by chaotic and/or hybrid inflation. The difference between these two models consists in the way inflation stops. On the contrary, a model where inflation occurs for small values of the inflaton vev is well represented by models in which the potential has a symmetry breaking shape. These classes of models were studied in great detail and compared to the WMAP third-year data in reference [34]. From this general perspective, the KKLMMT models with their above-mentioned Coulomb term generate inflation when the vev of the field is large, but with a potential bounded at infinity.

Another motivation, different in spirit from the previous one, lies in model building issues. The Coulomb type potential naturally arises in string inspired scenarios of inflation. Moreover, this type of potential has been known for a long time, even without relying on stringy inspiration, since it can occur in models of hybrid inflation from dynamical supersymmetry breaking [42]. Recently, in the context of String Theory, corrections to the Coulomb potential associated with the problem of moduli stabilisation have been explored [17, 24, 25, 26, 27, 29]. Although interesting from the theoretical point of view, they are not considered in the following. Including these effects in the analysis would greatly increase the number of free parameters relevant for the description of the inflationary part of the model and their degeneracy by opening the parameter space. As a result, given the current data, no constraint could be obtained (as it is the case, for instance, for running mass inflation [34]). We have therefore chosen to perform an exhaustive Bayesian analysis of the CMB data by considering only the generic Coulomb contribution to the potential in the context of string inspired brane inflation.

Compared to the existing literature [43, 44, 45, 46], our study uses a complete Markov-Chain Monte-Carlo (MCMC) analysis based on an exact numerical integration of this type of potential. In this respect, we do not consider particular values of the string length $\sqrt{\alpha'}$ and the string coupling g_s but, on the contrary, develop a parameter scanning strategy which allows to leave these parameters free[‡]. However, we will see in the following that, already with only the Coulomb part of the potential, degeneracies in the parameter space do not permit the WMAP data to fully constrain these stringy quantities. Nevertheless, the throat geometry and some combinations of the KKLMMT model parameters are constrained. Finally, we present new approximate solutions for the field evolution in the DBI regime and refine the analysis of inflationary quantum effects. In particular, it is shown that the approximate solutions usually considered are not sufficient to fully characterise this regime.

This article is organised as follows. In section 2, we briefly recall some basic facts about the KKLMMT scenario of brane inflation, deriving the governing equations from

[‡] Some conditions on these parameters must be nevertheless fulfilled as, for instance, $g_s < 1$ in order to be in the perturbative regime.

the effective four-dimensional action based on type IIB String Theory. In particular, we discuss the intrinsic string features of the model, which among others manifest themselves through an unusual kinetic behaviour as well as a restricted domain of validity for the model. In section 3, we briefly consider the impact of quantum fluctuations that may affect the classical trajectory in certain regions. Section 4 is devoted to the slow-roll phase of the scenario, which can be treated analogously to small field models. However, in the case of the KKLMNT scenario, the slow-roll discussion has to be complemented by a study of the stringy aspects: this is presented in section 5. After deriving the restrictions on the parameter space from model-intrinsic arguments in section 6, we present our results from the WMAP third-year data in sections 7 and 8. Conclusions are drawn in the final section 9. Finally, in Appendix A, we give details on the stochastic regime.

2. Brane inflation

In the following, we discuss the KKLMNT model of brane inflation, first proposed in reference [22] as a realisation of inflation within String Theory. Our goal here is to consider all aspects (string related or not) at play during the inflationary phase. We begin with a intuitive description of how the KKLMNT model arises in String Theory.

2.1. Qualitative description

The model considers a D3 and an anti-D3 brane in a ten-dimensional supergravity background whose world-volume (time-axis included) is aligned with the x^μ coordinate axes, μ varying from 0 to 3. The six extra dimensions y^A with $A = 4, \dots, 9$, are compactified such that the “radial” distance separating brane and anti-brane is $y^4 = r$, and their distance in the other coordinates vanishes. While inflationary models involving D3 (or higher dimensional) branes have been considered in the literature before, the KKLMNT model assumes that the six-dimensional section forms a so-called Klebanov-Strassler (KS) throat [47, 48, 49, 50, 51], i.e. a warped deformed conifold with background fluxes for certain background fields.

Intuitively, this background can be thought of as populated by \mathcal{N} heavy D3 branes with Ramond-Ramond (RR) charge. The anti-D3 brane is embedded at a fixed position r_0 (the bottom of the KS throat), representing an additional source of RR field strength that can be described as a small perturbation. The D3 brane is inserted into this perturbed background at $r_1 \gg r_0$ (far from the bottom of the throat) and is considered as a probe: it does not affect the geometry itself, but experiences the forces due to gravity and RR interaction, brought about by the exchange of light closed string modes between the branes. The distance $r = r_1 - r_0$ between the test D3 and the fixed anti-D3 brane corresponds (up to normalisation) to the inflaton field ϕ whose potential $V(\phi)$ can be calculated from the forces experienced by the test D3 brane in the limit $r \gg \ell_s$, $\ell_s = \sqrt{\alpha'}$ being the string length scale. Inflation takes place while ϕ “rolls down” along a

flat interaction potential in the direction of decreasing ϕ . When the branes become too close, in the sense that their proper distance approaches the string scale, a tachyon, the lightest open string mode stretching from one brane to the other, appears, and the long distance potential $V(\phi)$ is no longer valid. When the D3 brane reaches the bottom of the throat r_0 , the two branes annihilate in a complex process whose details are beyond the scope of the present paper. We will, however, introduce a phenomenological model which assumes that the brane annihilation triggers a reheating era.

2.2. The inflaton effective action

In this section, we use an effective field theory representation of the KKLM model, and our starting point will be the effective action of the inflaton field ϕ . Considering that the inflaton ϕ is itself an open string mode, it is related to the distance r between the brane and the anti-brane by

$$\phi = \sqrt{T_3} r, \quad (1)$$

and its effective four-dimensional action reads

$$\begin{aligned} S = & -\frac{1}{2\kappa} \int R\sqrt{-g} d^4x - T_3 \int \frac{1}{\tilde{h}(\phi)} \sqrt{-g} d^4x \\ & - T_3 \int \frac{1}{\tilde{h}(\phi)} \sqrt{1 + \frac{\tilde{h}(\phi)}{T_3} g^{\mu\nu} \partial_\mu \phi \partial_\nu \phi} \sqrt{-g} d^4x, \end{aligned} \quad (2)$$

where the quantity κ is defined by

$$\kappa \equiv \frac{8\pi}{m_{\text{Pl}}^2}, \quad (3)$$

and

$$T_3 = \frac{1}{(2\pi)^3 g_s \alpha'^2}, \quad (4)$$

is the D3 brane tension, g_s being the string coupling constant. The quantity $\tilde{h}(\phi)$ is the (perturbed) warp factor of the ten-dimensional metric whose form can be calculated from the full Einstein equations [51]. To simplify the notation, one can introduce the effective brane tension $T(\phi)$

$$T(\phi) \equiv \frac{T_3}{\tilde{h}(\phi)}, \quad (5)$$

allowing us to re-write equation (2) as [52]

$$\begin{aligned} S = & S_{\text{grav}} + S_{\text{DBI}} \\ = & -\frac{1}{2\kappa} \int R\sqrt{-g} d^4x \\ & - \int \left[T(\phi) \sqrt{1 + \frac{1}{T(\phi)} g^{\mu\nu} \partial_\mu \phi \partial_\nu \phi} + T(\phi) \right] \sqrt{-g} d^4x. \end{aligned} \quad (6)$$

It is clear that, for a slowly varying scalar field, the terms in $(\partial\phi)^2$ are small and the square root in S_{DBI} can be Taylor expanded in the field derivatives. The resulting action

at leading order identifies with the one of a canonically normalised scalar field evolving in a self-interaction potential.

2.3. The kinetic term

On a flat Friedmann–Lemaître–Robertson–Walker (FLRW) brane, the metric reads

$$ds^2 = a(\eta)^2 (-d\eta^2 + \delta_{ij} dx^i dx^j), \quad (7)$$

where η and x^i are the conformal time and spatial coordinates. In terms of the cosmic time $dt = a d\eta$, the metric tensor reduces to $\text{diag}[-1, a^2(t), a^2(t), a^2(t)]$. For such a homogeneous metric, ϕ can only depend on time and keeping the first non-trivial term in the square root expansion reproduces a standard kinetic term, namely

$$S_{\text{DBI}} = \int \left[\frac{1}{2} \dot{\phi}^2 - 2T(\phi) \right] a^3(t) d^4x, \quad (8)$$

where a dot denotes a derivative with respect to the cosmic time. However, this remains true as long as higher order terms in the expansion can be neglected, i.e. for

$$\dot{\phi}^2 \lesssim T(\phi). \quad (9)$$

Let us denote by ϕ_{DBI} the field value from which onwards the field evolution would be dominated by the string corrections to the standard kinetic term. Notice that equation (9) is also the condition required to have a positive square root argument in equation (6). In this sense, $\sqrt{T(\phi)}$ can be understood as the field maximum speed in the warped throat, and one can, by relativistic analogy, define a Lorentz factor γ such that [53]

$$\gamma(\dot{\phi}, \phi) \equiv \frac{1}{\sqrt{1 - \dot{\phi}^2/T(\phi)}}. \quad (10)$$

When $\gamma \sim \mathcal{O}(1)$, the field ϕ follows the dynamics of a canonically normalised scalar field which can slow-roll (and hence, produce inflation) on a sufficiently flat potential. However, there also exists an “ultra-relativistic” regime, $\gamma \gg 1$, where the string-intrinsic DBI form of the kinetic term is important. In this regime, inflation may be possible even if the scalar field potential is not flat.

2.4. The inflaton potential

Having established the inflaton dynamics, we now identify the potential $V(\phi)$. There is only one term in the expansion of equation (6) which does not contain field derivatives and hence we conclude that

$$V(\phi) = 2T(\phi) = \frac{2T_3}{\tilde{h}(\phi)}. \quad (11)$$

So far we have not specified the form of the warp factor $\tilde{h}(\phi)$. In the case of a KS background perturbed by one anti-D3 brane at the bottom of the throat, we have [22, 51]

$$\tilde{h}(\phi) = \frac{2T_3}{M^4} \left[1 + \left(\frac{\mu}{\phi} \right)^4 \right], \quad (12)$$

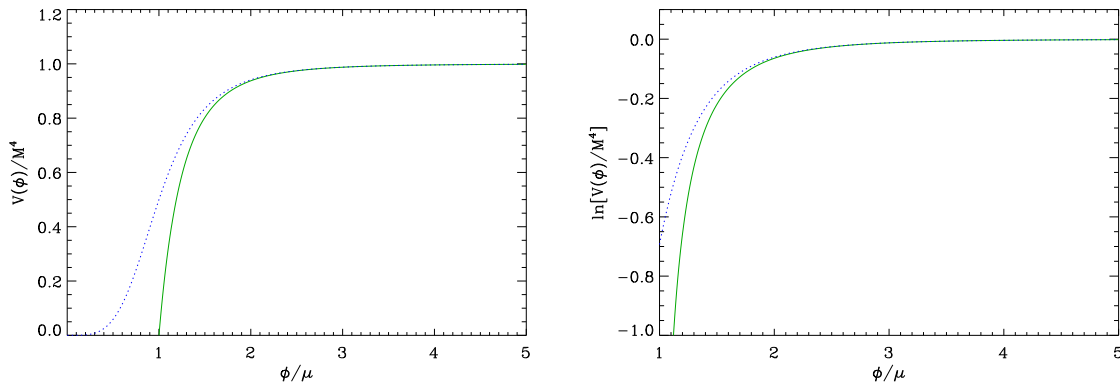


Figure 1. Left panel: The dotted blue line represents the potential given by equation (13). The solid green line shows the approximate potential for $\phi \gg \mu$, see equation (14). The conventional slow-roll phase occurs while the field is rolling on the extremely flat region to the right of the plot. Right panel: Same as the left panel, but in logarithmic unit for the potential.

leading to the potential

$$V(\phi) = \frac{M^4}{1 + (\mu/\phi)^4}. \quad (13)$$

In the case where $\phi \gg \mu$, the first order expansion in μ/ϕ reads

$$V(\phi) \simeq M^4 \left[1 - \left(\frac{\mu}{\phi} \right)^4 \right], \quad (14)$$

which is the most commonly used form of the KKLMNT Coulomb-type potential. The full expression of the potential as well as its approximate expression are represented in figure 1.

2.5. Parameter sets

From the String Theory point of view, a complete description of the KKLMNT model is given by the parameter set

$$(g_s, \alpha', v, \mathcal{M}, \mathcal{K}). \quad (15)$$

where we remind that g_s and $\sqrt{\alpha'}$ are the string coupling and length, respectively. The quantity v is the (dimensionless) volume ratio of the five-dimensional sub-manifold forming the basis of the six-dimensional conifold geometry to the volume of the five-sphere

$$v = \frac{\text{Vol}(X_5)}{\text{Vol}(S_5)}. \quad (16)$$

For instance, the base of the KS throat is the Einstein space $T_{1,1}$, hence in this case one has $v = 16/27$ [54]. The quantity \mathcal{M} and \mathcal{K} are two positive integers associated with the separately quantised background fluxes. They satisfy

$$\mathcal{N} = \mathcal{K}\mathcal{M}, \quad (17)$$

where \mathcal{N} is a positive integer representing the total background RR charge.

Another set of parameters equivalent to (15) is given in terms of the extra dimensions' geometry. The two natural length scales are the location of the bottom of the throat r_0 , which corresponds to the field value

$$\phi_0 = \sqrt{T_3} r_0, \quad (18)$$

and the throat edge r_{UV} . The position $r = r_{UV}$ where the throat is smoothly glued into the rest of the extra dimensional bulk. Provided the depth of the throat is comparable to its width, the edge field value can be approximated by [24]

$$\phi_{UV} = \sqrt{T_3} r_{UV}, \quad (19)$$

with

$$r_{UV}^4 = 4\pi g_s \alpha'^2 \frac{\mathcal{N}}{v}. \quad (20)$$

Consequently, one can deduce the maximum warp factor between the edge and the bottom of the throat [55]

$$\left(\frac{\phi_{UV}}{\phi_0}\right)^4 = \left(\frac{r_{UV}}{r_0}\right)^4 \simeq \exp\left(\frac{8\pi\mathcal{K}}{3g_s\mathcal{M}}\right), \quad (21)$$

where the anti-D3's small perturbation to the KS warp factor has been neglected. The set of geometrical parameters is therefore given by

$$(g_s, \alpha', \phi_0, \phi_{UV}, \mathcal{N}). \quad (22)$$

The potential expression in equation (13) contains the parameters M and μ , which are defined from the string parameters as

$$M^4 = \frac{4\pi^2 v \phi_0^4}{\mathcal{N}}, \quad \mu^4 = \frac{\phi_0^4}{\mathcal{N}} = \frac{M^4}{4\pi^2 v}. \quad (23)$$

Note that v can be expressed through M and μ ,

$$v = \frac{M^4}{4\pi^2 \mu^4}. \quad (24)$$

Since both M and μ are proportional to the ratio ϕ_0^4/\mathcal{N} , one has to provide another parameter to maintain equivalence with the set of equations (15) and (22), for instance \mathcal{N} . In that case, equation (23) can be inverted for ϕ_0 :

$$\phi_0 = \mu \mathcal{N}^{1/4} = \frac{M}{\sqrt{2\pi}} \left(\frac{\mathcal{N}}{v}\right)^{1/4}. \quad (25)$$

The model is thus equally well described by the ‘‘cosmological’’ parameter set

$$(g_s, \alpha', M, \mu, \mathcal{N}). \quad (26)$$

2.6. Domain of validity

We move on to discuss the domain of validity of the effective field theory description. It turns out that in order for equation (2) to be justified, one has to impose some constraints on the model parameters and the accessible field values ϕ .

2.6.1. *Throat within the overall six-dimensional volume.* In equation (3), the four-dimensional gravitational coupling constant κ is expressed as a function of the four-dimensional Planck mass, which, in a ten-dimensional geometry, depends on the volume of the compactified extra dimensions,

$$m_{\text{Pl}}^2 = 8\pi \frac{V_6^{\text{tot}}}{\kappa_{10}}, \quad (27)$$

where κ_{10} is related to the string parameters by

$$\kappa_{10} = \frac{1}{2}(2\pi)^7 g_s^2 \alpha'^4, \quad (28)$$

and V_6^{tot} is the total volume of the six compactified extra dimensions [56, 57]. Now remembering that the total six-dimensional volume consists in the volume V_6^{throat} of the KS throat, where inflation takes place, plus the bulk volume V_6^{bulk} , into which this throat is glued at $r = r_{\text{UV}}$, one has

$$V_6^{\text{tot}} = V_6^{\text{bulk}} + V_6^{\text{throat}}, \quad (29)$$

implying $V_6^{\text{tot}}/V_6^{\text{throat}} > 1$. Although we ignore the precise form of the six-dimensional bulk, the throat volume can be calculated from [24]

$$V_6^{\text{throat}} = 2\pi^4 g_s \mathcal{N} \alpha'^2 r_{\text{UV}}^2, \quad (30)$$

with r_{UV} given by equation (19). Then, re-writing equation (27) as

$$m_{\text{Pl}}^2 = 8\pi \frac{V_6^{\text{throat}}}{\kappa_{10}} \frac{V_6^{\text{tot}}}{V_6^{\text{throat}}}, \quad (31)$$

gives the total to throat volume ratio

$$\frac{V_6^{\text{tot}}}{V_6^{\text{throat}}} = \alpha' m_{\text{Pl}}^2 \sqrt{4\pi^3 g_s \frac{v}{\mathcal{N}^3}}. \quad (32)$$

Since this ratio must exceed one, we obtain a condition on the possible combinations of \mathcal{N} and v , depending on the choice of g_s and α' :

$$\mathcal{N}^{3/2} v^{-1/2} < 2\pi^{3/2} \alpha' m_{\text{Pl}}^2 g_s^{1/2}. \quad (33)$$

Note that this condition heavily depends on the choice of g_s and α' , the value of which can vary significantly according to the specific String Theory considered. It is also convenient to recast equation (33) in terms of ϕ_{UV} . From equations (19) and (32), one has

$$\kappa \phi_{\text{UV}}^2 = \frac{4}{\mathcal{N}} \frac{V_6^{\text{throat}}}{V_6^{\text{tot}}}, \quad (34)$$

and the volume ratio limit (33) implies

$$\phi_{\text{UV}} < \frac{m_{\text{Pl}}}{\sqrt{2\pi\mathcal{N}}}. \quad (35)$$

Let us also remark that, for the supergravity effective description to be valid, the volume of the extra dimensions, and therefore of the throat, should be larger than α'^3 , even when the volume of the five-dimensional conifold basis is very small. However, one can show that this condition does not play a role in the following analysis.

2.6.2. Inflation within a single throat. We will restrict our attention to the case where the D3 brane begins its journey towards the anti-D3 brane inside the KS throat, i.e. for

$$\phi < \phi_{\text{UV}}, \quad (36)$$

where ϕ_{UV} is the field value on the throat edge [see equation (19)]. In cosmological terms, this means that all the e-folds required to solve the Standard Big Bang Model problems occur inside one and the same throat. We will discuss in section 6 in which sense equation (36) allows us to impose restrictions on the parameter values.

2.6.3. End of brane motion by an instability-like mechanism. The derivation of (13) assumes that brane interaction is due to the exchange of the lightest closed string modes only. This is only approximately true: Firstly, one could include the contribution of heavier modes (whose propagation through the bulk is Yukawa suppressed) as well as consider more general effects such as the Kähler potential necessary to stabilise the moduli. In this case, deriving the full brane–anti-brane interaction potential is highly non-trivial. A phenomenological approach is to assume that these effects can be summarised in an additional potential term [e.g. of the form $V(\phi) = m^2\phi^2$] which can be added to equation (13). This route has been explored in the literature, see e.g. [45]. Very recently, the theoretical underpinning of form and origin of these terms has also received much attention [24, 25, 26, 27, 28]. For our cosmological purposes, these effects have not been considered, following the argumentation outlined earlier based on the accuracy of the present data. Secondly, in addition to the above-mentioned corrections to the potential, the effective field model intrinsically has a restricted domain of validity. When the two branes come too close in terms of their proper distance s (with respect to the string scale ℓ_s), an open string can stretch between them and a tachyon, being the lightest excitation of this open string, appears. Let us determine the value ϕ_{strg} for which the proper distance between the branes $s_{\text{end}} \simeq \ell_s$, where $\ell_s = \sqrt{\alpha'}$. It is solution of the following equation [45]

$$\int_{s_0}^{s_{\text{end}}} ds = \int_{r_0}^{r_{\text{strg}}} h^{1/4}(r) dr, \quad (37)$$

where the origin s_0 can be chosen at the brane annihilation location r_0 , i.e. $s_0 = 0$, with r_0 the radial coordinate of the bottom of the throat. Using the warp factor of the unperturbed background, $h(r) = r_{\text{UV}}^4/r^4$, one gets $s_{\text{end}} = r_{\text{UV}} \ln(r_{\text{strg}}/r_0)$. Since $s_{\text{end}} = \sqrt{\alpha'}$, we have $r_{\text{strg}} = r_0 e^{\sqrt{\alpha'}/r_{\text{UV}}}$, which after normalisation gives

$$\phi_{\text{strg}} = \phi_0 e^{\sqrt{\alpha'}/r_{\text{UV}}} = \mu \mathcal{N}^{1/4} \exp \left[\left(4\pi g_s \frac{\mathcal{N}}{v} \right)^{-1/4} \right], \quad (38)$$

where use has been made of equations (19) and (25). Notice that ϕ_{strg} explicitly depends on the background flux \mathcal{N} . As a consequence, another equivalent formulation of the parameter set (26) is therefore given by

$$(g_s, \alpha', M, \mu, \phi_{\text{strg}}). \quad (39)$$

From equation (38), one immediately gets

$$\phi_{\text{strg}} > \mu, \quad (40)$$

since the background flux number $\mathcal{N} \geq 1$. Although the String Theory details of the tachyon appearance and brane annihilation are out of the scope of this work, we will assume that these processes trigger a reheating era which precedes the cosmological radiation-dominated era (see section 8.1).

2.7. Equations of motion

The equations of motion for the inflaton in a FLRW metric on the brane can be obtained from the total action (6). From the stress-tensor associated with the scalar field ϕ , the energy density and pressure read

$$\rho = (\gamma - 1)T(\phi) + V(\phi), \quad P = \frac{\gamma - 1}{\gamma}T(\phi) - V(\phi), \quad (41)$$

from which one obtains the Friedmann–Lemaître equations

$$H^2 = \frac{\kappa}{3} [T(\phi)(\gamma - 1) + V(\phi)], \quad \dot{H} = \frac{\kappa}{2} T(\phi) \left(\frac{1}{\gamma} - \gamma \right). \quad (42)$$

When the velocity of the field is small, the Lorentz factor γ defined in (10) is close to one and its square root can be expanded. Likewise, varying the action with respect to the inflaton field leads to the following “Klein-Gordon like” equation of motion

$$\frac{d^2\phi}{dN^2} + \left(\frac{3}{\gamma^2} + \frac{d \ln H}{dN} \right) \frac{d\phi}{dN} + \left(\frac{3}{\gamma^2} - 1 \right) \frac{T'(\phi)}{2H^2} + \frac{V'(\phi) - T'(\phi)}{H^2\gamma^3} = 0, \quad (43)$$

where, in the present context, a prime denotes a derivative with respect to ϕ . Note that N here is the number of e-folds (not to be confused with the background flux \mathcal{N}), which will be used as a convenient measure of time. In the limit $\gamma \rightarrow 1$, equations (42) and (43) reduce to the standard Friedmann–Lemaître and Klein-Gordon equations. It will be important to establish in which regime the DBI corrections to the kinetic term (and therefore, deviation from the standard slow-roll dynamics) may be important.

2.8. Field evolution overview

Brane inflation according to the KKLMNT scenario incorporates both features of usual slow-roll inflation as well as intrinsic String Theory effects. Let us sketch the successive phases of the field evolution as ϕ rolls down the potential $V(\phi)$ towards its small values.

In figure 2 (left panel), one can distinguish a region (for very large field values, dark green shaded) in which the quantum character of the inflaton field cannot be neglected: Quantum fluctuations are of the same order as the classical ones where the potential is extremely flat, i.e. for ϕ exceeding a certain ϕ_{fluct} . This is notably of interest if the brane starts its journey above this limit. The peculiar properties of this regime will be discussed in section 3 and Appendix A.

For the moment, let us assume that the brane motion starts at $\phi_{\text{in}} < \phi_{\text{fluct}}$. In this region, the potential (13) is still very flat since $\phi \gg \mu$, allowing for most of the

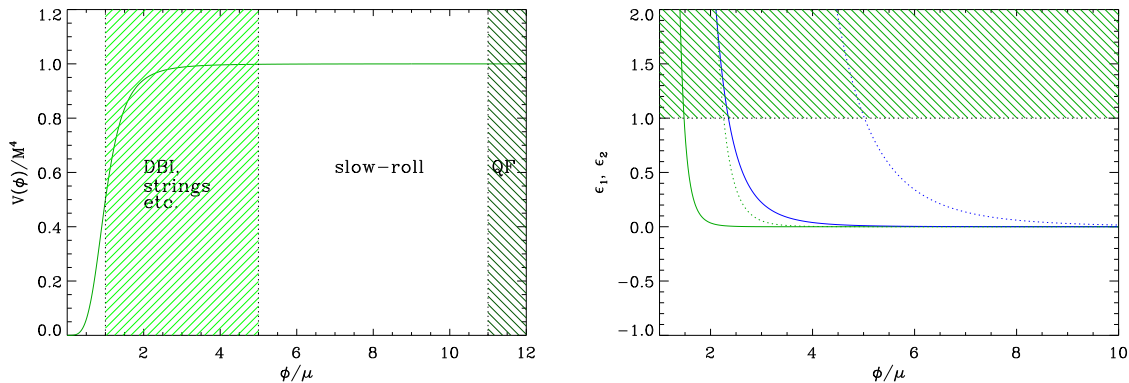


Figure 2. Left panel: Sketch of the expected dynamical regimes according to the vev of the inflaton field for the potential (13). The field starts out in the flat (no hatched) region of the potential and rolls towards smaller field values. Eventually, it will reach the light green hatched region where the slope of the potential becomes noticeable and where the DBI effects can no longer be neglected. This regime may or may not be reached according to the value of ϕ_{strg} for which the derivation of equation (13) breaks down. On the far right (dark green hatched region), the potential is extremely flat and quantum fluctuations are expected to dominate over the field classical evolution. Right panel: The slow-roll parameters ϵ_1 (green line) and ϵ_2 (blue line) for the KKLMMT potential. The solid curves have been obtained for $\mu/m_{\text{Pl}} = 0.1$ whereas the dotted ones for $\mu/m_{\text{Pl}} = 0.01$. Decreasing μ/m_{Pl} increases the differences between ϕ_{ϵ_1} and ϕ_{ϵ_2} , the field values for which $\epsilon_1 = 1$ and $\epsilon_2 = 1$, respectively. Notice that we always have $\phi_{\epsilon_2} > \phi_{\epsilon_1}$.

inflationary expansion to take place. One may therefore expect the usual slow-roll approximation to be valid and it will be used in section 4 to derive the shape of the induced primordial power spectra.

Rolling further to the left, the field ϕ eventually enters a region where the slope of the potential becomes noticeable (light green shaded region). Therefore, the conventional slow-roll approximations are certainly no longer sufficient to describe this evolution, and, since the field velocity should increase, one may expect the DBI dynamics to be the driving force for $\phi < \phi_{\text{DBI}}$. In addition, ϕ_{strg} is also located around this potential domain. The precise order of events in this region will be discussed in section 5.

3. Stochastic inflation

In this section, we will denote the *classically* predicted field value by ϕ_{cl} , and consider the effect of the quantum fluctuations on the classical trajectory [58, 59, 60, 61]. The field values for which quantum fluctuations are comparable to the classical ones can be obtained by first estimating the size of the classical fluctuations in the slow-roll regime. Denoting $V_{\phi_{\text{cl}}}$ the potential derivative with respect to the field, one gets

$$\Delta\phi_{\text{cl}} \simeq -\frac{V_{\phi_{\text{cl}}}}{3H(\phi_{\text{cl}})} \Delta t, \quad (44)$$

which comes from the Klein-Gordon equation by neglecting $\ddot{\phi}$. For Δt it is convenient to take the typical time scale at work during expansion, namely one Hubble time, $\Delta t = 1/H$. Concerning the quantum fluctuations, one has for a test field in de-Sitter space-time,

$$\Delta\phi_{\text{qu}} \simeq \frac{H(\phi_{\text{cl}})}{2\pi}. \quad (45)$$

The field value ϕ_{fluct} , for which classical and quantum fluctuations are of equal amplitude, verifies $\Delta\phi_{\text{cl}}(\phi_{\text{fluct}}) = \Delta\phi_{\text{qu}}(\phi_{\text{fluct}})$. From equations (44) and (45) it follows that

$$\frac{\phi_{\text{fluct}}}{\mu} \simeq \left[\frac{3}{8\pi} \left(\frac{m_{\text{Pl}}}{\mu} \right)^2 \left(\frac{m_{\text{Pl}}}{M} \right)^4 \right]^{1/10}. \quad (46)$$

Using equation (23), we can express (46) in terms of v and the overall scale of inflation M/m_{Pl} . According to their value, ϕ_{fluct} can generically be much larger than the minimal initial field value needed to produce $N_{\text{T}} \simeq 10^2$ e-folds of inflation. To ensure the consistency of the semi-classical approach, we require

$$\phi_{\text{in}} < \phi_{\text{fluct}}, \quad (47)$$

in the following. Quantum effects can be nevertheless described using the stochastic approach [60, 61] which is presented in detail in Appendix A. Since the initial value of the field is also limited by the requirement of having the D3 brane inside the throat, the effective semi-classical model remains valid only if $\phi_{\text{in}} < \min(\phi_{\text{fluct}}, \phi_{\text{UV}})$.

4. The slow-roll regime

In this section we analyse the KKLMMT potential according to its slow-roll characteristics. When denoted as in (13), the analogy between $V(\phi)$ and small field models (investigated in detail in reference [34]) is evident. Notice, however, that for small field inflation, ϕ is increasing while inflation is under way, whereas KKLMMT inflation proceeds from large to small field values (see figure 1).

4.1. Slow-roll parameters

Among the several definitions of the slow-roll parameters, we here use the Hubble-flow functions ϵ_n defined by [62, 63, 64]

$$\epsilon_{n+1} \equiv \frac{d \ln |\epsilon_n|}{dN}, \quad n \geq 0, \quad (48)$$

where N is the number of e-folds since some initial time η_{in} . The above hierarchy starts from $\epsilon_0 = H_{\text{in}}/H$. Slow-roll inflation proceeds as long as $|\epsilon_n| \ll 1$, for all $n > 0$, while inflation takes place if the scale factor is accelerating, i.e. $\epsilon_1 < 1$.

From the potential (13), the first two Hubble flow parameters in their slow-roll formulation read

$$\epsilon_1 = \frac{1}{\pi} \left(\frac{m_{\text{Pl}}}{\mu} \right)^2 \frac{\left(\frac{\phi}{\mu} \right)^{10}}{\left[1 + \left(\frac{\phi}{\mu} \right)^{-4} \right]^2}, \quad (49)$$

$$\epsilon_2 = \frac{1}{\pi} \left(\frac{m_{\text{Pl}}}{\mu} \right)^2 \left(\frac{\phi}{\mu} \right)^{-6} \frac{5 + \left(\frac{\phi}{\mu} \right)^{-4}}{\left[1 + \left(\frac{\phi}{\mu} \right)^{-4} \right]^2}, \quad (50)$$

and they are represented in figure 2 (right panel). They depend on the ratio ϕ/μ and the vev energy scale μ/m_{Pl} [or M/m_{Pl} , by virtue of equation (23)] only. As above-mentioned, inflation ends when $\epsilon_1 = 1$, while the slow-roll approximation itself breaks down when $\epsilon_2 = 1$ (and/or $\epsilon_1 = 1$). Let us stress again that the field theory description of the brane motion fails at $\phi = \phi_{\text{strg}}$.

4.2. Classical field trajectory

The next step is to obtain the classical field trajectory; this is possible while the slow-roll approximation is valid but even in this case, the trajectory is found only implicitly. The total number of e-folds $N(\phi)$ reads [65]

$$N(\phi) = 2\pi \frac{\mu^2}{m_{\text{Pl}}^2} \left[\frac{1}{6} \left(\frac{\phi_{\text{in}}}{\mu} \right)^6 + \frac{1}{2} \left(\frac{\phi_{\text{in}}}{\mu} \right)^2 - \frac{1}{6} \left(\frac{\phi}{\mu} \right)^6 - \frac{1}{2} \left(\frac{\phi}{\mu} \right)^2 \right]. \quad (51)$$

For the generic situation where $\phi/\mu \gg 1$, the two quadratic terms are sub-dominant. Neglecting them yields the following explicit solution

$$\frac{\phi(N)}{\mu} \simeq \left[\left(\frac{\phi_{\text{in}}}{\mu} \right)^6 - \frac{3}{\pi} \left(\frac{m_{\text{Pl}}}{\mu} \right)^2 N \right]^{1/6}. \quad (52)$$

As seen in figure 2, given that the field evolution starts on the very flat part of the potential (but outside the domain of quantum fluctuations), there will surely be an initial phase of evolution during which the slow-roll approximation, and hence the trajectory (52), is valid. However, moving towards smaller field values, this trajectory will eventually become inaccurate and one has to determine at which field value the slow-roll approximation breaks down and how this field value compares to the end of inflation and/or to ϕ_{strg} .

4.3. When does the slow-roll regime break down?

The slow-roll approximation breaks down when one of the slow-roll parameters becomes of order one, which need not coincide with the end of accelerated expansion ($\epsilon_1 = 1$). If slow-roll breaks down first, inflation can still proceed (typically during a very small

number of e-folds), but the evolution of the field is no longer described by the slow-roll trajectory (52). Let us define the field values ϕ_{ϵ_1} and ϕ_{ϵ_2} by

$$\epsilon_1(\phi_{\epsilon_1}) = 1, \quad \epsilon_2(\phi_{\epsilon_2}) = 1. \quad (53)$$

From equations (49) and (50), one obtains the algebraic equations

$$1 + 2 \left(\frac{\mu}{\phi_{\epsilon_1}} \right)^4 + \left(\frac{\mu}{\phi_{\epsilon_1}} \right)^8 - \frac{1}{\pi} \left(\frac{m_{\text{Pl}}}{\mu} \right)^2 \left(\frac{\mu}{\phi_{\epsilon_1}} \right)^{10} = 0, \quad (54)$$

and

$$1 + 2 \left(\frac{\mu}{\phi_{\epsilon_2}} \right)^4 + \left(\frac{\mu}{\phi_{\epsilon_2}} \right)^8 - \frac{5}{\pi} \left(\frac{m_{\text{Pl}}}{\mu} \right)^2 \left(\frac{\mu}{\phi_{\epsilon_2}} \right)^6 - \frac{1}{\pi} \left(\frac{m_{\text{Pl}}}{\mu} \right)^2 \left(\frac{\mu}{\phi_{\epsilon_2}} \right)^{10} = 0. \quad (55)$$

These equations cannot be solved explicitly (except numerically). Some approximate analytical solutions are derived in the following.

4.3.1. Case $\mu > m_{\text{Pl}}$ with $\phi_{\epsilon_1, \epsilon_2} < \mu$. In this case, keeping only the two dominant terms in equation (54) gives

$$\left(\frac{\mu}{\phi_{\epsilon_1}} \right)^8 - \frac{1}{\pi} \left(\frac{m_{\text{Pl}}}{\mu} \right)^2 \left(\frac{\mu}{\phi_{\epsilon_1}} \right)^{10} \simeq 0, \quad (56)$$

whose solution is

$$\frac{\phi_{\epsilon_1}}{\mu} \simeq \frac{m_{\text{Pl}}}{\mu} \frac{1}{\sqrt{\pi}}. \quad (57)$$

This expression is consistent with our assumptions: $\mu > m_{\text{Pl}}$ indeed implies $\phi_{\epsilon_1} < \mu$. Still in the same limit, the three remaining terms in equation (55) are

$$\left(\frac{\mu}{\phi_{\epsilon_2}} \right)^8 - \frac{5}{\pi} \left(\frac{m_{\text{Pl}}}{\mu} \right)^2 \left(\frac{\mu}{\phi_{\epsilon_2}} \right)^6 - \frac{1}{\pi} \left(\frac{m_{\text{Pl}}}{\mu} \right)^2 \left(\frac{\mu}{\phi_{\epsilon_2}} \right)^{10} \simeq 0. \quad (58)$$

This equation has an exact solution with two acceptable roots

$$\left(\frac{\phi_{\epsilon_2}}{\mu} \right)_{\pm} = \frac{m_{\text{Pl}}}{\mu} \sqrt{\frac{2}{\pi}} \left[1 \pm \sqrt{1 - \frac{20}{\pi^2} \left(\frac{m_{\text{Pl}}}{\mu} \right)^4} \right]^{-1/2}. \quad (59)$$

For $\mu > m_{\text{Pl}}$, slow-roll inflation can proceed till the field ϕ reaches $\max(\phi_{\epsilon_1}, \phi_{\epsilon_2}) < \mu$. By comparing equation (57) and (59), we further see that $\phi_{\epsilon_2} > \phi_{\epsilon_1}$, i.e. the slow-roll approximation breaks down before the end of inflation.

However, as already shown in section 5, the KKLMMT model itself is no longer well-defined for $\phi < \phi_{\text{strg}}$ due to the stringy origin of the potential (13). The value ϕ_{strg} given in equation (38) is always greater than μ . Hence, in the case where $\mu > m_{\text{Pl}}$, inflation will definitely come to an end at $\phi_{\text{strg}} > \max(\phi_{\epsilon_1}, \phi_{\epsilon_2})$. As a result, the entire field evolution occurs in the slow-roll regime and, as it will be shown in the following, we do not need to worry about DBI effects which remain negligible in that case.

4.3.2. *Case $\mu < m_{\text{Pl}}$ with $\phi_{\epsilon_1, \epsilon_2} > \mu$.* In this limit, the second and third term of equation (54) are small compared to one, which leads to

$$\frac{\phi_{\epsilon_1}}{\mu} \simeq \left(\frac{1}{\sqrt{\pi}} \frac{m_{\text{Pl}}}{\mu} \right)^{1/5}. \quad (60)$$

Similarly, in equation (55), the second and third term are small compared to one, while the last term is small compared to the fourth, so by keeping only the two dominant terms we obtain

$$\frac{\phi_{\epsilon_2}}{\mu} \simeq \left[\frac{5}{\pi} \left(\frac{m_{\text{Pl}}}{\mu} \right)^2 \right]^{1/6}. \quad (61)$$

Comparing equation (61) and (60) shows that one still has $\phi_{\epsilon_2} > \phi_{\epsilon_1}$, and the slow-roll approximation breaks down before inflation stops. This is confirmed in figure 2. However, this time, the field does not necessarily reach ϕ_{strg} first and non-slow-roll inflation may continue between ϕ_{ϵ_2} and ϕ_{ϵ_1} . Moreover, from ϕ_{ϵ_1} to ϕ_{strg} , the field encounters a transitory regime interpolating between the conventional slow-roll and DBI dynamics. As discussed above, all the slow-roll formulae are strictly speaking no longer valid after $\epsilon_2 = 1$. As a result, the region $\phi < \phi_{\epsilon_2}$ is only accessible numerically and we will show in this way that the number of e-folds occurring between ϕ_{ϵ_2} and ϕ_{ϵ_1} (or ϕ_{strg}) is actually small. The key lesson to be learned from $\phi_{\epsilon_2} > \phi_{\epsilon_1}$ is that whenever we want to rely on analytic results of the slow-roll calculus, we have to confine the field to values $\phi > \phi_{\epsilon_2}$ for consistency and keep in mind that the results will be applicable only if the number of e-folds occurring after ϕ_{ϵ_2} remains negligible.

To proceed further, let us summarise the possible field evolution given that $\mu < m_{\text{Pl}}$: The first option is that, also in this case, the field reaches the value ϕ_{strg} first, i.e. $\phi_{\text{strg}} > \phi_{\epsilon_2}$; this is possible depending on the values of \mathcal{N} and v for the chosen background geometry [see equation (38)]. In that case, the entire field evolution corresponds to slow-roll inflation and is described by the analytical trajectory (52).

If $\phi_{\text{strg}} < \phi_{\epsilon_2}$, then the situation is more complex and depends on the exact order of ϕ_{ϵ_1} , ϕ_{DBI} and ϕ_{strg} . For instance, if ϕ_{ϵ_1} is the next field value to be reached after ϕ_{ϵ_2} , the accelerated expansion would come to a halt here for a field ϕ with standard dynamics, rendering the number of e-folds between ϕ_{ϵ_2} and ϕ_{ϵ_1} extremely small. However, the subsequent evolution for $\phi < \phi_{\epsilon_1}$ could bring the field in the regime of DBI dominance and inflation may re-start. At the same time, ϕ_{strg} could be located between ϕ_{ϵ_1} and ϕ_{DBI} and, as a consequence, ϕ_{DBI} would never be reached. All other combinations are of course a priori possible. Which one is realised in practice depends on the value of the free parameters characterising the model.

5. String-intrinsic aspects

We now move on to investigating those aspects of the KKLMMT model due to its stringy origin. In particular, two questions remain to be properly addressed: the unusual DBI

dynamics, and the appearance of a tachyon once the proper brane distance approaches the string scale.

5.1. When does inflation end?

The potential (13) results from String Theory under the assumption that only the lightest closed string modes (gravitons and the RR particles) contribute to the brane interaction. When the proper distance s between the branes becomes comparable to the string length scale ℓ_s , the exchange of heavier closed modes become relevant, and an open string can stretch from one brane to the other. The appearance of a tachyon triggers the brane annihilation process, or reheating from a cosmological point of view.

We already calculated the field value ϕ_{strg} at which the tachyon appears in equation (38). The crucial question is, does the field first reach the value ϕ_{strg} or ϕ_{ϵ_2} ? If $\phi_{\epsilon_2} < \phi_{\text{strg}}$, inflation ends at brane annihilation for $\phi_{\text{end}} = \phi_{\text{strg}}$ and the field ϕ spends its entire “lifetime” in the usual slow-roll regime. Such is the course of events when $\mu > m_{\text{Pl}}$. For $\mu < m_{\text{Pl}}$, one has to compare ϕ_{ϵ_2} given in equation (61), with ϕ_{strg} given by equation (38). Their ratio reads

$$\frac{\phi_{\epsilon_2}}{\phi_{\text{strg}}} = \left(\frac{M}{m_{\text{Pl}}}\right)^{-1/3} \mathcal{N}^{-1/4} v^{1/12} 10^{1/6} \exp \left[- \left(4\pi g_s \frac{\mathcal{N}}{v}\right)^{-1/4} \right]. \quad (62)$$

This expression involves the energy scale M/m_{Pl} of the potential because ϕ_{ϵ_2} and ϕ_{strg} both depend on M/m_{Pl} , but not in the same way. However, from an observational point of view, this scale is involved in the amplitude of the cosmological perturbations and certainly fixed by the CMB normalisation. Therefore, we may go further and access the above ratio using the current WMAP measurement of the CMB quadrupole.

Let us call ϕ_* the field value at the time when the wavelength of the cosmological perturbations of physical interest today left the Hubble radius during inflation. The slow-roll field trajectory allows us to express ϕ_* in terms of N_* , the number of e-folds between the time of Hubble exit and the end of inflation at ϕ_{end} . Using the approximated classical trajectory (52), this leads to

$$\left(\frac{\phi_*}{\mu}\right)^6 \simeq \left(\frac{\phi_{\text{end}}}{\mu}\right)^6 + \frac{3}{\pi} \left(\frac{m_{\text{Pl}}}{\mu}\right)^2 N_*. \quad (63)$$

To proceed further, we have to specify when exactly inflation ends. But, at the same time, this is also the question we try to address. Changing the mechanism which stops inflation will change the scale M/m_{Pl} and, hence, will affect the ratio (62).

It is convenient to determine the frontier $\phi_{\epsilon_2} = \phi_{\text{strg}}$ in the parameter space. Setting for convenience $\phi_{\text{end}} = \phi_{\epsilon_2}$ in equation (63) gives

$$\frac{\phi_*}{\mu} \simeq \left[\frac{3}{\pi} \left(\frac{m_{\text{Pl}}}{\mu}\right)^2 \left(N_* + \frac{5}{3}\right) \right]^{1/6}. \quad (64)$$

Note that, had we used $\phi_{\text{end}} = \phi_{\epsilon_1}$ instead, the result would be (64) up to the replacement $N_* + 5/3 \rightarrow N_*$. Therefore, ending inflation at ϕ_{ϵ_2} instead of ϕ_{ϵ_1} only causes a small

shift in N_* . This is expected since, as soon as $\epsilon_2 > 1$, slow-roll is violated and the field starts to evolve rapidly: even if the precise evolution can only be probed numerically (see section 5.2), the number of e-folds spent in this regime is generically small. Inserting the result (64) into the expressions (49) and (50) for the slow-roll parameters, one arrives at

$$\epsilon_1 \simeq \frac{1}{\pi} \left(\frac{m_{\text{Pl}}}{\mu} \right)^2 \left[\frac{3}{\pi} \left(\frac{m_{\text{Pl}}}{\mu} \right)^2 \left(N_* + \frac{5}{3} \right) \right]^{-5/3}, \quad (65)$$

$$\epsilon_2 \simeq \frac{5}{3N_*} \left(1 + \frac{5}{3N_*} \right)^{-1} \simeq \frac{5}{3N_*}. \quad (66)$$

As can be seen in these equations, the value of ϵ_1 is generically much smaller than ϵ_2 . Moreover, the quantity ϵ_2 does not depend on the scale μ/m_{Pl} , at first order. The CMB quadrupole normalisation gives the additional relation [34]

$$\frac{V_*}{m_{\text{Pl}}^4} \simeq \frac{45\epsilon_1}{2} \frac{Q_{\text{rms-PS}}^2}{T^2}, \quad (67)$$

where, for $\phi_* \gg \mu$, one may approximate $V_* \simeq M^4$. Using the above expression (65) for ϵ_1 , we find the relations

$$\frac{M}{m_{\text{Pl}}} \simeq \left(45 \frac{Q_{\text{rms-PS}}^2}{T^2} \right)^{3/8} (6N_* + 10)^{-5/8} v^{-1/8}, \quad (68)$$

$$\frac{\mu}{m_{\text{Pl}}} \simeq \left(45 \frac{Q_{\text{rms-PS}}^2}{T^2} \right)^{3/8} (6N_* + 10)^{-5/8} (2\pi)^{-1/2} v^{-3/8}. \quad (69)$$

The numerical value of the WMAP quadrupole is [66]

$$\frac{Q_{\text{rms-PS}}}{T} \simeq 6 \times 10^{-6}. \quad (70)$$

Inserting this expression into equation (62), the ratio $\phi_{\epsilon_2}/\phi_{\text{strg}}$ becomes a function of \mathcal{N} and v only, at fixed string coupling g_s . Explicitly, one obtains

$$\frac{\phi_{\epsilon_2}}{\phi_{\text{strg}}} = \mathcal{C} \mathcal{N}^{-1/4} v^{1/8} 10^{1/6} \exp \left[- \left(4\pi g_s \frac{\mathcal{N}}{v} \right)^{-1/4} \right], \quad (71)$$

where the constant \mathcal{C} reads

$$\mathcal{C} = 10^{1/6} (6N_* + 10)^{5/24} \left(45 \frac{Q_{\text{rms-PS}}^2}{T^2} \right)^{-1/8}. \quad (72)$$

In the plane (v, \mathcal{N}) , the condition $\phi_{\epsilon_2} = \phi_{\text{strg}}$ is a curve separating the plane into the two domains $\phi_{\text{strg}} < \phi_{\epsilon_2}$ and $\phi_{\text{strg}} > \phi_{\epsilon_2}$. Notice that the shape and position of the frontier depend on the value of g_s ; this is illustrated in the left panel of figure 3.

It is convenient to re-scale the parameters g_s , \mathcal{N} and v to minimise the dependence on g_s of the contour $\phi_{\epsilon_2} = \phi_{\text{strg}}$. For this purpose, we define the new variables

$$x \equiv 4\pi g_s \frac{\mathcal{N}}{v}, \quad \bar{v} \equiv \frac{v}{(4\pi g_s)^2}. \quad (73)$$

Usually, the analysis is performed with some specific values of g_s . In this paper, our strategy is different and more general. With the help of the above rescaling, our results

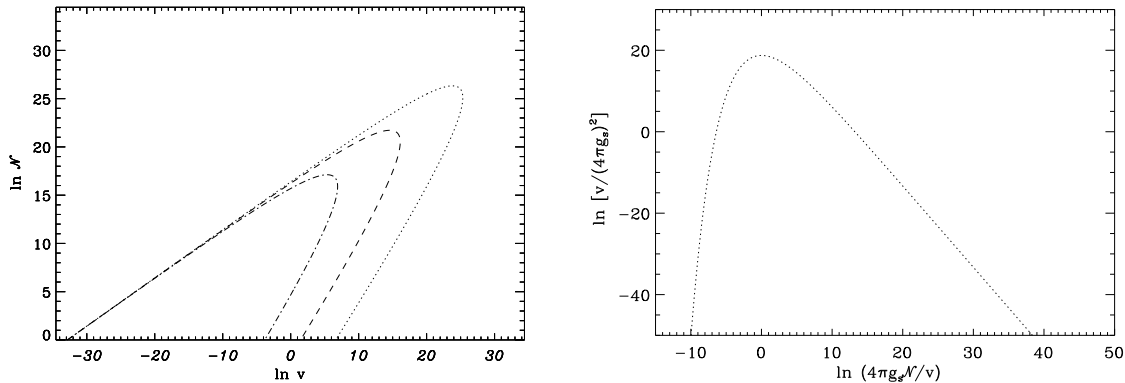


Figure 3. Left panel: The contour $\phi_{\epsilon_2} = \phi_{\text{strg}}$ in the plane $(\ln v, \ln \mathcal{N})$, obtained from equations (62) and (71) using the normalisation given by the CMB quadrupole with $N_* = 50$ [see equation (68)]. The dotted line corresponds to $g_s = 0.1$, the dashed line to $g_s = 10^{-3}$ and the dotted-dashed one to $g_s = 10^{-5}$. In each case, the area enclosed by the contour is the part of the parameter space where the slow-roll conditions are violated before brane annihilation and ϕ_{strg} does not play an important role for the end of inflation. It is clear from this plot that the contour sensitively depends on the value of g_s . However, such a dependence can be absorbed by an appropriate rescaling of the parameters as shown in the right panel. The same contour $\phi_{\epsilon_2} = \phi_{\text{strg}}$ is represented in the plane $(\ln x, \ln \bar{v})$, these parameters being defined in equation (73). It is universal for all values of the string coupling g_s .

will be valid for any values of the coupling constant. In terms of these new parameters, the condition $\phi_{\text{strg}} = \phi_{\epsilon_2}$ from equation (71) now reads, in logarithmic units

$$\ln \bar{v} = 8 \ln \mathcal{C} - 2 \ln x - 8x^{-1/4}. \quad (74)$$

This contour is represented in figure 3 (right panel). All dependence of this line on g_s has been absorbed in the rescaling, so one can now state universally that inside the contour, slow-roll breaks down before the model-intrinsic instability is reached ($\phi_{\text{strg}} < \phi_{\epsilon_2}$), whereas outside, slow-roll inflation proceeds all the way until brane annihilation ($\phi_{\text{strg}} > \phi_{\epsilon_2}$). In fact, this result is more general and we demonstrate in the following that the rescaling permits to absorb the g_s dependence in all the equations expressing a physically relevant condition for the model.

Note that in the above discussion, we have used $\phi_{\text{end}} = \phi_{\epsilon_2}$ to derive the normalisation (68). In doing so, we have in fact ignored the other “stringy” characteristic of the KKLMMT model, namely the DBI kinetic term. While brane evolution definitely ends at ϕ_{strg} , it is possible that, due to the unusual dynamics, a phase of “DBI inflation” occurs even after violation of the slow-roll conditions. If a considerable number of e-folds could be produced in the DBI regime, the value of N_* used in equation (68) would no longer be correct. In the following, we discuss for which field value ϕ_{DBI} those effects will be important and how much expansion may occur outside the slow-roll regime.

5.2. When is the DBI regime important?

An order of magnitude of the field value ϕ_{DBI} for which the DBI regime is relevant can be obtained from the potential (11) by use of the condition (9):

$$\dot{\phi}_{\text{DBI}}^2 \simeq V(\phi_{\text{DBI}}). \quad (75)$$

For a standard kinetic term ($\gamma = 1$), this value would precisely coincide with $\epsilon_1 = 1$. This suggests that the DBI regime appears when standard inflation ends. Of course, given the increasingly non-canonical dynamics as the field is approaching ϕ_{DBI} , the standard slow-roll formula is no longer valid and should be replaced by its generalised form

$$\epsilon_1 \equiv -\frac{d \ln H}{dN} = \frac{1}{2} \kappa \gamma \left(\frac{d\phi}{dN} \right)^2 = \frac{2}{\kappa \gamma} \left(\frac{d \ln H}{d\phi} \right)^2, \quad (76)$$

where use has been made of equation (10) and of the exact expression (42). Therefore, in the ultra-relativistic limit $\gamma \gg 1$, equation (76) suggests that the expansion of the universe may accelerate even with a steep potential. If such a second phase of inflation occurs for more than typically 60 e-folds, then the slow-roll phase becomes observationally irrelevant and the DBI regime crucial. We address this issue by analysing the DBI regime using both analytical and numerical methods.

The above expression for ϵ_1 can be further simplified by using equation (10) to express the field derivatives in terms of γ , H and T solely. The Friedmann–Lemaître equation (42) can then be used to remove any explicit dependency in the Hubble parameter in favour of γ :

$$H^2 = \kappa \frac{V}{3 - \frac{2\epsilon_1}{1 + \gamma^{-1}}}. \quad (77)$$

As a result, the first slow-roll parameter reads, in terms of γ , V and T

$$\epsilon_1 = \frac{3}{2} \frac{1 - \gamma^{-2}}{1 + \gamma^{-1} \left(\frac{V}{T} - 1 \right)}. \quad (78)$$

Equations (77) and (78) are exact and clearly enhance the effect of γ . In the limit $\gamma \rightarrow 1$, one recovers the usual slow-roll formulae obtained with a standard kinetic term, whereas an approximate analytic solution can be derived in the ultra-relativistic limit $\gamma \gg 1$. Under the assumption $V/T = \mathcal{O}(1)$, at leading order in γ^{-1} , one gets

$$\epsilon_1 = \frac{3}{2} + \mathcal{O}(\gamma^{-1}), \quad (79)$$

showing that deep in the DBI regime the universe is not inflating but expands as in a matter dominated era. In our case $V/T = 2$ which ensures the validity of the above expansion. Notice, however, that this relationship does no longer hold if one considers an additional term in the potential, e.g. $m^2 \phi^2$. In that case the V/T term in equation (78) can no longer be neglected and inflation may indeed proceed in the DBI regime [45, 46].

Although the universe is not inflating for $\gamma \gg 1$, we still have to check that the number of e-folds the field spends in the DBI “matter dominated” era remains small. From equations (76) and (79), the Hubble trajectory at leading order in γ^{-1} reads

$$H(N) = H_1 \exp \left[-\frac{3}{2} (N - N_1) \right], \quad (80)$$

where H_1 and N_1 respectively denote the Hubble parameter and the e-fold at which the limit $\gamma \gg 1$ becomes relevant. They could, for instance, be defined as the ones corresponding to the end of the slow-rolling phase provided that the transitory regime occurring between the conventional slow-roll and the region of DBI dominance is short. The field evolution at leading order is given in terms of γ by equation (76) and reads

$$\kappa \left(\frac{d\phi}{dN} \right)^2 = 3\gamma^{-1} + \mathcal{O}(\gamma^{-2}). \quad (81)$$

The system of equations is closed by using expression (42) for the Hubble parameter

$$H^2 = \frac{\kappa T}{3} (\gamma + 1), \quad (82)$$

which is exact since, in our case, one has $V/T = 2$. As a consequence, one gets the field trajectory (neglecting one compared to $\gamma \gg 1$)

$$\frac{d\phi}{dN} \simeq -\frac{\sqrt{T(\phi)}}{H_1} \exp \left[\frac{3}{2} (N - N_1) \right]. \quad (83)$$

This expression can be implicitly integrated in terms of the Gauss hyper-geometric function through use of equations (11) and (13), yielding

$$N = N_1 + \frac{2}{3} \ln \left(1 + \frac{3}{\sqrt{2}} \frac{\mu}{M} \frac{H_1}{M} \left\{ \frac{\sqrt{1+x^4}}{x} - \frac{\sqrt{1+x_1^4}}{x_1} - \frac{2}{x} \text{F} \left(-\frac{1}{4}, \frac{1}{2}; \frac{3}{4}; -x^4 \right) + \frac{2}{x_1} \text{F} \left(-\frac{1}{4}, \frac{1}{2}; \frac{3}{4}; -x_1^4 \right) \right\} \right), \quad (84)$$

where $x \equiv \mu/\phi$. A more illuminating form can be obtained in both limits $x \gg 1$ and $x \ll 1$. In the limit $x \ll 1$, that is to say $\phi \gg \mu$, using the Taylor series defining the hyper-geometric function, equation (84) becomes

$$N \simeq N_1 + \frac{2}{3} \ln \left[1 + \frac{3}{\sqrt{2}} \frac{H_1}{M} \frac{\mu}{M} \left(\frac{1}{x_1} - \frac{1}{x} \right) \right], \quad (85)$$

which gives for the field

$$\frac{\phi}{\mu} \simeq \frac{\phi_1}{\mu} - \frac{\exp \left[\frac{3}{2} (N - N_1) \right] - 1}{\frac{3}{\sqrt{2}} \frac{H_1}{M} \frac{\mu}{M}}. \quad (86)$$

Similarly, in the limit $x \gg 1$ or $\phi \ll \mu$, using the linear transformation formulae associated with the Gauss hyper-geometric function [67], equation (84) yields

$$N \simeq N_1 + \frac{2}{3} \ln \left[1 + \frac{3\sqrt{2}}{2} \frac{H_1}{M} \frac{\mu}{M} (x - x_1) \right], \quad (87)$$

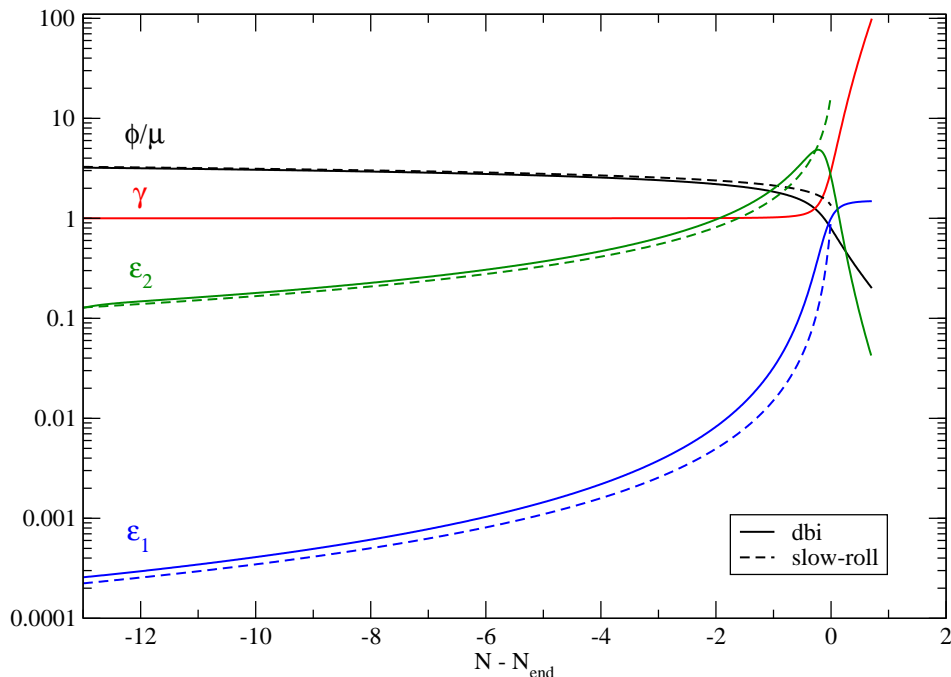


Figure 4. Evolution of the field ϕ , the Hubble-flow functions ϵ_1 , ϵ_2 and the DBI parameter γ in the last e-foldings of an extreme model living close to the throat edge ($\mu = m_{\text{Pl}}/\sqrt{32\pi}$). This model has been chosen to emphasise the DBI effects: the solid lines correspond to an exact numerical integration of the full action (6) whereas the dashed lines are obtained by using the slow-roll approximations (49), (50) and (51). The DBI regime smoothly connects the slow-roll evolution ($\gamma \simeq 1$) to the ultra-relativistic matter-like expansion ($\gamma \gg 1$). Note that in the model at hand, brane annihilation occurs at $\phi_{\text{strg}} > \mu$ preventing any observable effects coming from the DBI evolution.

and, therefore, inverting the previous relation, one obtains

$$\frac{\phi}{\mu} \simeq \left\{ \frac{\mu}{\phi_1} + \frac{\exp\left[\frac{3}{2}(N - N_1)\right] - 1}{\frac{3\sqrt{2} H_1 \mu}{2 M M}} \right\}^{-1}. \quad (88)$$

In fact, the limit $x \gg 1$ ($\phi \ll \mu$) cannot be reached in the model under scrutiny since the tachyonic instability occurs for $\phi \simeq \phi_{\text{strg}} \geq \mu$. As a result, the ultra-relativistic DBI regime could only occur for $\phi > \mu$. As can be seen in equation (86), the corresponding field evolution is exponentially fast implying that the number of e-foldings during which $\phi > \phi_{\text{strg}}$ and $\gamma \gg 1$ is negligible, provided ϕ_1/μ and the denominator are not too large. This is indeed the case for the following reasons. Firstly, as already mentioned, equation (78) shows that γ can deviate from unity only if ϵ_1 is also of order unity, i.e. the field should be in the non-flat region of the potential and therefore $\phi_1 \gtrsim \mu$. Concerning the denominator, as can be seen from equation (77), $H_1/M^2 \lesssim 1/m_{\text{Pl}}$ and this term is at most of order μ/m_{Pl} . The constraint (35) coming from the size of the throat, together

with the fact that brane annihilation occurs at $\phi_{\text{strg}} > \mu$, require that

$$\mu < \frac{m_{\text{Pl}}}{\sqrt{2\pi}}, \quad (89)$$

ensuring that $H_1\mu/M^2$ cannot be large.

To end this section, we have numerically checked that the previous analysis was still qualitatively valid during the intermediate regime in which neither the slow-roll nor the ultra-relativistic approximations can be used. Figure 4 shows the last e-foldings of evolution for an extreme model, close to the limit (89), for which the effects of the DBI regime can be seen. The differences between the slow-roll approximation (under the standard kinetic term hypothesis) and the exact DBI integration appear only during less than an e-fold and close to the region where $\epsilon_1 = 1$. Remembering that the effective field description of the brane motion physically ends at ϕ_{strg} , we conclude that for all practical purposes, the DBI regime has no cosmological observable effects for the model based on the potential (13). The situation, however, can be entirely different in models that include additional terms (e.g. $m^2\phi^2$) in the potential, as shown in reference [45].

6. Theoretical restrictions on the parameter space

We are ready to conclude our analytical investigation of the KKLMMT inflationary model by deriving restrictions on its free parameters. For our numerical calculations and for comparison with the WMAP3 data, we use the observable parameter set (M, μ, \mathcal{N}) , where M and μ are related by equation (24). There are essentially three theoretical consistency relations to be satisfied.

6.1. Constraints from the size of the throat

For the model to be consistent, the warped throat in which the D3 and anti-D3 branes are located should be smaller than the total size of the compactified sub-manifold spanned by the extra dimensions. Earlier, we derived the restriction (33) from this condition. It turns out that this condition can be conveniently re-written in terms of our rescaled parameters (x, \bar{v}) defined in equation (73) as

$$\ln \bar{v} < \ln(\alpha' m_{\text{Pl}}^2 \pi) - \frac{3}{2} \ln x. \quad (90)$$

This is a straight line in the plane $(\ln x, \ln \bar{v})$ whose offset depends on α' (see figure 5). A significant fraction of the parameter space is cut-out by this requirement. Notice that, as announced above, the rescaling (73) has removed any dependence of this bound on g_s and it is universal in the sense that it does not involve the precise inflationary trajectory, nor the mechanism that ends inflation.

6.2. Constraints from starting inflation inside the throat

For all the e-folds to occur inside one throat, we enforce $\phi < \phi_{\text{UV}}$. Since ϕ decreases during inflation, this restriction applies to the initial field value ϕ_{in} . On the other hand,

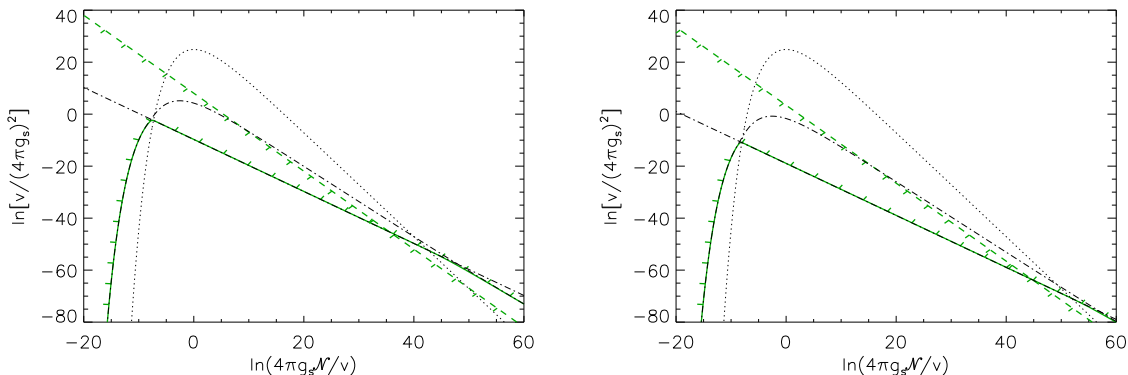


Figure 5. Allowed regions (ticks in) in the rescaled parameter plane $(\ln x, \ln \bar{v})$ for $\alpha' m_{\text{Pl}}^2 = 1000$ (left panel) and $\alpha' m_{\text{Pl}}^2 = 10$ (right panel) with the fiducial values $N_* = 50$ and $N_{\text{T}} = 60$. The black dotted curve is the contour $\phi_{\epsilon_2} = \phi_{\text{strg}}$ of figure 3. For all points located inside this contour, the slow-roll conditions are violated before brane annihilation. The green dashed line (with ticks down) represents the volume ratio constraint (90), whose slope is universal but whose offset depends on $\alpha' m_{\text{Pl}}^2$. Regions above this line are therefore excluded. The solid green curve (with ticks up) represents the condition that all of the brane evolution occurs within one throat, and has been obtained through a numerical integration. All points below that curve would not satisfy this condition. Its shape can be piecewise analysed. In the region $\phi_{\text{strg}} < \phi_{\epsilon_2}$ (inside the black dotted contour), this is a straight line given by equation (92). The slope of this line is universal, but the offset again depends on $\alpha' m_{\text{Pl}}^2$. Outside the dotted contour, namely for $\phi_{\text{strg}} > \phi_{\epsilon_2}$, and in the limit $\phi_{\text{strg}} \gg \phi_{\epsilon_2}$, this boundary is described by equation (101). Combined, these pieces lead to the solid green curve with ticks up; to make the shape of both pieces visible individually, they have been extended outside their respective domains of validity (dotted-dashed black curve).

there is a lower bound on ϕ_{in} such that at least N_{T} e-folds are produced. This bound in turn depends on the mechanism ending the inflationary expansion.

Let us start with the case in which the slow-roll approximation is violated before brane annihilation. Making use of the classical trajectory (52), the initial field value necessary to produce N_{T} e-folds before ϕ_{ϵ_2} can be derived from equation (61) and reads

$$\frac{\phi_{\text{in}, \epsilon_2}}{\mu} \simeq \left\{ \frac{3}{\pi} \left(\frac{m_{\text{Pl}}}{\mu} \right)^2 \left[\frac{5}{3} + N_{\text{T}} \right] \right\}^{1/6}. \quad (91)$$

For the KKLMMT case, imposing the CMB normalisation (69) calculated earlier and using equation (19), one can recast the bound $\phi_{\text{in}, \epsilon_2} < \phi_{\text{UV}}$ in terms of the rescaled variables

$$\ln \bar{v} > -\ln x - 4 \ln \mathcal{D}, \quad (92)$$

where the constant \mathcal{D} reads

$$\mathcal{D} = (\pi \alpha' m_{\text{Pl}}^2)^{-1/2} (6N_* + 10)^{5/12} (6N_{\text{T}} + 10)^{-1/6} \left(45 \frac{Q_{\text{rms-PS}}^2}{T^2} \right)^{-1/4}. \quad (93)$$

This is also a straight line in the plane (x, \bar{v}) and further constrains from below the parameter space (see figure 5). As before, all the g_s dependence has been removed and only the α' one remains in the expression of the offset. This offset also depends on N_* and N_T but only weakly because these two quantities appear in a logarithm. In the following, the fiducial values $N_* = 50$ and $N_T = 60$ will be used

Notice that by using the normalisation (69) derived from $\phi_{\text{end}} = \phi_{\epsilon_2}$, the previous result is valid only inside the contour (74). Therefore, we still have to treat the case where inflation ends prematurely at $\phi_{\text{strg}} > \phi_{\epsilon_2}$. Since the entire field evolution occurs in the slow-roll regime, the trajectory (52) remains valid all the time. The minimal initial field value $\phi_{\text{in, strg}}$ leading to N_T e-folds of inflation is therefore obtained by setting $\phi_{\text{end}} = \phi_{\text{strg}}$. This leads to

$$\frac{\phi_{\text{in, strg}}}{\mu} = \left[\frac{3N_T}{\pi} \left(\frac{m_{\text{Pl}}}{\mu} \right)^2 + \left(\frac{\phi_{\text{strg}}}{\mu} \right)^6 \right]^{1/6}, \quad (94)$$

where ϕ_{strg} is given by equation (38). In order to use the CMB normalisation, the new value of ϕ_* has to be derived from equation (63) where, now, $\phi_{\text{end}} = \phi_{\text{strg}}$. One obtains

$$\frac{\phi_*}{\mu} = \left[\left(\frac{\phi_{\text{strg}}}{\mu} \right)^6 + \frac{3}{\pi} \left(\frac{\mu}{m_{\text{Pl}}} \right)^{-2} N_* \right]^{1/6}. \quad (95)$$

The slow-roll parameter associated with this field value reads

$$\epsilon_1 \simeq \frac{1}{\pi} \left(\frac{\mu}{m_{\text{Pl}}} \right)^{-2} \left(\frac{\phi_*}{\mu} \right)^{-10}, \quad (96)$$

and can be plugged into equation (67) to give the CMB normalisation condition

$$\left(\frac{M}{m_{\text{Pl}}} \right)^6 = 45 \frac{Q_{\text{rms-PS}}^2}{T^2} v^{1/2} \left[\left(\frac{\phi_{\text{strg}}}{\mu} \right)^6 + 6N_* \left(\frac{M}{m_{\text{Pl}}} \right)^{-2} v^{1/2} \right]^{-5/3}. \quad (97)$$

Unlike the case $\phi_{\text{end}} = \phi_{\epsilon_2}$, this equation for M/m_{Pl} cannot be made explicit but one can use equation (61) to replace the last term in the square brackets and obtain

$$\left(\frac{M}{m_{\text{Pl}}} \right)^6 = 45 \frac{Q_{\text{rms-PS}}^2}{T^2} v^{1/2} \left[\left(\frac{\phi_{\text{strg}}}{\mu} \right)^6 + \frac{3N_*}{5} \left(\frac{\phi_{\epsilon_2}}{\mu} \right)^6 \right]^{-5/3}. \quad (98)$$

An explicit analytical solution can be derived in the limit $\phi_{\text{strg}} \gg \phi_{\epsilon_2}$. Due to the presence of the N_* term, this approximation may be violated only for large N_* values. But if we are not in this extreme situation, in the limit $\phi_{\text{strg}} \gg \phi_{\epsilon_2}$, one gets

$$\frac{M}{m_{\text{Pl}}} \simeq \left(45 \frac{Q_{\text{rms-PS}}^2}{T^2} \right)^{1/6} v^{1/12} \left(\frac{\phi_{\text{strg}}}{\mu} \right)^{-5/3}, \quad (99)$$

$$\frac{\mu}{m_{\text{Pl}}} \simeq \left(45 \frac{Q_{\text{rms-PS}}^2}{T^2} \right)^{1/6} (2\pi)^{-1/2} v^{-1/6} \left(\frac{\phi_{\text{strg}}}{\mu} \right)^{-5/3}. \quad (100)$$

Enforcing $\phi_{\text{in, strg}} < \phi_{\text{UV}}$ from equations (19) and (94) gives, in terms of the rescaled parameters,

$$\ln \left[1 + 6N_T \left(45 \frac{Q_{\text{rms-PS}}^2}{T^2} \right)^{-1/3} x^{-2/3} \bar{v}^{-1/3} \exp \left(-\frac{8}{3} x^{-1/4} \right) \right] < 4x^{-1/4}$$

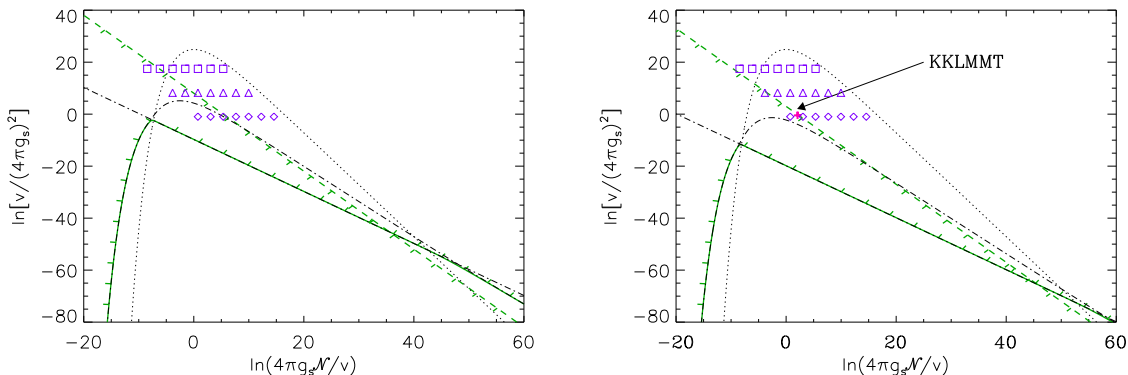


Figure 6. Plots similar to those in figure 5, for $\alpha' m_{\text{Pl}}^2 = 1000$ on the left and for $\alpha' m_{\text{Pl}}^2 = 6.4$ (as chosen in [22]) on the right. The quantities N_* and N_{T} are fixed to their fiducial values $N_* = 50$ and $N_{\text{T}} = 60$. The additional symbols correspond to various models selected according to the values of v , \mathcal{N} and g_s . All purple symbols correspond to the KS throat value of $v = 16/27$, and respectively have $\mathcal{N} = 1, 10, 100, 10^3, 10^4, 10^5$ and 10^6 from left to right. The diamond-shaped points are for $g_s = 0.1$, the triangles for $g_s = 10^{-3}$, and the squares for $g_s = 10^{-5}$. The original KKLMMT model [22] is indicated by a red cross in the right panel; it corresponds to $v = 1$, $\mathcal{N} = 160$ and $g_s = 0.1$ at $\alpha' m_{\text{Pl}}^2 = 6.4$.

$$+ 2 \ln \bar{v} + \frac{5}{2} \ln x - 3 \ln (\pi \alpha' m_{\text{Pl}}^2) - \ln \left(45 \frac{Q_{\text{rms-PS}}^2}{T^2} \right). \quad (101)$$

Again, there is no trace of g_s left after rescaling, but instead of a straight line as was the case for equations (90) and (92), this is an implicit contour in the $(\ln x, \ln \bar{v})$ plane. It is represented in figure 5. Let us recall that equation (101) is only valid far enough from the contour $\phi_{\text{strg}} = \phi_{\epsilon_2}$ in such a way that $\phi_{\text{strg}} \gg \phi_{\epsilon_2}$. In the intermediate regime where inflation does end by instability at ϕ_{strg} , but the two terms in the square brackets of equation (98) are of comparable value, the correct normalisation of M/m_{Pl} to the CMB quadrupole is only accessible numerically and has been also represented in figure 5 for convenience. It is remarkable that when one normalises with either (68) (obtained from $\phi_{\text{end}} = \phi_{\epsilon_2}$) or with (99) (assuming $\phi_{\text{strg}} \gg \phi_{\epsilon_2}$), the g_s dependence can be absorbed into the unique rescaling given in equation (73).

Finally, in figure 6, various concrete models for different values of v , \mathcal{N} and g_s are compared with the consistency conditions derived above. In particular, one notices that the volume ratio constraint is quite restrictive and that many possible models are already ruled out by this condition.

6.3. Constraints from stochastic inflation

If the field ϕ starts out at a value comparable to ϕ_{fluct} given in equation (46), then stochastic effects will be important and the classical field trajectory does no longer suffice to describe the field evolution. As a minimum requirement, in the case where

brane annihilation occurs after ϕ_{ϵ_2} , one has to impose

$$\phi_{\text{in},\epsilon_2} \ll \phi_{\text{fluct}}, \quad (102)$$

where $\phi_{\text{in},\epsilon_2}$ is given by equation (91). Comparing equation (91) with equation (46), and using the correct normalisation (68), we notice that the dependence on \mathcal{N} and v disappears. As a result, the restriction coming from (102) concerns the maximal total number of e-folds N_{T} achievable,

$$N_{\text{T}} < -\frac{5}{3} + (3^2 2^{11})^{-1/5} (6N_* + 10) \left(45 \frac{Q_{\text{rms-PS}}^2}{T^2} \right)^{-3/5},$$

which gives $\max(N_{\text{T}}) \simeq 10^7$ for $N_* \simeq 50$. Similarly, if inflation ends at $\phi_{\text{strg}} > \phi_{\epsilon_2}$, one imposes

$$\phi_{\text{in,strg}} \ll \phi_{\text{fluct}}, \quad (103)$$

to avoid quantum fluctuation dominance. In this case, using equations (46) and (94), together with the normalisation given in equation (99), gives

$$\begin{aligned} \ln \left[1 + 6N_{\text{T}} \left(45 \frac{Q_{\text{rms-PS}}^2}{T^2} \right)^{-1/3} x^{-2/3} \bar{v}^{-1/3} \exp \left(-\frac{8}{3} x^{-1/4} \right) \right] \\ < \frac{3}{5} \ln \frac{3}{4} - \frac{3}{5} \ln \left(45 \frac{Q_{\text{rms-PS}}^2}{T^2} \right). \end{aligned} \quad (104)$$

As usual, the rescaling allows us to get rid of any explicit dependence in g_s . We do not pursue this issue further here. For a detailed study of the presence of quantum fluctuation effects in the throat, see Appendix A.

7. Implications of the WMAP slow-roll bounds

In this section, the theoretically predicted values of the KKLMMT slow-roll parameters are confronted with the third year WMAP data (WMAP3). The WMAP3 bounds on the Hubble-flow parameters ϵ_1 and ϵ_2 have been discussed in reference [34, 33, 68] under various prior choices and hypotheses. For the sake of robustness, in the following we use the constraints derived in reference [34] on the first order Hubble-flow parameters obtained by marginalising over the second order slow-roll parameter ϵ_3 and under an uniform prior choice for $\log(\epsilon_1)$ in $[-5, 0]$ and for ϵ_2 in $[-0.2, 0.2]$. The resulting one and two-sigma contour intervals of the two-dimensional marginalised posteriors are represented in figure 7.

Let us first consider the situation where violation of the slow-roll conditions occurs before brane annihilation. In this case, if one chooses for instance $N_* = 50$, the CMB normalisation from equations (68) and (69) yields

$$\frac{\mu}{m_{\text{Pl}}} \simeq 5.6 \times 10^{-6} v^{-3/8}, \quad \frac{M}{m_{\text{Pl}}} \simeq 1.4 \times 10^{-5} v^{-1/8}. \quad (105)$$

Hence these two parameters become functions of v only. The resulting numerical values for ϵ_1 and ϵ_2 are given by equations (65) and (66) and read

$$\epsilon_1 \simeq 4.8 \times 10^{-11} v^{-1/2}, \quad \epsilon_2 \simeq 0.03. \quad (106)$$

This has two very important consequences: it is clear that except for very small values of the volume ration $v < 10^{-18}$, ϵ_1 remains negligible compared to ϵ_2 . In particular, since the spectral indices of the scalar and tensor primordial power spectra, at first order in the Hubble-flow parameters, read

$$n_s - 1 = -2\epsilon_1 - \epsilon_2, \quad n_T = -2\epsilon_1, \quad (107)$$

we have unobservably small tensor modes and a scalar spectral index

$$n_s \simeq 0.97. \quad (108)$$

In figure 7, we have studied the slow-roll predictions in more detail. The slow-roll parameters have been calculated exactly in the sense that equation (55) has been solved numerically, that is to say we have obtained the exact value of ϕ_{ϵ_2} . The same has been done for ϕ_* . Then, the corresponding values of the Hubble-flow parameters have been derived with the help of equations (65) and (66) for different N_* such that $N_* \in [40, 60]$. For each value of N_* , this gives a point in the space (ϵ_1, ϵ_2) and for the range under consideration, a segment line spanning twenty e-folds (see figure 7). The “left” end of this segment line corresponds to the largest value of N_* , namely $N_* = 60$ and the “right” end corresponds to $N_* = 40$. The left panel assumes $v = 1$, while the right one was plotted for $v = 10^{-6}$. The dotted-dashed blue contours are the WMAP3 constraints on the slow-roll parameters and corresponds to the 68% and 95% confidence intervals of the two-dimensional marginalised posteriors. The dotted black lines are the lines of constant n_s , the red one tracing the scale invariant case $n_s = 1$. The figure confirms the previous analysis. The gravitational waves level is generically very low and the spectral index is slightly red in full agreement with the WMAP3 data. Moreover, changing the size of the extra dimension changes ϵ_1 without affecting ϵ_2 . However, for reasonable values of v , ϵ_1 remains so small that there is no hope to detect primordial gravitational waves in the future.

Let us now turn to the situation where the parameters of the model are such that inflation ends by instability at ϕ_{strg} . In this case, the WMAP normalisation leads to the scale M/m_{pl} given by equation (99). Then, straightforward calculations lead to the following expressions for the Hubble-flow parameters

$$\epsilon_1 = \frac{v^{1/3}}{2\pi^2} \left(45 \frac{Q_{\text{rms-PS}}^2}{T^2} \right)^{-1/3} \left(\frac{\phi_{\text{strg}}}{\mu} \right)^{-20/3}, \quad (109)$$

$$\epsilon_2 = \frac{5v^{1/3}}{2\pi^2} \left(45 \frac{Q_{\text{rms-PS}}^2}{T^2} \right)^{-1/3} \left(\frac{\phi_{\text{strg}}}{\mu} \right)^{-8/3}. \quad (110)$$

In the limit $\phi_{\text{strg}}/\mu \gg 1$, one has $\epsilon_1 \ll \epsilon_2 \ll 1$ except maybe for extreme values of v . Therefore, n_s is now pushed towards one, while n_T becomes even smaller for all values of N_* . As a consequence, one expects this scenario to be disfavoured by the data. Indeed, as can be noticed in figure 7, a scale invariant power spectrum is not likely if the gravitational waves level is low (this is no longer true if $\epsilon_1 > 10^{-2}$).

To conclude this section, let us recap what can be deduced from the slow-roll analysis. Firstly, the situation where inflation ends by violation of the slow-roll

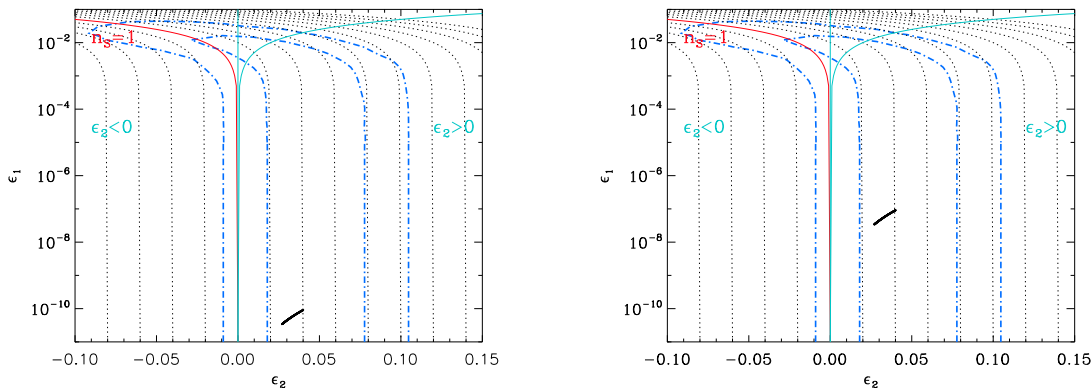


Figure 7. Left panel: Predictions for the KKLMNT model with $v = 1$ in the case where one considers that inflation stops at $\epsilon_2 = 1$. Right panel: Same as left panel but with $v = 10^{-6}$.

condition is favoured by the data as compared to the case where inflation stops by brane annihilation. Secondly, one expects the level of gravitational waves to be extremely low. The stringy interpretation of this result is linked to the so-called Lyth bound [69, 24] which relates the tensor to scalar ratio to the total variation of the inflaton field value. In our case, this gives $\Delta\phi = \sqrt{T_3}(r_{UV} - r_0) \simeq \sqrt{T_3}r_{UV} = \phi_{UV}$. Therefore, given equation (35), the volume bound on the throat limits the gravitational wave contribution, as recovered here. Thirdly, the constraint $\epsilon_1 \lesssim 3 \times 10^{-2}$ implies the limit

$$\log(4\pi^2 v) \gtrsim -16. \quad (111)$$

This is clearly not a very stringent constraint. In the next section, we will see that, combined with the constraint on the size of the throat, the data can lead to a better limit.

8. WMAP constraints in the exact numerical approach

In this section, the cosmological consequences of the KKLMNT model are investigated using a numerical integration of the brane motion up to its linear perturbations to extract the exact scalar and tensor primordial power spectra. The tachyonic instability occurring at the bottom of the throat triggering a reheating era is considered through a simple phenomenological model. The predicted CMB power spectra can then be computed by integrating the seeded cosmological perturbations through the radiation and matter era and we have used a modified version of the **CAMB** code for this purpose [70]. This method allows a Markov-Chain Monte-Carlo (MCMC) analysis of the WMAP third year data involving the usual cosmological parameters together with the KKLMNT parameters. A modified version of the **COSMOMC** code [71] has been used to derive the probability density distributions of the cosmological, KKLMNT and reheating parameter values given the data.

8.1. Method and hypotheses

The numerical method used has been introduced in references [34, 35] and consists in the mode by mode integration of both the background and the perturbed quantities till the end of inflation (see also Refs. [72, 73, 74, 75, 76, 77, 78]). As shown in section 5.2, the DBI regime is not relevant for the model under scrutiny and we have chosen to integrate the background equations stemming from the action (6) in the standard kinetic-term limit. The resulting equations of motion are obtained from equations (43), (76) and (77) in the $\gamma = 1$ limit and for the KKLMMT potential (13).

In the longitudinal gauge, we consider the scalar and tensor linear perturbations to the flat FLRW metric (7),

$$ds^2 = a^2 \left\{ -(1 + 2\Phi)d\eta^2 + [(1 - 2\Psi)\delta_{ij} + h_{ij}] dx^i dx^j \right\}, \quad (112)$$

where Φ and Ψ are the Bardeen potentials [79] and h_{ij} is a transverse and traceless tensor. From the perturbed Einstein and Klein-Gordon equations, the dynamics of the scalar and tensor modes, in Fourier space, reduces to the equations of motion of two uncoupled parametric oscillators [7, 80, 81, 82]

$$\frac{d^2 \mu_{s,T}}{d\eta^2} + \omega_{s,T}^2(k, \eta) \mu_{s,T} = 0, \quad (113)$$

where the frequencies are respectively

$$\omega_s^2(k, \eta) = k^2 - \frac{(a\sqrt{\epsilon_1})''}{a\sqrt{\epsilon_1}}, \quad \omega_T^2(k, \eta) = k^2 - \frac{a''}{a}, \quad (114)$$

the prime denoting differentiation with respect to conformal time. The scalar and tensor mode functions are gauge invariant and read [7]

$$\mu_s = a\sqrt{2\kappa} \left(\delta\phi + \frac{d\phi}{d\eta} \frac{\Phi}{\mathcal{H}} \right), \quad \mu_T = ah_{ij}, \quad (115)$$

where $\delta\phi$ stands for the linear perturbations, in the longitudinal gauge, of the inflaton field ϕ [see equation (1)]. The initial conditions for the perturbed quantities $\mu_{s,T}$ are set in the decoupling limit $k \gg \mathcal{H}$ where the deep sub-Hubble modes behave as free quantum fields. Assuming their initial state to be the usual Bunch-Davies vacuum, one gets [83]

$$\lim_{k/\mathcal{H} \rightarrow \infty} \mu_{s,T} = \sqrt{k} \frac{e^{-ik(\eta-\eta_i)}}{\sqrt{k}}, \quad (116)$$

with η_i some (arbitrary) initial conformal time. These initial conditions uniquely determine the solutions of equation (113) which can be numerically integrated along the lines described in reference [35]. From such a numerical integration, the primordial scalar and tensor power spectra can be evaluated at the end of inflation for all the relevant observable wavenumbers

$$\mathcal{P}_\zeta \equiv k^3 P_\zeta(k) = \frac{k^3}{8\pi^2} \left| \frac{\mu_s}{a\sqrt{\epsilon_1}} \right|^2, \quad \mathcal{P}_h \equiv k^3 P_h(k) = \frac{2k^3}{\pi^2} \left| \frac{\mu_T}{a} \right|^2. \quad (117)$$

Concerning the background quantities, the attractor mechanism during inflation ensures that the initial field value ϕ_{in} has no direct observable effects since it determines only the total number of e-folds N_{T} . Its value can therefore be, a priori, arbitrarily chosen provided N_{T} is big enough to solve the problems of the standard hot Big-Bang phase and allows the observable perturbations to be sub-Hubble initially. As thoroughly discussed in sections 5 and 6, the brane motion ends by the appearance of a tachyon from its coalescence with the anti-brane at the bottom of the throat, and this determines the field value at which the above classical evolution cannot longer be used, namely $\phi \simeq \phi_{\text{strg}}$. The initial field value ϕ_{in} can therefore be chosen in such a way that the brane motion generates N_{T} e-folds of inflation before reaching ϕ_{strg} . However, one still has to impose that the brane motion starts inside the throat for the model to be consistent, i.e. $\phi_{\text{in}} < \phi_{\text{UV}}$.

According to the previous discussion, it is natural to assume that the reheating era starts when the brane alights on the anti-brane. Although, strictly speaking, brane annihilation occurs at the bottom of the throat r_0 , the String Theory details of the evolution for $\phi < \phi_{\text{strg}}$ are out of the scope of our simple approach [84, 85, 86]. As a result, we have adopted the phenomenological reheating model discussed in references [34, 35]. It assumes that the reheating can only influence the observed perturbations through its effects on the cosmological redshift z_{strg} , which will be identified with the beginning of the reheating era. Such an assumption is motivated by the fact that adiabatic super-Hubble perturbation modes should not be significantly modified during reheating, at least in the absence of entropy modes (here, we deal with a single field model). The influence of z_{strg} can be seen by rewriting equation (113) in terms of the number of e-folds as a time variable. The wavenumbers to be considered during inflation always appear in the ratio k/\mathcal{H} which should be determined from the observable wavenumbers k/a_0 measured today, typically three decades around $k_* = 0.05 \text{ Mpc}^{-1}$. At a given e-fold N during inflation,

$$\frac{k}{\mathcal{H}} = \frac{k}{a_0} (1 + z_{\text{strg}}) \frac{e^{N_{\text{T}} - N}}{H(N)}. \quad (118)$$

Assuming instantaneous transitions between the successive expansion eras, the redshift z_{strg} is given by

$$\ln(1 + z_{\text{strg}}) = \frac{1}{4} \ln(\kappa^2 \rho_{\text{reh}}) - \ln \frac{a_{\text{strg}}}{a_{\text{reh}}} - \frac{1}{2} \ln \left(\sqrt{3\Omega_{\text{rad}} \kappa H_0} \right), \quad (119)$$

where ρ_{reh} is the total energy density at the end of the reheating era, and Ω_{rad} , H_0 are the density parameter of radiation and the Hubble parameter today. The first two terms in equation (119) are clearly reheating dependent and in absence of a microscopic model we can define a phenomenological reheating parameter R_{rad} such that

$$\ln R_{\text{rad}} \equiv -\frac{1}{4} \ln \left(\frac{\rho_{\text{reh}}}{\rho_{\text{strg}}} \right) + \ln \frac{a_{\text{strg}}}{a_{\text{reh}}}. \quad (120)$$

This parameter has a simple physical interpretation: it encodes the global deviation the dynamics of the reheating era may have with respect to a pure radiation-like era (for

which R_{rad} vanishes). Notice that, from the numerical integration, the energy density ρ_{strg} when $\phi = \phi_{\text{strg}}$ is known and only depends on ϕ_{strg} and the potential parameters.

Under the previous assumptions, the KKLMMT inflation era requires the knowledge of five primordial parameters: the KKLMMT potential parameters, namely M and μ , the reheating parameter R_{rad} and the field values ϕ_{UV} and ϕ_{strg} encoding the observable properties of the throat and the branes. The resulting CMB anisotropies are uniquely determined once the ‘‘low energy’’ cosmological model is fixed. We are considering the Λ CDM flat universe model which adds four cosmological parameters: the number density of baryons Ω_{b} , of cold dark matter Ω_{dm} , the reduced Hubble parameter today h , and the redshift of reionisation z_{re} .

8.2. MCMC parameters and priors

Due to parameter degeneracies with respect to the CMB temperature and polarisation angular power spectra, some parameter combinations are more appropriate for an efficient MCMC exploration. Concerning the Λ CDM parameters, instead of directly sampling models according to the values of the set $(\Omega_{\text{b}}, \Omega_{\text{dm}}, z_{\text{re}}, H_0)$, it is more convenient to use the equivalent set $(\Omega_{\text{b}}h^2, \Omega_{\text{dm}}h^2, \tau, \theta)$, where τ is the optical depth and θ measures the ratio of the sound horizon to the angular diameter distance [71].

Similarly, it is more convenient to use an optimal derived set for the primordial parameters. The amplitude of the scalar primordial power spectrum at a given observable wavenumber $\mathcal{P}_* = \mathcal{P}_\zeta(k_*)$ is a well measured quantity [see equation (67)]. It is therefore more convenient to directly sample the models according to the values of \mathcal{P}_* rather than the potential energy scale M/m_{Pl} . This can be done by integrating the perturbations with the artificial value $M/m_{\text{Pl}} = 1$ and then perform a rescaling of M/m_{Pl} from unity to its physical value that would be associated with the wanted \mathcal{P}_* . As shown in reference [34], under the rescaling $M/m_{\text{Pl}} \rightarrow sM/m_{\text{Pl}}$, the power spectra become $\mathcal{P}(k) \rightarrow s\mathcal{P}(s^{1/2}k)$. As a result, the value of s required is the ratio $\mathcal{P}_*/\mathcal{P}_\diamond^{(M=1)}$, where $\mathcal{P}_\diamond^{(M=1)}$ is the amplitude of the scalar power spectrum obtained with $M/m_{\text{Pl}} = 1$ and evaluated at $k_\diamond = k_*s^{-1/2}$. In fact, to circumvent such a rescaling on the wavenumbers, it is more convenient to introduce the rescaled reheating parameter R defined by

$$\ln R \equiv \ln R_{\text{rad}} + \frac{1}{4} \ln(\kappa^2 \rho_{\text{strg}}). \quad (121)$$

The quantity R represents an effective energy, in Planck units, at the time of brane merging, which is exactly equal to $\sqrt{\kappa}\rho_{\text{strg}}^{1/4}$ for a radiation-like reheating. The advantage of R with respect to R_{rad} is that, at fixed R , one has $k_\diamond = k_*$ [34]. Finally, as shown in section 5, one may expect some observable effects coming from the situations in which there is violation of the slow-roll conditions before brane annihilation, i.e. according to the value of $\phi_{\text{strg}}/\phi_{\text{e}_2}$. Since ϕ_{e_2} is determined by μ/m_{Pl} only [see equation (61)], we have chosen to perform the MCMC exploration on the parameter ϕ_{strg}/μ instead of ϕ_{strg} .

Finally, the nine MCMC parameters are: $\Omega_{\text{b}}h^2$, $\Omega_{\text{dm}}h^2$, τ , θ on the cosmological side, \mathcal{P}_* , μ/m_{Pl} , ϕ_{UV} , ϕ_{strg}/μ for the primordial parameters and R for the reheating era.

We still have to specify their prior probability distributions according to the theoretical constraints and our best knowledge on their value. For the base cosmological parameters $\Omega_b h^2$, $\Omega_{\text{dm}} h^2$, τ and θ , wide top hat uniform distributions have been chosen centred over their preferred value from the previous analysis of the CMB data [87, 71]. For the primordial parameters, \mathcal{P}_* fixes the amplitude of the cosmological perturbations and we have chosen a uniform prior on the logarithm compatible with the amplitude of the CMB fluctuations:

$$2.7 \leq \ln(10^{10} \mathcal{P}_*) \leq 4.0. \quad (122)$$

The parameter μ/m_{Pl} is related to the underlying String Theory model by equation (23) and we will assume that the order of magnitude of the volume ratio v is not known. As a result, it is natural to also use a uniform prior probability distribution on $\log(\mu/m_{\text{Pl}})$ to ensure its conformal invariance. The same considerations hold for the two other primordial parameters, ϕ_{UV} and ϕ_{strg} , whose dependency with respect to the fundamental string theory parameters is given in equations (19) and (38). Our ignorance on the values of \mathcal{N} , g_s and α' motivates the use of uninformative uniform logarithmic priors. However, the analysis of section 6 imposes various bounds. The maximal size of the throat in equation (35) and the requirement $\mathcal{N} \geq 1$ give the upper limit

$$\log(\sqrt{\kappa} \phi_{\text{UV}}) \leq \log 2. \quad (123)$$

Similarly, the definition (38) of ϕ_{strg} ensures that $\phi_{\text{strg}} \geq \mu$ implying the lower limit

$$\log(\phi_{\text{strg}}/\mu) \geq 0. \quad (124)$$

Since $\phi_{\text{strg}} < \phi_{\text{UV}}$, these conditions impose

$$\log(\sqrt{\kappa} \mu) < \log 2, \quad (125)$$

which will be our upper prior limit for the parameter μ/m_{Pl} . However, we should ensure that there are enough e-folds of inflation to solve the flatness problem and to set the sub-Hubble initial conditions (116) for the observable perturbations. As shown in reference [88], only for some extreme reheating models the values of N_{T} may exceed 10^2 . In order to include all the models, we have implemented a ‘‘hard prior’’ which, during the MCMC exploration, rejects any model that does not support at least 110 e-folds of inflation inside the throat. This is implemented in the following way. Once ϕ_{strg} is known [from $\log(\phi_{\text{strg}}/\mu)$ and $\log(\sqrt{\kappa} \mu)$], one can determine ϕ_{in} such that there are 110 e-folds of inflation in between: the model is accepted if $\phi_{\text{in}} < \phi_{\text{UV}}$ and rejected otherwise. The prior limits on $\ln R$ are determined by requiring that the end of reheating occurs before nucleosynthesis, characterised by ρ_{nuc} , and that the instantaneous equation of state parameter w_{reh} satisfies the strong and dominant energy conditions $-1/3 < w_{\text{reh}} < 1$. Under these assumptions, one gets [34]

$$\frac{1}{4} \ln(\kappa^2 \rho_{\text{nuc}}) < \ln R < -\frac{1}{12} \ln(\kappa^2 \rho_{\text{nuc}}) + \frac{1}{3} \ln(\kappa^2 \rho_{\text{strg}}). \quad (126)$$

This equation clearly involves ρ_{strg} and the upper prior limit on $\ln R$ depends on the other primordial parameters. We have therefore coded another ‘‘hard prior’’ checked

during the MCMC exploration to dismiss any model violating this limit. The energy density ρ_{nuc} at nucleosynthesis time has been quite extremely set around the MeV scale: $\ln R > -46$. Finally, we have to set a lower limit on the $\log(\sqrt{\kappa}\mu)$ prior. According to the values of v , μ/m_{Pl} may be extremely small. Our choice has been motivated by numerical convenience and we have chosen $\log(\sqrt{\kappa}\mu) > -3$. Indeed, it turns out that, for smaller values, one runs into tricky numerical difficulties. The dependency of the results with respect to this choice will be carefully discussed in the following. Notice that the lower limit of the $\log(\sqrt{\kappa}\phi_{\text{UV}})$ prior is implicitly set by the others since $\phi_{\text{UV}} > \phi_{\text{in}}$ and we ensure that there are at least 110 e-folds of inflation in between ϕ_{in} and ϕ_{strg} .

8.3. Data used

As already mentioned, the CMB measurements used are the WMAP third year data [89, 87, 66, 90]. The degeneracies between some cosmological parameters have been reduced by adding the Hubble Space Telescope (HST) constraint $H_0 = 72 \pm 8$ km/s/Mpc [91] and a uniform top hat prior on the age of the universe between 10 Gyrs and 20 Gyrs [71]. The likelihood estimator is provided by the WMAP team[§] and we have used the current 2.2.2 version. Use has been made of the eigenvalue compression option at low multipoles to decrease the computing time. The convergence of the Markov chain simulations has been monitored from the Gelman and Rubin R -test implemented in COSMOMC [92]. The MCMC exploration has been stopped once the ratio of the variance of the means to the mean of the variances between the different chains was less than $R - 1 < 0.2\%$. The total number of samples obtained from this convergence criterion and drawing the posterior distributions is around 1.5 millions. In the following, we present and interpret the posterior marginalised probability distributions for the nine model parameters obtained from the previous priors and data.

8.4. Cosmological parameters

The marginalised posteriors and mean likelihoods of the cosmological parameters and power spectra amplitude are the same than those found in previous analysis of the same data but that were using other primordial power spectra, such as the first and second order slow-roll spectra in reference [34] or the phenomenological power law models in reference [87]. This is expected since these parameters are rather well constrained and supported by the slow-roll analysis of section 7 showing that the KKLMMT model can indeed produce the preferred value of the power spectra amplitude and spectral indices. The best fit model is found with a $\chi^2 \simeq 3538.1$ for nine parameters (or 3517 degrees of freedom after eigenvalue compression). This may be compared with the WMAP power law best fit model having $\chi^2 \simeq 3540.8$ with three parameters less. Although it shows that the KKLMMT model can provide a good fit to the data, it is not currently favoured because of its intrinsic numbers of parameters.

[§] <http://lambda.gsfc.nasa.gov>

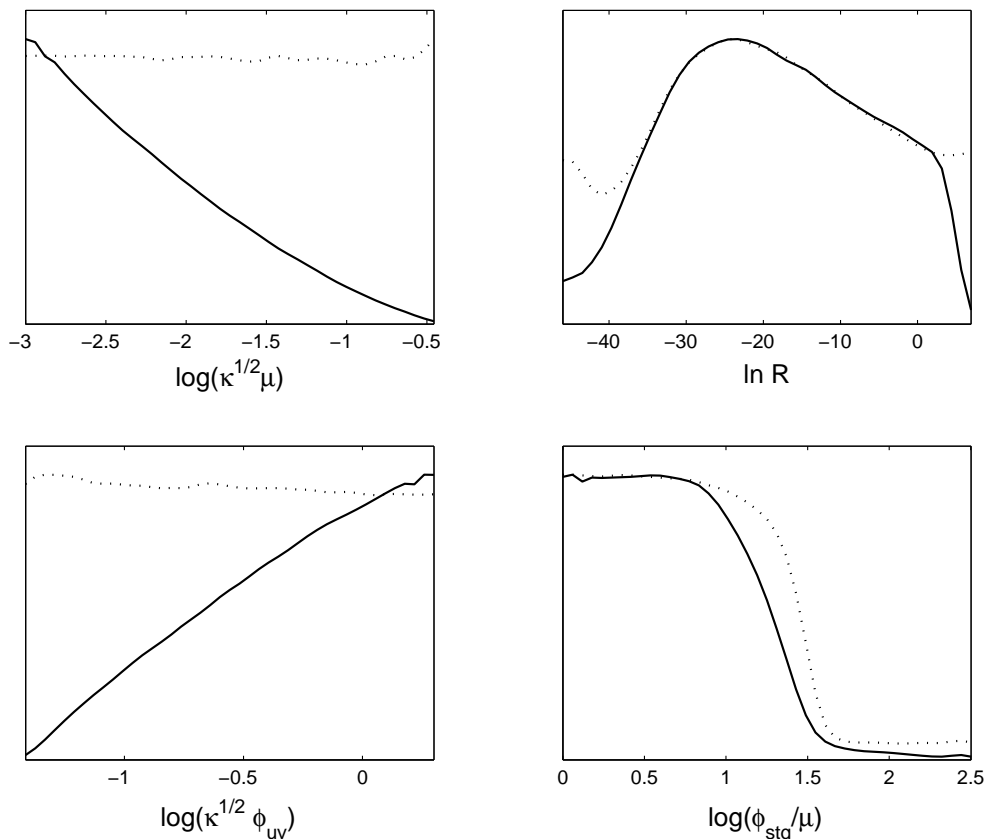


Figure 8. Marginalised posterior probability distributions (solid lines) and mean likelihoods (dotted lines) for the sampled primordial parameters of the Λ CDM–KKLMMT model.

8.5. Primordial parameters

The marginalised posteriors and mean likelihoods for the sampled primordial parameters $\log(\sqrt{\kappa}\mu)$, $\log(\sqrt{\kappa}\phi_{UV})$, $\log(\phi_{\text{strg}}/\mu)$ and $\ln R$ are represented in figure 8. The fact that the mean likelihood (dotted curves) remains uniform for $\log(\sqrt{\kappa}\mu)$ and $\log(\sqrt{\kappa}\phi_{UV})$ shows that, on the prior range explored, these parameters do not help to improve the fit to the data. On the other hand, their probability distributions are not flat and show that large values of μ/m_{Pl} and small values of ϕ_{UV} are strongly disfavoured: $\log(\sqrt{\kappa}\mu) < -1.1$ at 95% confidence level. As discussed in reference [93], discrepancies between the marginalised probability and the mean likelihood occur when “volume effects” are induced by strong correlations between the parameters. The full likelihood in the multi-dimensional parameter space can be uniform along peculiar regions whose volume may be parameter dependent. The shape of the μ/m_{Pl} and ϕ_{UV} probabilities come from the amount of fine tuning required to have a successful model of inflation when μ/m_{Pl} is close to the throat edge. In that case, there is indeed not too much parameter space available for the brane motion since ϕ_{UV} has to saturate its maximal value to allow both $\phi_{\text{strg}} > \mu$ and $\phi_{\text{strg}} < \phi_{\text{in}} < \phi_{UV}$. As a result of these correlations,

the marginalised probabilities for μ/m_{Pl} and ϕ_{UV} penalise the values for which strong fine-tunings are required to satisfy the theoretical priors. Let us mention again that these priors are imposed by the consistency of the model.

On the other hand, the marginalised posteriors and mean likelihoods associated with \mathbf{R} and ϕ_{strg}/μ show that these parameters are directly constrained by the data. Clearly, $\phi_{\text{strg}} \gg \mu$ is disfavoured and at 95% confidence level one has $\log(\phi_{\text{strg}}/\mu) < 1.4$. This result can be understood from section 7. Large values of ϕ_{strg}/μ correspond to models in which brane annihilation occurs well inside the slow-roll regime, i.e. $\phi_{\text{strg}} > \phi_{\epsilon_2}$. As a result, the observable perturbation modes are generated during the brane motion in the flat part of the potential (see figure 2) and both the slow-roll parameters are small: the spectral index is close to $n_s \simeq 1$ while the amplitude of the tensor modes is negligible with respect to the scalar modes. As already mentioned in section 7, this situation is disfavoured by the WMAP data. The upper bound on ϕ_{strg}/μ is in fact slightly dependant on the lower limit of the μ prior due to the presence of some correlations with the other parameters. As discussed in the following, a μ -prior independent upper limit can be more conveniently given for the rescaled parameter $\phi_{\text{strg}}/\mu^{2/3}$ and one gets, at 95% confidence level,

$$\log\left(\frac{\kappa^{1/6}\phi_{\text{strg}}}{\mu^{2/3}}\right) < 0.52. \quad (127)$$

The marginalised probability distribution for the reheating parameter is peaked around $\ln \mathbf{R} \simeq -22$. Its behaviour at large values directly comes from the prior (126) which is a function of ρ_{strg} . As will be discussed in the following, ρ_{strg} is related to the energy scale of inflation which is bounded from above by the amplitude of the cosmological perturbations. Here again, the differences between the marginalised probability and the mean likelihood trace the correlations induced by the prior hypothesis between these two parameters, namely that reheating occurs after inflation. The lower tail of the distribution is driven by the data and falls off till the prior lower bound is saturated at $\ln \mathbf{R} = -46$ (nucleosynthesis limit). This posterior is very similar to the one derived for the small field models in reference [34] where it has been shown that the CMB data were disavouring a low energy scale reheating for these models. In the present case, the $\ln \mathbf{R}$ posterior of figure 8 does not fall-off to zero in its lower part but still yields a limit

$$\ln \mathbf{R} > -38, \quad (128)$$

at a 95% confidence level.

The physical interpretation of this limit comes from the influence of \mathbf{R} on N_* , the e-fold at which an observable perturbation mode with wavenumber k_* crossed the Hubble radius during inflation. Indeed, one has $a_*/a_0 = a_*/a_{\text{strg}} \times a_{\text{strg}}/a_0$, with, by definition, $a_*/a_0 \simeq k_*/(a_0\kappa^{1/2}V_*^{1/2})$, where we have expressed the Hubble parameter in terms of the potential. The quantity a_*/a_{strg} can be expressed in terms of N_* and $a_{\text{strg}}/a_0 = (1 + z_{\text{strg}})^{-1}$ is given by equations (119), (120) and (121), expressing ρ_{strg} in

terms of the potential evaluated at ϕ_{strg} . One gets [34]

$$N_* \simeq 58 - \ln \left[\frac{k_*}{a_0} (\text{Mpc}^{-1}) \right] + \ln R + \frac{1}{2} \ln \frac{V_*}{V_{\text{strg}}}. \quad (129)$$

As shown in section 7, since the WMAP data prefer a slightly red-tilted spectral index in the absence of tensor modes, it is not surprising that, for a given model of inflation, some values of N_* , and therefore R , end up being favoured. This interpretation can be further explored by using the slow-roll approximation. As already mentioned, the KKLMPT model generically leads to observable ϵ_1 values much smaller than ϵ_2 . Let us first determine N_* such that $\epsilon_2(\phi_*) = \epsilon_{2\text{obs}}$, where $\phi_* = \phi(N_*)$ and $\epsilon_{2\text{obs}} \simeq 0.05$ is the preferred observed value (see figure 7). Using the classical trajectory given by equation (51), one finds that

$$N_* \simeq \frac{\kappa\mu^2}{24} \left[\left(\frac{\phi_*}{\mu} \right)^6 - \left(\frac{\phi_{\text{end}}}{\mu} \right)^6 \right], \quad (130)$$

and using the expression of the second horizon flow parameter (50), one arrives at

$$\epsilon_2 \simeq \frac{40}{\kappa\mu^2} \left(\frac{\phi_*}{\mu} \right)^{-6}. \quad (131)$$

Combining these two last equations, one obtains

$$N_* = \frac{5}{3\epsilon_{2\text{obs}}} \left[1 - \frac{\kappa\mu^2\epsilon_{2\text{obs}}}{40} \left(\frac{\phi_{\text{end}}}{\mu} \right)^6 \right]. \quad (132)$$

As already discussed, if the slow-roll is violated before brane annihilation, we can use the slow-roll trajectory with the approximation $\phi_{\text{end}} \simeq \phi_{\epsilon_2} = [40/(\kappa\mu^2)]^{1/6}$, from which one deduces that

$$N_* \simeq \frac{5}{3\epsilon_{2\text{obs}}}. \quad (133)$$

Inserting this value into formula (129) with $k_*/a_0 \simeq 0.05 \text{ Mpc}^{-1}$ and neglecting the potential term gives $\ln R \simeq -28$. This is the preferred value of $\ln R$ that would give an observable spectral index at k_* compatible with the favoured value and in agreement with the shape of the marginalised posterior of figure 8. Let us notice that the two-sigma limit (128) is the best that can be extracted from the data. Indeed, the three-sigma lower limit matches the nucleosynthesis prior bound. This differs from the results obtained in reference [34] for the small field models and is due to the marginalised posterior which does not vanish for low value of $\ln R$. Moreover, the mean likelihood appears to increase again in that region. This effect comes from correlations between parameters and suggests that some, but quite fine-tuned, models provide a good fit to the data even for $\ln R$ small. To understand this property, we have represented in figure 9 the two-dimensional marginalised posterior and mean likelihood in the plane $[\ln R, \log(\phi_{\text{strg}}/\mu)]$ (left panel). One recovers the favoured value for $\ln R \simeq -22$ as the central vertical broad region (one-sigma contour), and as shown above, this domain is associated with the models in which slow-roll inflation ends before the branes collide. The two-sigma contour extends towards the left side of the plot but only for $1 < \log(\phi_{\text{strg}}/\mu) < 1.5$.

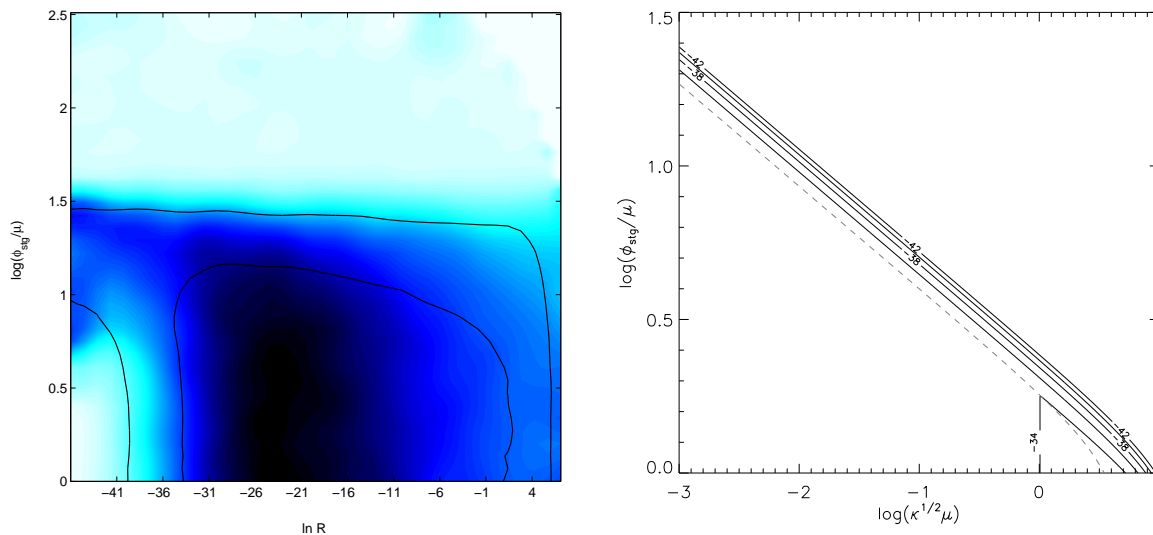


Figure 9. The left panel shows the one- and two-sigma confidence intervals of the two-dimensional marginalised posterior as a function of the parameters $\ln R$ and $\log(\phi_{\text{strg}}/\mu)$. The shading traces the corresponding two-dimensional mean likelihood. The right panel is a contour plot of $\ln R$ as a function of $\log(\sqrt{\kappa}\mu)$ and $\log(\phi_{\text{strg}}/\mu)$ obtained from the slow-roll approximation by assuming that $\epsilon_2 = \epsilon_{2\text{obs}} \simeq 0.05$. The dashed line marks the limit $\phi_{\text{strg}} = \phi_{\epsilon_2}$. This plot shows that, although $\phi_{\text{strg}} > \mu$ is generically disfavoured (see figure 8), it is still possible to obtain a good fit to the data provided some fine tuning is performed between ϕ_{strg}/μ , μ/m_{Pl} and $\ln R$: a low energy reheating allows for some models where brane annihilation occurs before slow-roll violation to have red-tilted power spectra.

This tail is associated with the models in which brane annihilation occurs before the slow-roll conditions are violated. To see why such models are not disfavoured we can still use equations (129) and (132) but, now, with $\phi_{\text{end}} = \phi_{\text{strg}}$ to get

$$\ln R \simeq -61 + \frac{5}{3\epsilon_{2\text{obs}}} \left[1 - \frac{\kappa\mu^2\epsilon_{2\text{obs}}}{40} \left(\frac{\phi_{\text{strg}}}{\mu} \right)^6 \right]. \quad (134)$$

The $\ln R$ contour plot coming from this function is represented on the right panel of figure 9 for different values of ϕ_{strg} and μ/m_{Pl} . One sees that it is indeed possible to get $\epsilon_{2\text{obs}} \simeq 0.05$ for $\phi_{\text{strg}} > \phi_{\epsilon_2}$ provided $\ln R \simeq -40$, in agreement with the plot. The physical interpretation is that a low energy reheating allows the observable window of wavenumbers to be shifted towards the end of brane evolution in such a way that, although brane annihilation occurs before violation of the slow-roll conditions, it is possible to get not so small values for ϵ_2 . Of course, this requires some amount of fine tuning between $\ln R$, μ/m_{Pl} and ϕ_{strg} , which is statistically penalised and explains why these models are out of the one-sigma contour.

8.6. Derived primordial parameters

As described in section 8.1, the Markov chains have been performed on the power spectra amplitude \mathcal{P}_* and its posterior probability distribution is plotted in figure 8. Since \mathcal{P}_* and M/m_{Pl} are in direct relation (see section 8.2), it is possible to derive the marginalised probability distribution of M/m_{Pl} from the one of \mathcal{P}_* . The same considerations apply to the volume ratio v which is given by equation (24): using importance sampling, one can extract its posterior distribution from the one of μ/m_{Pl} and M/m_{Pl} [71]. Both probability distributions are plotted in figure 10 and seem to favour some peculiar values of M/m_{Pl} and v . Once again, the discrepancies between the posteriors and the mean likelihoods come from the correlations with other parameters and may hide some effects coming from the priors. The right panel of figure 10 represents the two-dimensional probability distribution (point density), as well as its one- and two-sigma confidence level regions, obtained without marginalising over the parameter $\log(\sqrt{\kappa}\mu)$. As can be seen on these plots, the narrow highly probable regions trace the strong correlations between M/m_{Pl} and μ/m_{Pl} , and between v and μ/m_{Pl} . Remembering that the lower limit on the μ/m_{Pl} parameter comes from our numerically convenient prior $\sqrt{\kappa}\mu > 10^{-3}$, one immediately sees that this choice has a direct influence on the upper limit, and respectively the lower limit, of the $\log(4\pi^2v)$ and $\log(\sqrt{\kappa}M)$ probability distributions. If we had chosen a smaller limit for μ/m_{Pl} , the v posterior would have been shifted towards larger values, whereas the M/m_{Pl} one towards the smaller. As a result, we conclude that there is no upper, respectively lower, constraints on v and M/m_{Pl} .

The same correlations are at work for the other tails of the probability distribution associated with v and M/m_{Pl} . However, this time, we are probing the highest allowed values for μ/m_{Pl} which are disfavoured due to the amount of fine-tuning required for a successful inflation nearby the throat edge (see previous section). As a result, we obtain the 95% confidence levels

$$\log(\sqrt{\kappa}M) < -2.9, \quad \log(4\pi^2v) > -8.5. \quad (135)$$

Let us stress that these bounds come from both the data and the requirement that inflation proceeds inside the throat, as imposed by the self-consistency of the model used.

To understand how the data lead to the correlations observed between the parameters μ/m_{Pl} , M/m_{Pl} and v , we have plotted in figure 11 the one- and two-sigma contours (solid curves) of the two-dimensional posteriors associated with various pairs of primordial parameters. The corresponding two-dimensional mean likelihood is traced by the shaded areas. The highly probable region spanning the plane $[\log(\sqrt{\kappa}M), \log(\sqrt{\kappa}\mu)]$ directly comes from the constraints on the power spectrum amplitude and spectral index. This can be shown by using the slow-roll approximations. Indeed, if one assumes that the slow-roll conditions are violated before brane annihilation, namely $\phi_{\text{strg}} < \phi_{\epsilon_2}$, then the WMAP normalisation through equations (68) and (69) leads to

$$\log(\sqrt{\kappa}M) = \log \left[\left(45 \frac{Q_{\text{rms-PS}}^2}{T^2} \right)^{1/4} (6N_* + 10)^{-5/12} (4\pi^2)^{1/12} (8\pi)^{1/3} \right]$$

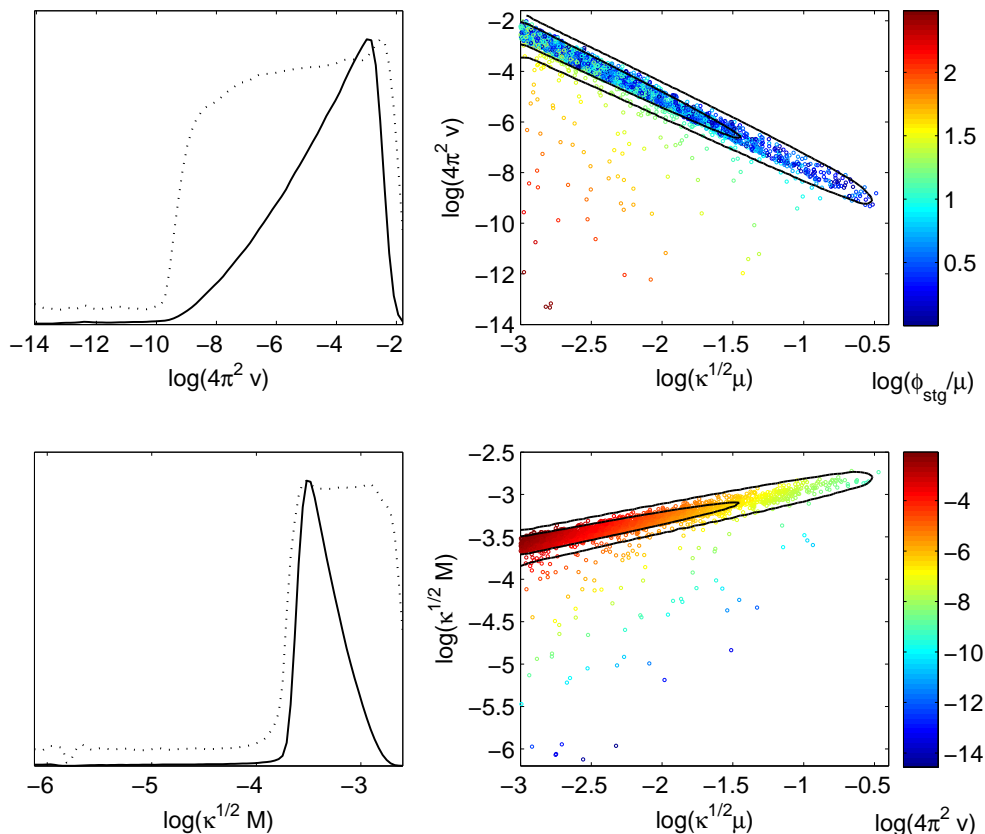


Figure 10. Marginalised posterior probability distributions for the M/m_{Pl} and v parameters (solid curves) and their associated mean likelihoods (dotted curves). The right panel shows the corresponding one- and two-sigma contour of the two-dimensional posteriors obtained without marginalising over $\log(\sqrt{\kappa}\mu)$. The two-dimensional probability is proportional to the point density while the colormap traces correlations with a third parameter.

$$+ \frac{1}{3} \log(\sqrt{\kappa}\mu). \quad (136)$$

This is a straight line with slope equal to $1/3$, exactly as observed for the high probable regions in figure 11. Using a fiducial value for the quadrupole and $N_* = 50$, the offset is around -2.6 . Consequently, for $\log(\sqrt{\kappa}\mu) \simeq -3$ one gets $\log(\sqrt{\kappa}M) \simeq -3.6$, as confirmed by the plot. The effect of the spectral index is indirect and, as previously discussed, tends to favour the models in which $\phi_{\text{strg}} < \phi_{\epsilon_2}$. This suggests that the less probable and wider shaded region in the plane $[\log(\sqrt{\kappa}M), \log(\sqrt{\kappa}\mu)]$ corresponds to the cases where $\phi_{\text{strg}} > \phi_{\epsilon_2}$. Again, the slow-roll approximation in this limit gives the relation

$$\left(\frac{M}{m_{\text{Pl}}}\right)^6 \simeq 45 \frac{Q_{\text{rms-PS}}^2}{T^2} v^{1/2} \left(\frac{\phi_{\text{strg}}}{\mu}\right)^{-10}. \quad (137)$$

Since v is also a function of M/m_{Pl} and μ/m_{Pl} , this is a three parameters relation, or a surface in the plane $[\log(\sqrt{\kappa}M), \log(\sqrt{\kappa}\mu)]$. We can, however, derive the slope

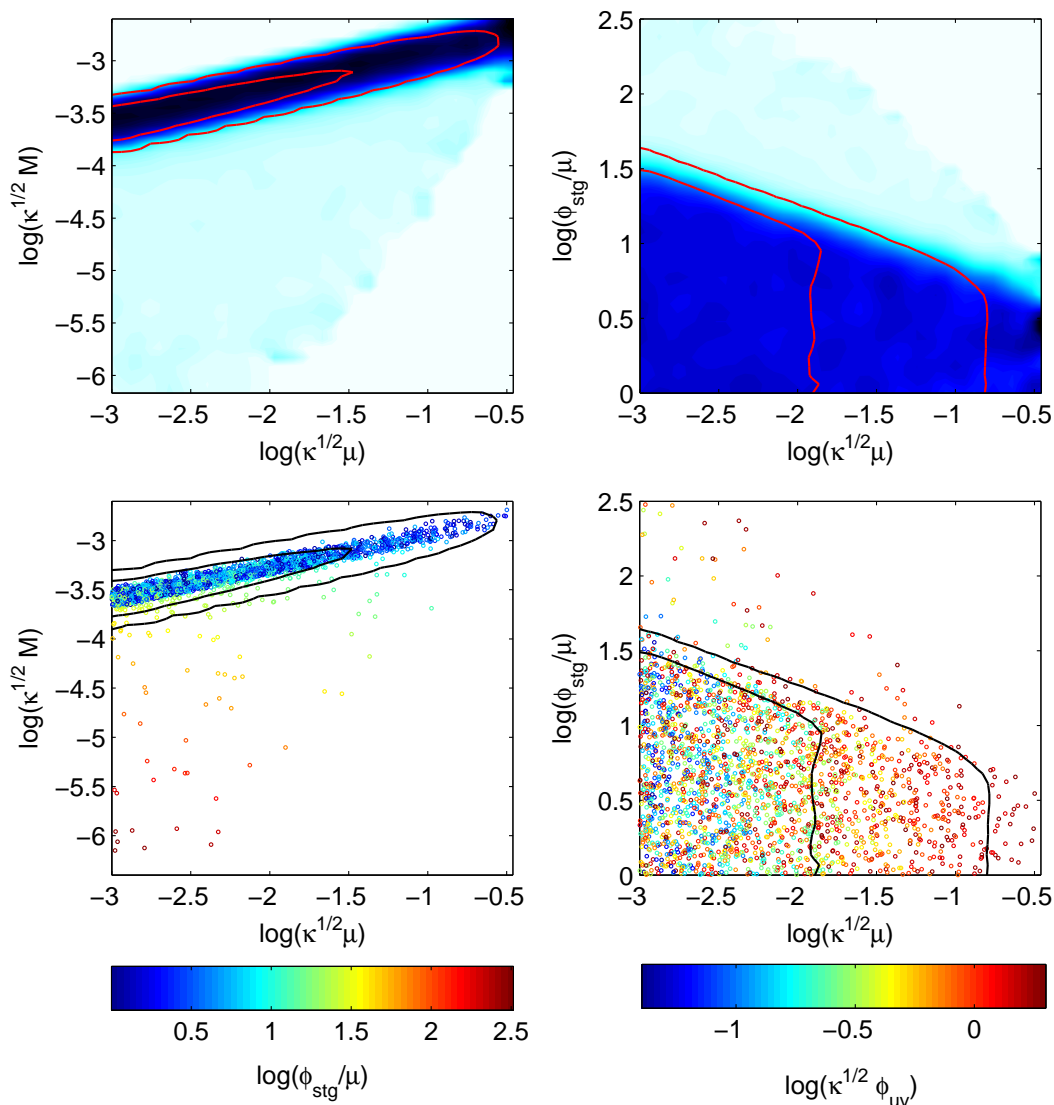


Figure 11. One- and two-sigma contours (solid curves) of the two-dimensional marginalised probability distribution for various pairs of the primordial parameters. The two-dimensional mean likelihood is traced by the shading intensity. The bottom panels show the two-dimensional posterior (point density) and its correlation with a third parameter (colorbar).

associated with the lower boundary of the blurred region (beyond which there is no acceptable models). This boundary is reached for the largest ϕ_{strg} compatible with the throat size, i.e. for $\phi_{\text{in, strg}} = \max(\phi_{\text{UV}}) = m_{\text{Pl}}/\sqrt{2\pi}$ [see equation (35)]. This limit is reached when the ratio of throat to bulk volume is maximal. Using the expression of $\phi_{\text{in, strg}}$ given by equation (94) and solving for ϕ_{strg} leads to

$$\frac{\phi_{\text{strg}}}{\mu} = \left[\left(\frac{m_{\text{Pl}}}{\sqrt{2\pi}\mu} \right)^6 - \frac{3N_{\text{T}}}{\pi} \left(\frac{m_{\text{Pl}}}{\mu} \right)^2 \right]^{1/6}. \quad (138)$$

This expression can now be inserted into equation (137) and one gets

$$\begin{aligned} \log(\sqrt{\kappa}M) &\simeq \log \left[\left(45 \frac{Q_{\text{rms-PS}}^2}{T^2} \right)^{1/4} 4\sqrt{\pi} \right] - \frac{1}{2} \log(\sqrt{\kappa}\mu) \\ &\quad - \frac{5}{12} \log \left[\frac{64}{(\sqrt{\kappa}\mu)^6} - \frac{24N_{\text{T}}}{\sqrt{\kappa}\mu} \right]. \end{aligned} \quad (139)$$

For not too large values of $\sqrt{\kappa}\mu$ (in practice $\sqrt{\kappa}\mu \lesssim 0.1$), the term proportional to N_{T} can be neglected and one obtains

$$\begin{aligned} \log(\sqrt{\kappa}M) &\simeq \log \left[\left(45 \frac{Q_{\text{rms-PS}}^2}{T^2} \right)^{1/4} 4\sqrt{\pi} \right] - \frac{5}{12} \log(64) \\ &\quad + 2 \log(\sqrt{\kappa}\mu). \end{aligned} \quad (140)$$

This is a straight line in the plane $[\log(\sqrt{\kappa}M), \log(\sqrt{\kappa}\mu)]$ the slope of which is +2: this matches with the observed lower boundary of the blurred region in figure 11. The offset is around -2.1 giving $\log(\sqrt{\kappa}M) \simeq -4.1$ for $\log(\sqrt{\kappa}\mu) \simeq -1$, again in agreement with the figure. One might also notice that the boundary curve in figure 11 slightly bends over for small values of μ/m_{Pl} as the effects of the terms proportional to N_{T} start to appear. The previous interpretation is confirmed by the left bottom panel of figure 11. The point density clearly decreases in the domain of low likelihood which appears blurred in the upper left panel. As traced by the colormap, this region indeed corresponds to large value of ϕ_{strg}/μ . Let us notice that, although this region is out of the 95% confidence contour, it remains inside the three-sigma one.

The previous discussion also applies to the right plots of figure 10. The above-described relations between M/m_{Pl} , μ/m_{Pl} and ϕ_{strg} are directly converted into correlations between v and the other parameters through equation (24). As a result, the main degeneracy seen in the plane $[\log(\sqrt{\kappa}\mu), \log(4\pi^2v)]$ is also a consequence of both the power spectra normalisation and spectral index constraints. The bottom right panel illustrates the degeneracy between M/m_{Pl} and μ/m_{Pl} coming from the data and differs from the one associated with equation (24): this difference explains the two-sigma lower limit on $\log(4\pi^2v)$. Let us elaborate on this point. The limit on v can be understood from the slow-roll result even if, at first sight, there is a mismatch between the constraint obtained above and equation (111). In fact, equation (105) implies

$$\log(4\pi^2v) \simeq -\frac{8}{3} \log(\sqrt{\kappa}\mu) - 9. \quad (141)$$

This relation is consistent with the top right panel in figure 10. Let us notice that, in this context, it is relevant to use equation (105), which is derived under the assumption that inflation stops by violation of the slow-roll conditions, since one observes in figure 10 that the two-sigma contour corresponds to “small” values of ϕ_{strg} . Moreover, if one inserts the limit (89), namely $\sqrt{\kappa}\mu < 2$, in the above relation then the constraint (135) is reproduced. This constraint is different from equation (111) because it has a different origin. The limit (111) assumes that the maximum allowed contribution of tensor modes to the observed CMB data can indeed be generated during KKLMMT

inflation. However, the requirement that the brane motion proceeds inside the throat strongly limits the generation of tensor modes and leads to the stronger bound of equation (135). Therefore, the two limits are consistent and the stronger bound is given by equation (135).

Finally, we have plotted in the right hand panels of figure 11 the two-dimensional probability distribution and mean likelihood in the plane $[\log(\sqrt{\kappa}\mu), \log(\phi_{\text{strg}}/\mu)]$, as well as the effect of ϕ_{UV} . These plots exhibit the volume effects associated with the large values of the parameter μ/m_{Pl} . Clearly, the allowed range of both ϕ_{strg}/μ and ϕ_{UV} are all the more reduced as μ/m_{Pl} increases, thereby decreasing the statistical weight of these domains in the marginalised posterior of μ/m_{Pl} (see figure 8). The two-sigma contours are found to follow the high likelihood region, and as before, it corresponds to models in which brane annihilation occurs after violation of the slow-roll conditions ($\phi_{\text{strg}} < \phi_{\epsilon_2}$). Indeed, the edge between the dark and the blurred regions is just given by the equation $\phi_{\text{strg}} = \phi_{\epsilon_2}$. Using equation (61), which gives ϕ_{ϵ_2} when $\sqrt{\kappa}\mu$ is small, one gets

$$\log\left(\frac{\phi_{\text{strg}}}{\mu}\right) \simeq \frac{1}{6}\log(40) - \frac{1}{3}\log(\sqrt{\kappa}\mu). \quad (142)$$

This is a straight line in the plane $[\log(\sqrt{\kappa}\mu), \log(\phi_{\text{strg}}/\mu)]$ with a $-1/3$ slope, as observed in the figure. The offset is close to 0.3 implying that for $\log(\sqrt{\kappa}\mu) = -3$ one would have $\log(\phi_{\text{strg}}/\mu) \sim 1.3$. There is a slight difference since the contour seems to intercept the vertical axis at $\log(\phi_{\text{strg}}/\mu) \sim 1.5$. Such a difference may be due to the fact that ϕ_{strg} must significantly deviate from ϕ_{ϵ_2} for the effect to be visible. Moreover, the reheating effects already mentioned are not considered in the derivation of equation (142). Equation (142) renders explicit the μ -prior dependence previously noted on the upper two-sigma limit associated with the marginalised probability distribution of ϕ_{strg}/μ (see figure 8). The $-1/3$ slope explains why the prior independent limit of equation (127) is more conveniently express in terms of $\phi/\mu^{2/3}$. Finally, the upper edge of the blurred region is, as before, given by the condition $\phi_{\text{in, strg}} = \max(\phi_{\text{UV}})$ (see lower right panel of figure 11). Using equation (138), one finds

$$\log\left(\frac{\phi_{\text{strg}}}{\mu}\right) \simeq \log(2) - \log(\sqrt{\kappa}\mu). \quad (143)$$

Again, one can check that the slope and the offset are consistent with what is observed in figure 11. Beyond that limit, inflation would not take place in the throat and those models are rejected.

8.7. Fundamental parameters

Our choice of MCMC parameters is minimal as far as observable effects are concerned. The cosmological consequences of the KKLMNT model are described by the set of four parameters $(M, \mu, \phi_{\text{strg}}, \phi_{\text{UV}})$ whereas, as discussed in section 2.5, the underlying string theory model involves five parameters: $(g_s, \alpha', M, v, \mathcal{N})$. As a result, it is impossible without additional assumption to extract more information for the string parameters.

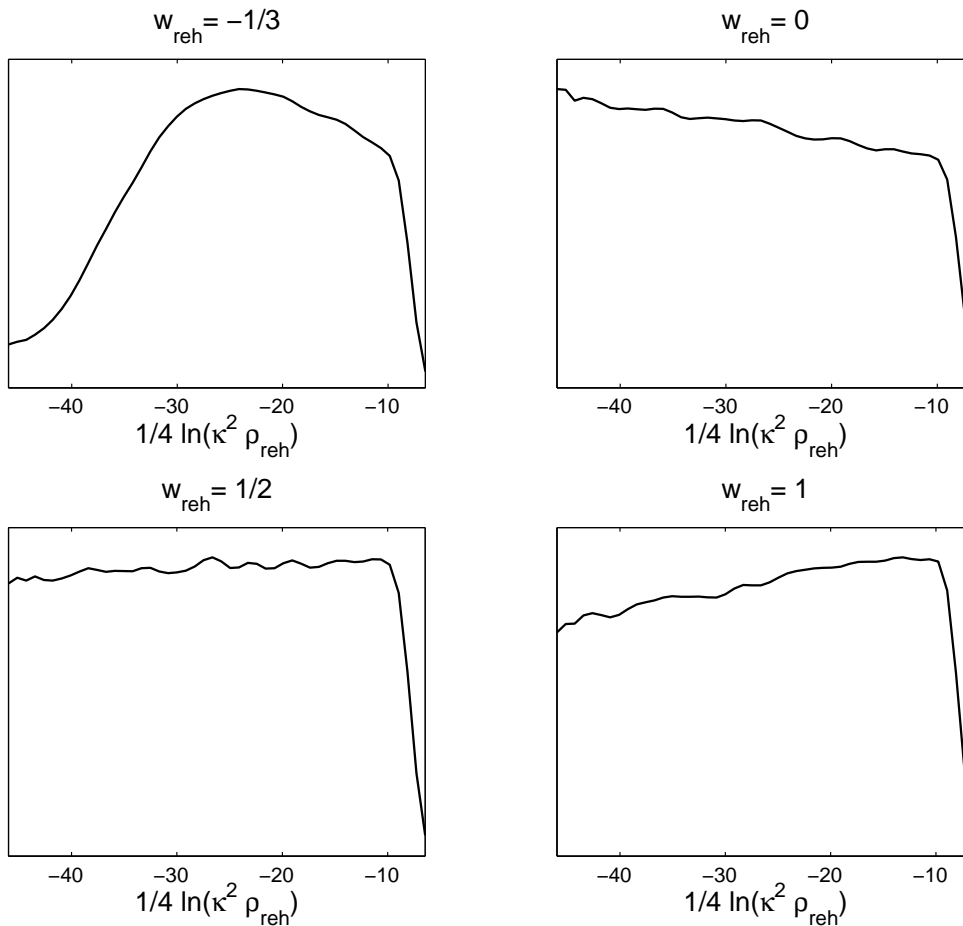


Figure 12. Marginalised probability distributions on the reheating energy scale derived from the WMAP data under the assumption that the reheating proceeds with a constant equation of state: $P = w_{\text{reh}}\rho$. For an extreme equation of state $w_{\text{reh}} \gtrsim -1/3$, one finds a weak (non-trivial) lower bound $\rho_{\text{reh}}^{1/4} > 20$ GeV at two-sigma level. For all the other cases, the reheating can occur at any energy scale higher than nucleosynthesis (from the CMB point of view).

As found in the previous section, the CMB data, however, allow some constraints to be derived for the M/m_{Pl} and v parameters. Their probability distributions do not assume anything on the value of g_s , α' or \mathcal{N} (apart from consistency requirements) and are also robust against the reheating as long as it can be described by our phenomenological model. If one wants to go further on the fundamental theory parameters, additional assumptions have to be made. In the following, such a step is performed first on the reheating model by assuming that it proceeds with a constant equation of state $P = w_{\text{reh}}\rho$. Then, a similar approach is adopted to derive some posterior probability distributions on the remaining string parameters by assuming that the value of α' is known. As a working example, $\alpha' = 10^3 m_{\text{Pl}}^{-2}$ and $\alpha' = 10^5 m_{\text{Pl}}^{-2}$ are considered.

For a constant equation of state parameter during reheating, $\rho \propto a^{-3(1+w_{\text{reh}})}$ and

equation (121) can be further simplified into

$$\ln R = \frac{1 - 3w_{\text{reh}}}{12 + 12w_{\text{reh}}} \ln(\kappa^2 \rho_{\text{reh}}) + \frac{1 + 3w_{\text{reh}}}{6 + 6w_{\text{reh}}} \ln(\kappa^2 \rho_{\text{strg}}). \quad (144)$$

From the MCMC analysis performed in the previous section, samples on R and ρ_{strg} can be used to extract by importance sampling the probability distribution associated with ρ_{reh} (the prior choice remains that the reheating occurs before nucleosynthesis). The resulting posteriors are plotted in figure 12 for four values of w_{reh} spanning the range allowed by the dominant and strong energy conditions in General Relativity. For an extreme equation of state with $w_{\text{reh}} \gtrsim -1/3$, i.e. which is on the verge of an accelerated expansion, one has the 95% confidence limit

$$\rho_{\text{reh}}^{1/4} > 20 \text{ GeV}. \quad (145)$$

Although this kind of models are certainly already ruled out by particle physics experiments, let us notice that this limit comes from CMB data only. As can be seen in figure 12, all the other cases associated with more reasonable values of the equation of state parameter are not constrained.

A similar method has been applied to the parameters g_s and \mathcal{N} by assuming that the value of α' is known. In figure 13, we have plotted the two-dimensional marginalised probability distributions, as well as their one- and two-sigma contours, in the plane $(\log \mathcal{N}, \log g_s)$ and for the two fiducial values of α' . As can be seen on these plots (right panels), there is basically no constraint coming from the data for the case $\alpha' = 10^3 m_{\text{Pl}}^{-2}$. Indeed, on one hand, the two-dimensional posterior is limited by the consistency conditions $\mathcal{N} \geq 1$ and $g_s < 1$ to satisfy flux quantisation and perturbative treatment. On the other hand, the colorbar shows that the two-sigma contour simply traces the high values of v which have been shown in section 8.6 to be essentially related to our lower prior on μ/m_{Pl} . The case $\alpha' = 10^5 m_{\text{Pl}}^{-2}$ is slightly different. As can be seen in the lower right panel of figure 13, the two-sigma contour is detached from the axes and therefore the data give slightly more information than the prior consistency limit. Again, the right end of the contour is not physical since it comes only from our μ/m_{Pl} prior, as before. However, the observed degeneracy between $\log \mathcal{N}$ and $\log g_s$ is a non-trivial information. It means that for a given flux number, a value of g_s is favoured by the data. We have not represented any one-dimensional posterior for g_s or \mathcal{N} since there is typically no more information than the above-mentioned degeneracy. To do so, another assumption would have to be made, such as some prior knowledge on the flux number or on the coupling constant. On the left panels of figure 13, we have plotted the corresponding two-dimensional posteriors in the plane $\{\ln(4\pi g_s \mathcal{N}/v), \ln[v/(4\pi g_s)^2]\}$ to allow a comparison with the slow-roll results of section 6 (see also figure 5). As expected, all the models lie in the range predicted by the slow-roll analysis, up to the prior limit fixed by the numerically convenient lower limit on μ/m_{Pl} . The associated g_s values are traced by the colormap.

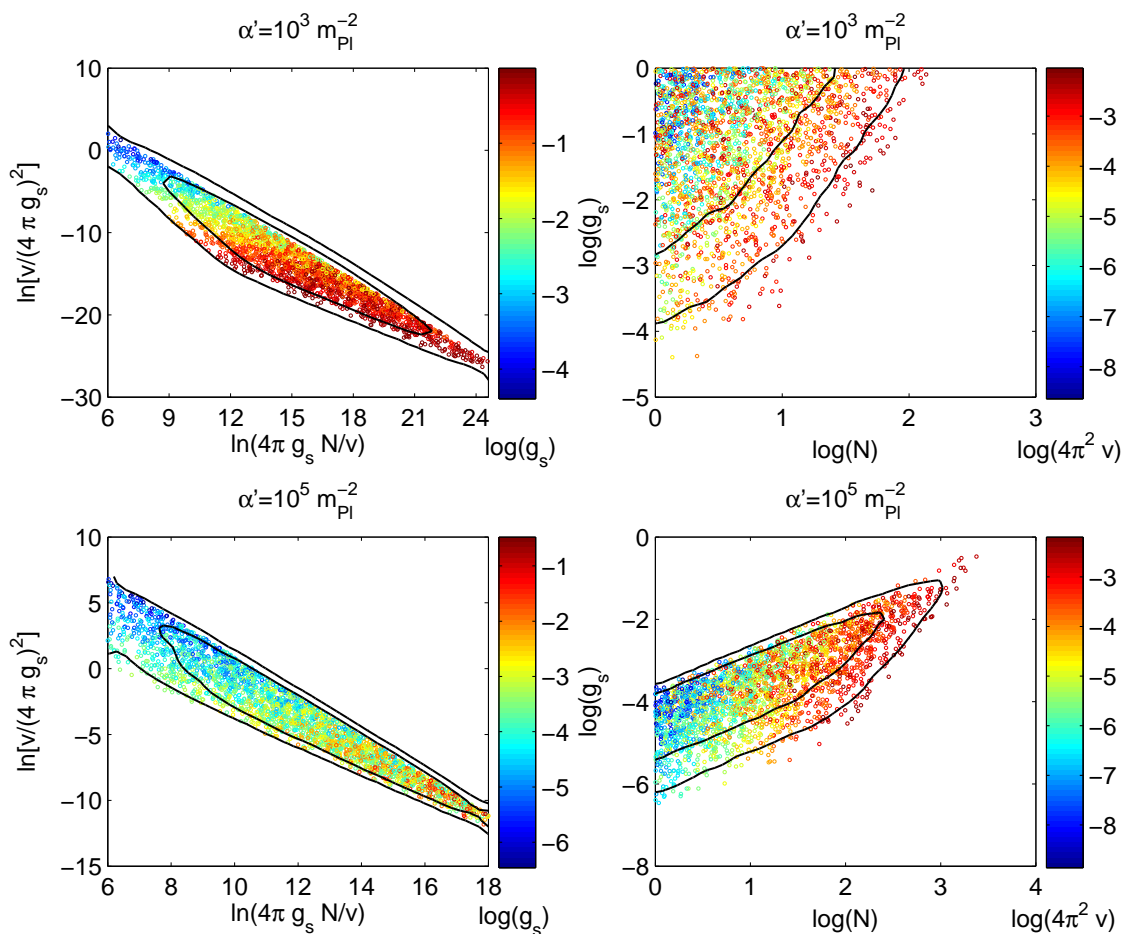


Figure 13. Two-dimensional posteriors of the string parameters and their one- and two-sigma contours obtained by importance sampling for two fiducial values of α' : $\alpha' = 10^3 m_{\text{Pl}}^{-2}$ and $\alpha' = 10^5 m_{\text{Pl}}^{-2}$. Correlations with a third parameter are traced by the colormap. The CMB data give some non-trivial constraints only for large values of α' . This appears as the degeneracy observed between \mathcal{N} and g_s in the bottom right panel. The left panels show that the models lie in the regions predicted by the slow-roll analysis in section 6.

9. Conclusions

To conclude, let us summarise and discuss the main results obtained in this article. Our goal was to compare a typical model of string-inspired brane inflation to the CMB data. In this scenario, the inflaton field is interpreted as the distance between two branes moving in six dimensions along a warped throat. The end of inflation either occurs by violation of the slow-roll conditions or by tachyonic instability at brane annihilation. Our MCMC analysis was carried out by using an exact numerical approach in which the only approximation used is the linear theory of cosmological perturbations. Moreover, various effects have been considered as, for instance, the presence of a DBI kinetic term or the possible quantum effects. The MCMC exploration has also been performed for

arbitrary values of g_s and α' .

From this analysis, we have obtained the following results. Firstly, the WMAP data favour a scenario where inflation ends by violation of the slow-roll conditions before brane annihilation rather than by the tachyonic instability brought about by the annihilation. In other words, ϕ_{strg} cannot be too close to the edge of the throat and one finds

$$\log \left(\frac{\kappa^{1/6} \phi_{\text{strg}}}{\mu^{2/3}} \right) < 0.52, \quad (146)$$

at 95% confidence level. This constraint originates from the fact that ending inflation by instability pushes the spectral index towards one while preserving a low level of gravitational waves, a situation which is disfavoured by the data.

Secondly, one has obtained a limit on v , the volume ratio of the five-dimensional sub-manifold forming the basis of the six-dimensional conifold to the volume of the five-sphere. This limit reads

$$\log v > -10, \quad (147)$$

at 95% confidence level. This constraint comes both from the data and a requirement of self-consistency of the model, namely that inflation proceeds inside the throat.

Thirdly, we find that the reheating period is slightly constrained. Although we have not considered the detailed process of brane annihilation, the total number of e-folds for which the universe reheats may change the part of the inflaton potential probed by the observations. Combined with the power spectra generated during brane inflation, the WMAP data provide the 95% confidence limit

$$\ln R > -38. \quad (148)$$

In the case where the reheating proceeds with a constant equation of state parameter, we find that if $w_{\text{reh}} \gtrsim -1/3$ then $\rho_{\text{reh}}^{1/4} > 20\text{GeV}$ (at two-sigma). This limit is certainly already ruled out by particle physics experiments, but it is worth recalling that it has been obtained from the CMB data only. With more accurate data, it will certainly be possible to improve this bound, and hopefully for other values of the equation of state parameter.

Fourthly, on the theoretical side, we have obtained approximate solutions in the case where the DBI kinetic term does not reduce to the standard one. The regime where the initial conditions are such that the quantum effects are important has also been considered in detail, see Appendix A. In this case, using a perturbative treatment, we have computed how the trajectory (with or without volume effects) can deviate from the classical motion. We have also shown that this approximative scheme breaks down when the brane approaches the bottom of the throat. In this regime, only a numerical integration of the Langevin equation could allow us to go further and, for instance, to see whether the field really starts to climb the potential as indicated by the calculation presented in the appendix. Clearly, this discussion is relevant in order to know whether a regime of eternal inflation can be established in this model.

Finally, let us discuss how the present work could be improved. Recently, various works have been devoted to the type of model studied here. In particular, special attention has been paid to the general set up and exactly calculable corrections to the potential (13) have been proposed. It was also shown that, in some situations, these corrections play a crucial role [24, 25, 26, 27, 28]. The next step would therefore be to include them in our analysis. Since they introduce new parameters into the problem, and given the weakness of the constraints obtained here, this would probably be meaningful only at the expense of including other more accurate data sets to break the degeneracies. Time dependent KS-like compactifications have also been discussed in the literature to provide a late-time acceleration of the universe [94, 95]. These models may provide an alternative to the standard Λ CDM universe we have considered at low energy. Concerning the approach of the present paper, more precise data would certainly help to disentangle the correlations between \mathcal{N} and g_s , and might therefore allow to use astrophysical data to constrain String Theory, at least under the strong theoretical prejudice that the relevant model of inflation is indeed the one described here.

Acknowledgments

It is a pleasure to thank Philippe Brax and Dan Israël for helpful discussions and careful reading of the manuscript. We wish to thank Andrew Frey for useful clarifications. The computations have been performed at the Institut du Développement des Ressources en Informatique Scientifique^{||} and at the French Data Processing Center for Planck-HFI[¶] hosted in the Institut d’Astrophysique de Paris. This work is partially supported by the Belgian Federal Office for Scientific, Technical and Cultural Affairs, under the Inter-University Attraction Pole grant P6/11. LL acknowledges financial support through a DAAD PhD scholarship.

Appendix A. Stochastic inflation

Appendix A.1. Regime of quantum fluctuations within the throat

We previously stated (section 2.6) that all e-folds of inflation should occur within a single throat and hence $\phi < \phi_{UV}$ always, ϕ_{UV} being the field value at the edge of the throat. In section 3, we further calculated the field value ϕ_{fluct} above which quantum fluctuations have an impact on the classical trajectory. It seems reasonable to ask under which conditions, if any, the field value ϕ_{fluct} is located within the throat and hence stochastic inflation effects can, at least in principle, affect the field evolution. Let us try to derive the parameter restriction resulting from

$$\phi_{\text{fluct}} < \phi_{UV}. \tag{A.1}$$

^{||} <http://www.idris.fr>

[¶] <http://www.planck.fr>

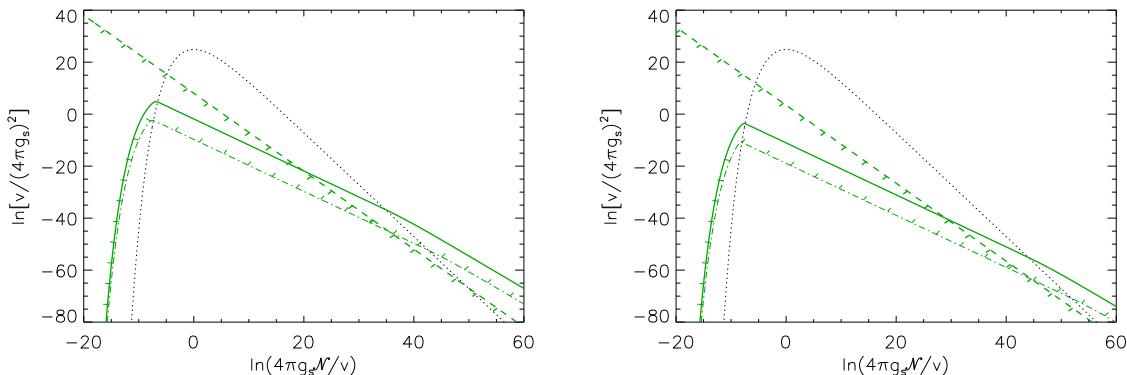


Figure A1. The panels illustrate the parameter regions allowing the stochastic regime to take place inside the throat, for $\alpha' m_{\text{Pl}}^2 = 1000$ (left panel) and $\alpha' m_{\text{Pl}}^2 = 10$ (right panel). All curves are the same as in figure 5, but in addition a solid green curve illustrates the condition $\phi_{\text{fluct}} = \phi_{\text{UV}}$. Stochastic inflation may occur inside the throat only for the parameter values lying above the solid green curve, and below the volume constraint (dashed green curve with ticks down).

Again, it will be important to decide which normalisation is used to express ϕ_{fluct} given by equation (46). With ϕ_{UV} from equation (19), consider first the normalisation (68) valid for $\phi_{\text{end}} = \phi_{\epsilon_2}$. In this case, the rescaled parameters (x, \bar{v}) of equation (73) are again a useful set to express (A.1) in a simple form,

$$\ln \bar{v} > 4 \ln \mathcal{F} - \ln x, \quad (\text{A.2})$$

where the constant \mathcal{F} can be expressed as

$$\mathcal{F} = 3^{1/10} 2^{-1/5} \left(45 \frac{Q_{\text{rms-PS}}^2}{T^2} \right)^{3/20} (6N_* + 10)^{-1/4} (\pi \alpha' m_{\text{Pl}}^2)^{1/2}. \quad (\text{A.3})$$

This is a condition of the same type as the one given by equation (92) (from $\phi_{\text{in}, \epsilon_2} < \phi_{\text{UV}}$), but more restrictive. The parameter region in the $(\ln x, \ln \bar{v})$ plane for which stochastic effects can occur within the throat is therefore smaller than the one obtained from equation (92) (see figure A1).

Now let us investigate the case of equations (99) and (100) where the WMAP normalisation is done using $\phi_{\text{end}} = \phi_{\text{strg}} \gg \phi_{\epsilon_2}$. Inserting this normalisation into equation (46) for ϕ_{fluct} , we find the following inequality in terms of $(\ln x, \ln \bar{v})$:

$$\ln \mathcal{G} < \frac{5}{12} \ln x + \frac{1}{3} \ln \bar{v} + \frac{2}{3} x^{-1/4}, \quad (\text{A.4})$$

where

$$\mathcal{G} = 3^{1/10} 2^{-1/5} (\pi \alpha' m_{\text{Pl}}^2)^{1/2} \left(45 \frac{Q_{\text{rms-PS}}^2}{T^2} \right)^{1/15}. \quad (\text{A.5})$$

This is another curve in the plane $(\ln x, \ln \bar{v})$, analogous to (101) though slightly simpler. Again, equation (A.4) constrains the possible parameter space outside the contour $\phi_{\epsilon_2} = \phi_{\text{strg}}$ in the same manner, but somewhat tighter than equation (101). Note

that inside and outside of the contour $\phi_{\epsilon_2} = \phi_{\text{strg}}$, the requirements $\phi_{\text{in},\epsilon_2} < \phi_{\text{UV}}$ and $\phi_{\text{fluct}} < \phi_{\text{UV}}$ are consistent with each other. Both are represented in figure A1. We have therefore shown that the condition (A.1) can be met for sufficiently generic parameter combinations, and hence stochastic effects may occur inside the throat.

Appendix A.2. Detailed analysis of the stochastic regime

In the following, we apply the treatment established in reference [60] to the case of the brane inflationary potential (13). The underlying approach of stochastic inflation consists in describing the evolution of a coarse-grained field φ corresponding to the original scalar field ϕ averaged over e.g. Hubble patch. The quantum fluctuations correspond in this picture to stochastic noise due to small-scale Fourier modes. Therefore, the dynamics of the coarse-grained field are controlled by a Langevin equation, whose solution enables one to calculate the probability density function of the field φ . In the slow-roll approximation, this coarse-grained field obeys the equation

$$\dot{\varphi} + \frac{V_\varphi}{3H} = \frac{H^{3/2}}{2\pi} \xi(t), \quad (\text{A.6})$$

where the Hubble parameter H is entirely described by the coarse-grained field as well, i.e. one has (in the slow-roll approximation)

$$H^2 \simeq \frac{\kappa}{3} V(\varphi). \quad (\text{A.7})$$

In equation (A.6), $\xi(t)$ is the noise field and its mean and two-point correlation function satisfy

$$\langle \xi(t) \rangle = 0, \quad \langle \xi(t) \xi(t') \rangle = \delta(t - t'), \quad (\text{A.8})$$

where δ is the Dirac delta function. The approach in [60] has been to solve this system of equations using a perturbative expansion in the noise, that is, one writes φ as

$$\varphi(t) = \phi_{\text{cl}}(t) + \delta\varphi_1(t) + \delta\varphi_2(t) + \dots, \quad (\text{A.9})$$

where $\phi_{\text{cl}}(t)$ is the solution of the Langevin equation without the noise, and $\delta\varphi_1(t)$ is linear in $\xi(t)$, $\delta\varphi_2(t)$ quadratic and so on. To avoid notational confusion, the classical field value, which is denoted by ϕ in the rest of this article, is called ϕ_{cl} in this Appendix. As discussed in reference [60], there are, up to second order, two resulting probability distributions for φ . The first of these, $P_c(\varphi, t)$, is the probability of the stochastic process to assume a given field value at a given time in a single coarse-grained domain. The second distribution, $P_v(\varphi, t)$, takes into account volume effects, namely the dependence of the volume size on the field value within this domain. These two distributions are given by

$$P_c(\varphi, t) \equiv \langle \delta(\varphi - \varphi[\xi]) \rangle = \frac{1}{\sqrt{2\pi \langle \delta\varphi_1^2 \rangle}} \exp \left[-\frac{(\varphi - \langle \varphi \rangle)^2}{2 \langle \delta\varphi_1^2 \rangle} \right], \quad (\text{A.10})$$

and

$$\begin{aligned}
 P_v(\varphi, t) &= \frac{\langle \delta(\varphi - \varphi[\xi]) \exp [3 \int d\tau H(\varphi[\xi])] \rangle}{\langle \exp [3 \int d\tau H(\varphi[\xi])] \rangle} \\
 &= \frac{1}{\sqrt{2\pi} \langle \delta\varphi_1^2 \rangle} \exp \left[-\frac{(\varphi - \langle \varphi \rangle - 3I^T J)^2}{2 \langle \delta\varphi_1^2 \rangle} \right], \tag{A.11}
 \end{aligned}$$

where the mean field value is given by $\langle \varphi \rangle \approx \phi_{\text{cl}} + \langle \delta\varphi_2 \rangle$ and where I and J are two continuous vectors [60]. The influence of stochastic effects therefore requires three quantities to be determined for any given inflationary potential, namely $\langle \delta\varphi_1^2 \rangle$, $\langle \delta\varphi_2 \rangle$, and $I^T J$. These quantities have been calculated in reference [60] as functions of the Hubble parameter (in the slow-roll approximation) and read

$$\langle \delta\varphi_1^2 \rangle = \frac{\kappa}{2} \left(\frac{H'}{2\pi} \right)^2 \int_{\phi_{\text{cl}}}^{\phi_{\text{in}}} \left(\frac{H}{H'} \right)^3 d\phi, \tag{A.12}$$

$$\langle \delta\varphi_2 \rangle = \frac{H''}{2H'} \langle \delta\varphi_1^2 \rangle + \frac{H'}{4\pi m_{\text{Pl}}^2} \left[\frac{H_{\text{in}}^3}{H_{\text{in}}'^2} - \frac{H^3}{H'^2} \right], \tag{A.13}$$

where, in the present context, a prime denotes a derivative with respect to φ . In the slow-roll approximation, the Hubble parameter can be directly replaced by $\sqrt{\kappa V/3}$ and the correction due to volume effects can be expressed as

$$3I^T J = \frac{12H'}{m_{\text{Pl}}^4} \int_{\phi_{\text{cl}}}^{\phi_{\text{in}}} \frac{H^4}{H'^3} d\phi - 12\pi \frac{H}{H'} \frac{\langle \delta\varphi_1^2 \rangle}{m_{\text{Pl}}^2}. \tag{A.14}$$

In the stochastic inflation regime, we are dealing with very large field values $\phi \gg \mu$ and one can use the expansion (14) of the potential. Equation (A.12) then yields

$$\begin{aligned}
 \frac{\langle \delta\varphi_1^2 \rangle}{\mu^2} &= \frac{\kappa^2 M^4}{48\pi^2} \left(\frac{\mu}{\phi_{\text{cl}}} \right)^6 \left[\left(\frac{\phi_{\text{cl}}}{\mu} \right)^4 - 1 \right]^{-1} \left\{ \frac{1}{16} \left[\left(\frac{\phi_{\text{in}}}{\mu} \right)^{16} - \left(\frac{\phi_{\text{cl}}}{\mu} \right)^{16} \right] \right. \\
 &\quad - \frac{3}{12} \left[\left(\frac{\phi_{\text{in}}}{\mu} \right)^{12} - \left(\frac{\phi_{\text{cl}}}{\mu} \right)^{12} \right] + \frac{3}{8} \left[\left(\frac{\phi_{\text{in}}}{\mu} \right)^8 - \left(\frac{\phi_{\text{cl}}}{\mu} \right)^8 \right] \\
 &\quad \left. - \frac{1}{4} \left[\left(\frac{\phi_{\text{in}}}{\mu} \right)^4 - \left(\frac{\phi_{\text{cl}}}{\mu} \right)^4 \right] \right\}, \tag{A.15}
 \end{aligned}$$

Since the brane motion in the throat occurs only for $\phi_{\text{cl}} > \mu$ (see section 4), one gets in the regime $\phi_{\text{cl}} \ll \phi_{\text{in}}$

$$\frac{\langle \delta\varphi_1^2 \rangle}{\mu^2} \simeq \frac{\kappa^2 M^4}{768\pi^2} \left(\frac{\phi_{\text{cl}}}{\mu} \right)^{-10} \left(\frac{\phi_{\text{in}}}{\mu} \right)^{16}. \tag{A.16}$$

Since ϕ_{cl}/μ is decreasing, the variance is, as expected, increasing as inflation proceeds.

Let us now determine the correction to the mean value. As can be seen from (A.13), no additional integration is necessary to calculate $\langle \delta\varphi_2 \rangle$, and after some algebra one finds

$$\frac{\langle \delta\varphi_2 \rangle}{\mu} = \frac{1}{2} \left[3 - 5 \left(\frac{\phi_{\text{cl}}}{\mu} \right)^4 \right] \left(\frac{\phi_{\text{cl}}}{\mu} \right)^{-1} \left[\left(\frac{\phi_{\text{cl}}}{\mu} \right)^4 - 1 \right]^{-1} \frac{\langle \delta\varphi_1^2 \rangle}{\mu^2}$$

$$\begin{aligned}
 & + \frac{\kappa^2 M^4}{192\pi^2} \left(\frac{\mu}{\phi_{\text{cl}}}\right)^5 \left[1 - \left(\frac{\mu}{\phi_{\text{cl}}}\right)^4\right]^{-1/2} \left\{ \left(\frac{\phi_{\text{in}}}{\mu}\right)^{10} \right. \\
 & \times \left. \left[1 - \left(\frac{\mu}{\phi_{\text{in}}}\right)^4\right]^{5/2} - \left(\frac{\phi_{\text{cl}}}{\mu}\right)^{10} \left[1 - \left(\frac{\mu}{\phi_{\text{cl}}}\right)^4\right]^{5/2} \right\}. \quad (\text{A.17})
 \end{aligned}$$

Finally, in order to evaluate the volume effects characterised by the term $3I^T J$, one needs to calculate the integral in equation (A.14). For the potential (14), this can still be solved exactly. One obtains

$$\begin{aligned}
 \frac{3I^T J}{\mu} &= \frac{\kappa^3 M^4 \mu^2}{128\pi^2} \left(\frac{\mu}{\phi_{\text{cl}}}\right)^5 \left[1 - \left(\frac{\mu}{\phi_{\text{cl}}}\right)^4\right]^{-\frac{1}{2}} \times \left[S\left(\frac{\phi_{\text{in}}}{\mu}\right) - S\left(\frac{\phi_{\text{cl}}}{\mu}\right) \right] \\
 & - \frac{3\kappa\mu^2}{4} \left[1 - \left(\frac{\mu}{\phi_{\text{cl}}}\right)^4\right] \left(\frac{\phi_{\text{cl}}}{\mu}\right)^5 \frac{\langle\delta\varphi_1^2\rangle}{\mu^2}, \quad (\text{A.18})
 \end{aligned}$$

where the function S is defined by

$$\begin{aligned}
 S(x) &\equiv \frac{1}{383} \left[x^2 \sqrt{x^4 - 1} (-279 + 326x^4 - 200x^8 + 48x^{12}) \right. \\
 & \left. + 105 \ln \left(x^2 + \sqrt{x^4 - 1} \right) \right]. \quad (\text{A.19})
 \end{aligned}$$

The corresponding trajectory is plotted in figure A2 (left panel). The solid line represents the classical trajectory without the quantum effects. Since we are using ϕ_{cl} as a clock, this line is just the straight line “ $y = x$ ”. The dotted line gives $\langle\varphi\rangle = \phi_{\text{cl}} + \langle\delta\varphi_2\rangle$, i.e. the mean value of the field in the situation where the volume effects are ignored. The two dashed lines above and below this line are $\phi_{\text{cl}} + \langle\delta\varphi_2\rangle \pm \sqrt{\langle\delta\varphi_1^2\rangle}$. As discussed at length in reference [60], the quantum effects accumulate and manifest themselves only once the field is approaching the end of inflation. As clearly shown in figure A2, the quantum effects are such that the field rolls down the potential more quickly than its classical counterpart. However, the story is different when volume effects are taken into account. The corresponding trajectory is represented by the dotted-dashed line, the two dashed lines above and below being the limits of the one sigma interval. In this case, the field is first slowed down and starts moving back to even climb up the potential. Then, at some point, it stops and rolls down again the potential. However, as we will see in the next subsection, this last part of the evolution can not be tracked within our approximation since it is outside its domain of validity (represented by the shaded regions).

In figure A2 (right panel), we have represented the corresponding distributions without and with volume effects as given by equations (A.10) and (A.11) respectively. The vertical dotted lines corresponds to the classical values of the field at three successive times (denoted “1”, “2” and “3”), namely $\phi_{\text{cl}}^{(1)}/\mu = 300$, $\phi_{\text{cl}}^{(2)}/\mu = 200$ and $\phi_{\text{cl}}^{(3)}/\mu = 150$. The solid lines are the three distributions P_c corresponding to the three classical field values while the dashed lines are the three P_v 's. This plot essentially confirms the above analysis. In particular, one notices that the maximum of P_c is ahead the classical vacuum expectation value as discussed before. On the contrary, the volume effects “retain” the

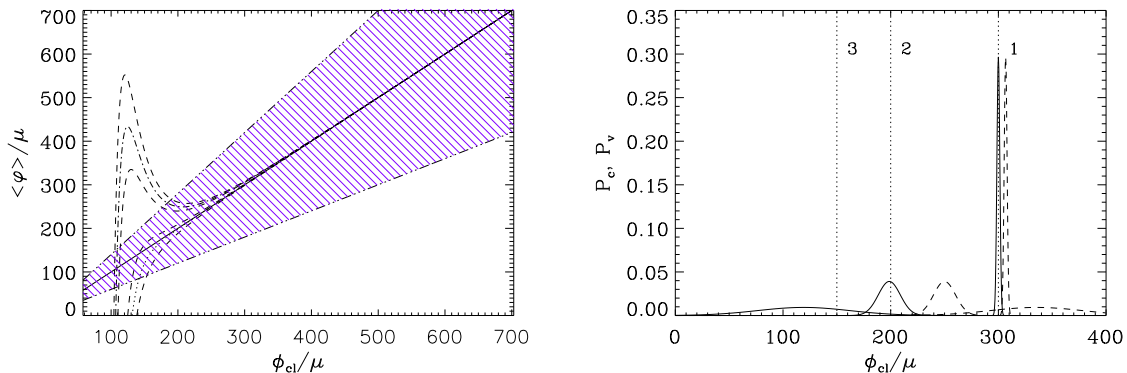


Figure A2. Left panel: Evolution of the inflaton field when the quantum effects (with or without volume effects) are taken into account. The underlying model is such that “classical” inflation stops by violation of the slow-roll conditions. Hence, the WMAP normalisation is calculated with the help of equation (68). With $v = 1$ and $N_* = 50$, this leads to $\phi_{\text{fluct}}/\mu \sim 793.5$. The initial condition is chosen to be $\phi_{\text{in}}/\mu = 700$. The solid line represents the classical trajectory, the dotted line the mean value without the volume effects and the dotted-dashed line the mean value with the volume effects. Right panel: Evolution of the probability distribution $P_c(\varphi)$ (solid lines) and $P_v(\varphi)$ (dashed lines). As in figure A2, the case displayed here corresponds to $v = 1$ and $N_* = 50$, leading to $\phi_{\text{fluct}}/\mu \sim 793.5$. The initial shape of the probability density function has been chosen to be $\delta(\phi - \phi_{\text{in}})$ with $\phi_{\text{in}}/\mu = 700$. The vertical dashed lines represent the location of the field at successive points of the classical trajectory (the field moves “from right to left”).

field and this one can even change the direction of its motion (from right to left to left to right). Finally, the two distributions strongly spread out while inflation is proceeding.

Appendix A.3. Reliability of the perturbative treatment

In this section, we discuss in which range of field values $\langle \varphi \rangle \in [\phi_{\text{cl}} - |\Delta\varphi_{\text{min}}(\phi_{\text{cl}})|, \phi_{\text{cl}} + \Delta\varphi_{\text{max}}(\phi_{\text{cl}})]$ the previous analysis is valid. Indeed, as discussed above, in order to estimate the mean value of the field with or without the volume effects, a perturbative expansion in the noise has been used which may break down at some point. It has been shown in [61] that $\Delta\varphi_{\text{min}}$ and $\Delta\varphi_{\text{max}}$ can be found from requesting that the two conditions

$$\max_{x \in [\phi_{\text{cl}}, \phi_{\text{cl}} + \Delta\varphi_{\text{max}}(\phi_{\text{cl}})]} \left| \frac{H^{(4)}(x)}{6} \Delta\varphi^3 \right| \ll \left| \frac{H_{\text{cl}}'''}{2} \right| \Delta\varphi^2, \quad (\text{A.20})$$

$$\max_{x \in [\phi_{\text{cl}}, \phi_{\text{cl}} + \Delta\varphi_{\text{max}}(\phi_{\text{cl}})]} \left| \frac{[H^{3/2}(x)]''}{2} \right| \Delta\varphi^2 \ll \left| (H_{\text{cl}}^{3/2})'' \right| \Delta\varphi, \quad (\text{A.21})$$

are simultaneously satisfied. The strongest bounds on $\Delta\varphi_{\text{min}}$ and $\Delta\varphi_{\text{max}}$ that follow from (A.20) and (A.21) then give the reliability interval for the distributions $P_c(\varphi, t)$

and $P_v(\varphi, t)$. In the present case, a straightforward calculation leads to

$$\frac{\Delta\varphi_{\min}}{\mu} \approx -\frac{2}{5} \frac{\phi_{\text{cl}}}{\mu}, \quad \frac{\Delta\varphi_{\max}}{\mu} = \frac{2}{5} \frac{\phi_{\text{cl}}}{\mu}. \quad (\text{A.22})$$

The resulting reliability region is plotted in figure A2 and corresponds to the purple hatched region. We see that the approximation breaks down more quickly for $P_v(\varphi, t)$ than for $P_c(\varphi, t)$. In particular, the conclusion that, due to volume effects, the field reverses its motion comes from a regime which is at the border of the reliability interval. We conclude that, in order to have access to this phenomenon and, in particular, to discuss eternal inflation in this model, a more powerful method is needed, as, for instance, a full numerical integration of the Langevin equation (A.6).

Appendix B. Brane inflation from String Theory

Appendix B.1. The background action of type IIB Superstring Theory

We begin by considering the background action only, and to that end place ourselves in the context of ten-dimensional type IIB Superstring Theory. In the string frame, the effective action reads (see e.g. references [49, 57, 96])

$$\begin{aligned} \mathcal{S}_{\text{tot}} = & -\frac{1}{2\hat{\kappa}} \int d^{10}x \sqrt{-g} \left\{ e^{-2\Phi} \left[R + 4(\nabla\Phi)^2 - \frac{1}{12} (dB_{(2)})^2 \right] \right. \\ & \left. - \frac{1}{2} (dC_{(0)})^2 - \frac{1}{12} [dC_{(2)} - C_{(0)}dB_{(2)}]^2 - \frac{1}{480} (F_{(5)})^2 \right\} \\ & + \frac{1}{4\hat{\kappa}} \int C_{(4)} \wedge dB_{(2)} \wedge dC_{(2)}, \end{aligned} \quad (\text{B.1})$$

where $\hat{\kappa}$ stands for

$$\hat{\kappa} = \frac{1}{2}(2\pi)^7 \alpha'^4. \quad (\text{B.2})$$

The field strength denoted by $F_{(5)}$ in equation (B.1) is given by

$$F_{(5)} = dC_{(4)} + \frac{1}{2} [B_{(2)} \wedge dC_{(2)} - C_{(2)} \wedge dB_{(2)}]. \quad (\text{B.3})$$

The brackets (i) indicate the number of indices of the corresponding field. The fields in this theory are therefore the scalars Φ (the dilaton) and $C_{(0)}$ (the axion), g_{mn} (ten-dimensional gravity) as well as the antisymmetric fields $B_{(2)}$ (Kalb-Ramond), $C_{(2)}$, and $C_{(4)}$. Note that the totally antisymmetric ϵ tensor refers to curved space, where we define

$$\epsilon_{(10)} = \pm 1 \quad \text{for pair/odd permutation of the indices,} \quad (\text{B.4})$$

$$\epsilon_{(10)} = 0 \quad \text{if two or more indices are equal,} \quad (\text{B.5})$$

$$\epsilon^{(10)} = \frac{1}{g} \epsilon_{(10)}. \quad (\text{B.6})$$

The first line of (B.1) describes the Neveu-Schwarz–Neveu-Schwarz (NS-NS) sector, while the second line results from the Ramond-Ramond (RR) sector. The third line

is the Chern-Simons (C-S) coupling between the sources of $C_{(4)}$ (that is, RR charged objects such as D3 branes) and background fluxes. From the definition (B.3) of $F_{(5)}$ it is clear that if $(dB_{(2)})$ and $(dC_{(2)})$ have non-zero background values, they can produce a non-zero $F_{(5)}$ field strength even in the absence of localised $C_{(4)}$ sources. Turning this argument around, one can also interpret such fluxes as intrinsic “background” $C_{(4)}$ sources.

Appendix B.2. The equations of motion

From equation (B.1), it is straightforward to derive the equations of motion for these fields. The resulting system of equations has been studied in the references [48, 49, 50, 51] and we now present the solutions found there. Note that in addition to finding simultaneous solutions for *all* equations of motion, one has to impose the condition of self-duality of the 5-form field strength, $F_{(5)} = \star F_{(5)}$, onto these solutions.

Appendix B.2.1. Ansatz for the metric. Let us focus on the Einstein equations first, which follow from (B.1) by variation with respect to the ten-dimensional metric g_{mn} ⁺. In this section, the ten-dimensional set of coordinates we use is $(x^0, x^i, r, \psi, \theta_1, \phi_1, \theta_2, \phi_2)$, $i = 1, 2, 3$. A super-gravity motivated ansatz for the metric reads

$$ds^2 = \frac{1}{\sqrt{h(r)}} \eta_{\mu\nu} dx^\mu dx^\nu + \sqrt{h(r)} ds_6^2, \quad (\text{B.7})$$

which involves a natural splitting into a four-dimensional extended space-time and the six compactified extra dimensions. Note that in (B.7), the four-dimensional metric has been set to Minkowski $\eta_{\mu\nu} = \text{diag}(-1, +1, +1, +1)$, multiplied by a factor depending on the fifth dimension r . In principle one can also choose e.g. a FLRW universe for the four-dimensional section of the metric by replacing $\eta_{\mu\nu}$ with $g_{\mu\nu} = \text{diag}(-1, a^2, a^2, a^2)$. For the six-dimensional section, the choice of interest here is

$$ds_6^2 = dr^2 + r^2 ds_{T_{1,1}}^2, \quad (\text{B.8})$$

where $ds_{T_{1,1}}^2$ is the metric on the Einstein space $T_{1,1}$ [47]. Note that the choice of geometry and compactification for the extra dimensions is an input parameter for the resulting inflationary model. In particular, one can enforce “warping” on the conifold $T_{1,1}$ by giving non-vanishing background values to $(dB_{(2)})$ and $(dC_{(2)})$. The main virtue of these fluxes is that in general they stabilise the scalar fields corresponding to the complex structure moduli of the extra dimensions. The warped conifold geometry was studied in reference [50] and has become known as the Klebanov-Strassler (KS) throat. Interest in the KS geometry is due to the fact that it represents an exactly solvable example of field strengths background fluxes. Nevertheless, this scenario can be viewed

⁺ Small Latin indices m, n, \dots run from 0 to 9 (with the exception of $i = 1, 2, 3$), while small Greek indices μ, ν, \dots run from 0 to 3. Capital Latin indices M, N, \dots run over the extra dimensions coordinates only, i.e. from 4 to 9.

as generic because “warped throats” appear in many flux compactifications invoked to stabilise the moduli. The metric of the $T_{1,1}$ space reads

$$\begin{aligned} ds_{6, T_{1,1}}^2 &= dr^2 + r^2 ds_{T_{1,1}}^2 \\ &= dr^2 + \frac{r^2}{9} (d\psi + \cos \theta_1 d\phi_1 + \cos \theta_2 d\phi_2)^2 \\ &\quad + \frac{r^2}{6} \sum_{i=1}^2 (d\theta_i^2 + \sin^2 \theta_i d\phi_i^2), \end{aligned} \tag{B.9}$$

whereas the one on its deformed counterpart is

$$\begin{aligned} ds_{6, \text{warped}}^2 &= \frac{1}{K(r)} dr^2 + \frac{r^2}{9} K(r) (d\psi + \cos \theta_1 d\phi_1 + \cos \theta_2 d\phi_2)^2 \\ &\quad + \frac{r^2}{6} (d\theta_1^2 + \sin^2 \theta_1 d\phi_1^2) \\ &\quad + \frac{1}{6} (r^2 + 6z^2) (d\theta_2^2 + \sin^2 \theta_2 d\phi_2^2), \end{aligned} \tag{B.10}$$

where the warping function $K(r)$ is given by

$$K(r) = \frac{r^2 + 9z^2}{r^2 + 6z^2}. \tag{B.11}$$

The quantity $z \neq 0$ (in general complex) is the warping number introduced in the definition of the deformed conifold (see below).

We begin our investigation with the simple conifold (B.9). Using our coordinates $(r, \psi, \theta_1, \phi_1, \theta_2, \phi_2)$ for the six-dimensional section of the metric, equation (B.9) shows that we are dealing with a generalised “cone” whose base is given by two spheres, $\mathcal{S}_3 \times \mathcal{S}_2$ [47]. However, the defining equation of the conifold is more readily written in terms of four complex coordinates w_i , $i = 1 \dots 4$ which obey [97]

$$\sum_{i=1}^4 w_i^2 = 0. \tag{B.12}$$

From equation (B.12), one sees that the geometry becomes singular at $w_i = 0$ for all $i = 1 \dots 4$. In this case, \mathcal{S}_2 and \mathcal{S}_3 are shrinking to a point at the tip of the conifold where $r = 0$. Using the six-dimensional metric (B.9) within the ten-dimensional ansatz (B.7), the components of the Einstein equations can be combined to yield the differential equation

$$\left(\frac{\partial^2}{\partial r^2} h \right) + \frac{5}{r} \left(\frac{\partial}{\partial r} h \right) = 0, \tag{B.13}$$

whose solutions read

$$h(r) = C_2 + \frac{C_1}{4r^4}. \tag{B.14}$$

Note that it is possible to choose $C_2 = 0$ and that the ten-dimensional space is Ricci flat. Equation (B.13) can indeed be obtained by setting the Ricci scalar $R = 0$.

For the time being, we have considered the case of a simple (and singular) conifold, where a priori no background fluxes have to be present, i.e. it is consistent to choose

$B_{(2)} = C_{(2)} = 0$. One can now turn these fluxes on; the resulting effect is to induce corrections in equation (B.14) which are proportional to the ratio of the flux quanta \mathcal{M} , \mathcal{K} in the NS-NS and the RR sector respectively, namely $(dB_{(2)})$ and $(dC_{(2)})$. This was the route taken in references [48, 49]. In the presence of fluxes, the singular conifold is replaced by its deformed counterpart and this amounts to modify equation (B.12) into

$$\sum_{i=1}^4 w_i^2 = z, \quad (\text{B.15})$$

where the warping number z is a non-vanishing complex number. The solution for $h(r)$ in the deformed conifold case (again found from the Einstein equations or from $R = 0$) is [51]

$$h(r) = C_3 + C_4 \left[\frac{1}{18r^2 z^2} - \frac{1}{162z^4} \ln \left(1 + \frac{9z^2}{r^2} \right) \right]. \quad (\text{B.16})$$

The constants C_3 , C_4 can again be determined from the chosen compactified geometry.

In “cone” terminology, equation (B.15) implies that the \mathcal{S}_2 still shrinks to a point at the tip of the cone, but the \mathcal{S}_3 remains finite. As mentioned above, this is achieved by turning on background fluxes for $(dB_{(2)})$ and $(dC_{(2)})$, i.e. aligning them with two Poincaré dual 3-cycles. Two such cycles which verify equation (B.12) are described by

$$\mathcal{A} : \sum_{i=1}^4 x_i^2 = z, \quad \mathcal{B} : x_4^2 - \sum_{i=1}^3 y_i^2 = z, \quad (\text{B.17})$$

where the complex coordinates w_i have been decomposed into their real and imaginary parts, x_i and y_i respectively. Alignment of the 3-forms leads to a Dirac quantisation of the fluxes along the 3-cycles

$$\frac{1}{2\pi\alpha'} \int_{\mathcal{A}} (dC_{(2)}) = 2\pi\mathcal{M}, \quad \frac{1}{2\pi\alpha'} \int_{\mathcal{B}} (dB_{(2)}) = -2\pi\mathcal{K}. \quad (\text{B.18})$$

These conditions impose restrictions on the possible ansätze for the fields, and eventually on the constants C_3 , C_4 in equation (B.16).

The difference between the simple and the deformed conifold will be most remarkable close to the tip of the cone at $r = r_0$. Let us notice that $r_0 \neq 0$ since by deforming the conifold, we have replaced the “sharp” tip by a finite size sphere \mathcal{S}_3 . However, at some distance from the tip, both metrics should essentially give the same description of the geometry and in particular, we can “glue” the warped metric (B.16) to its simple version (B.14) at a certain radius r_* . From this matching, the constants C_1 and C_2 become some function of C_3 , C_4 and r_* . Far from the singularity, the metric (B.14) expressed in terms of those constants provides an accurate enough description of the warped conifold geometry. Let us now link this setup with the brane inflation model we are interested in. We place two branes (D3 and anti-D3) into the background, and r will denote the coordinate distance between them. Now, one of these branes (the anti-D3 brane) is placed at the tip r_0 while ensuring r to be large. In that case, the metric in the vicinity of the D3 brane located at $r_1 \gg r_0$ can still be accurately described

by equation (B.14). It is for this reason that, while the solution (B.16) for the warped metric is known, for all “practical” applications the simple solution (B.14) suffices.

While we do not write down the exact solutions for the other fields in this theory exactly, let us state that the solution for the 4-form $C_{(4)}$, in the string frame, is found to be [22, 48, 49, 50, 54, 97]

$$[C_{(4)}]_{0123}(r) = g_s^{-1} \frac{1}{h(r)}. \quad (\text{B.19})$$

This form turns out to be crucial in the derivation of the effective inflaton potential as it is demonstrated below.

Appendix B.2.2. Interpretation of the background fluxes. We conclude our investigation of the background with some comments on an intuitive interpretation of background fluxes. If we consider a simple (singular) conifold geometry with non-zero fluxes, it can be viewed as a stack of $\mathcal{N} = \mathcal{MK}$ branes with RR charge placed at the $r = 0$ singularity. The total RR charge \mathcal{N} is therefore the product of the fluxes. If one uses the deformed conifold instead, this singularity is replaced by a three-sphere \mathcal{S}_3 with radius r_0 , and the charge \mathcal{N} of the branes is literally smeared out across the three-sphere. In the following sections, we first add one more D3 brane (so that there are $(\mathcal{N} + 1)$ RR charged branes in total) to this background. This additional brane can be treated as a perturbation of the metric background (B.14). We then probe the perturbed background using a test anti-D3 brane and calculate the force it experiences.

Appendix B.3. Perturbed geometry

In order to describe a Dp brane inserted into this super-gravity background, one has to consider two additional contributions to the action (B.1) [57]. In the string frame, they are the DBI action of a Dp brane,

$$\mathcal{S}_{Dp} = -\mu_p \int_{M_p} d^{p+1} \xi e^{-\Phi} [-\det(G_{\alpha\beta} + B_{\alpha\beta} + 2\pi\alpha' F_{\alpha\beta})]^{1/2}, \quad (\text{B.20})$$

plus its Chern-Simons coupling

$$\mathcal{S}_{C-S, \text{brane}} = \pm q_p \int_{M_p} C_{(p+1)}, \quad (\text{B.21})$$

since Dp branes in type IIB Superstring Theory are localised sources of $C_{(p+1)}$ field strength*. The RR charge q_p is given by $q_p = \mu_p$. For stabilised dilaton $g_s = e^{\langle\Phi\rangle}$, the effective brane tension T_p is related to the fundamental brane tension μ_p by

$$T_p = \frac{\mu_p}{g_s}, \quad (\text{B.22})$$

and can be calculated from [57]

$$T_p^2 = \frac{\pi}{\kappa_{10}} (4\pi^2 \alpha')^{3-p}. \quad (\text{B.23})$$

* More generally, a Dp brane in type IIB theory can source $C_{(l)}$ fields for all even $l \leq p + 1$ [57].

The gravitational coupling constant κ_{10} was given in equation (28). The upper sign in equation (B.21) refers to the case of a Dp brane, the lower to an anti- Dp brane. The quantities ξ^i are the coordinates on the brane, $G_{\alpha\beta}$ is the induced four-dimensional metric and $B_{\alpha\beta}$ the induced anti-symmetric tensor (Kalb-Ramond field) on the brane. These two are given by

$$G_{\alpha\beta} = g_{mn} \frac{\partial x^m}{\partial \xi^\alpha} \frac{\partial x^n}{\partial \xi^\beta}, \quad (\text{B.24})$$

$$B_{\alpha\beta} = B_{mn} \frac{\partial x^m}{\partial \xi^\alpha} \frac{\partial x^n}{\partial \xi^\beta}, \quad (\text{B.25})$$

g_{mn} and B_{mn} being ten-dimensional. It is moreover possible (notably for parallel branes) to choose a configuration in which the gauge field on the brane $F_{\alpha\beta}$ vanishes.

In our case, the brane has three spatial dimensions, and we may choose the ξ^α to be parallel to the (x^0, x^i) , $i = 1, 2, 3$ coordinate axes. If the coordinates y_1^A , $A = 4 \dots 9$ of the brane are assumed to be static and independent of the location *on* the brane, it can be shown that there is no $B_{(2)}$ “pull-back” onto the brane. Then equation (B.24) implies

$$G_{00} = g_{00}, \quad G_{ii} = g_{ii}, \quad \text{for } i = 1, 2, 3. \quad (\text{B.26})$$

The determinant of this induced metric, given that the ten-dimensional metric is (B.7), reads

$$\det G_{\alpha\beta} = G = -\frac{1}{h^2(r_1)}. \quad (\text{B.27})$$

Notice that we would pick up an additional $a^6(t)$ factor if we were to use a FLRW universe on the brane instead of $\eta_{\mu\nu}$.

D3 branes are sources of $C_{(4)}$ fields, and thus of the corresponding $F_{(5)}$ field strength, as can be seen from the Chern-Simons coupling (B.21)

$$\mathcal{S}_{\text{C-S}} = \pm \sum_i \mu_3^{(i)} \int_{M_4^{(i)}} d\tau d\sigma_1^{(i)} d\sigma_2^{(i)} d\sigma_3^{(i)} \frac{dx^m}{d\tau} \frac{dx^n}{d\sigma_1^{(i)}} \frac{dx^k}{d\sigma_2^{(i)}} \frac{dx^l}{d\sigma_3^{(i)}} C_{mnkl}, \quad (\text{B.28})$$

the summation over i running over all the D3 branes present [16, 19]. In this equation, the integration is carried out over the world volume $M_4^{(i)}$ of each brane, and $\mu_3^{(i)}$ denotes their respective RR charge. It then follows from equations (B.20) and (B.21) that the presence of one D3 brane at r_1 adds the following terms to the action

$$\mathcal{S}_{\text{D3}} = -T_3 \int_{M_3} d^4\xi \sqrt{-G} + \mu_3 \int_{M_3} C_{(4)}, \quad (\text{B.29})$$

where G is given by equation (B.27). The D3 brane will manifest itself as a small perturbation of the background, i.e. the function $h(r)$ calculated in Appendix B.1 is replaced by

$$\tilde{h}(r, r_0) = h(r) + \delta h(r_0). \quad (\text{B.30})$$

Let us consider the effect of replacing $h(r)$ by $\tilde{h}(r, r_1)$ in the Einstein equations. Since $h(r)$ already fulfils equation (B.13), the resulting equation for $\delta h(r_1)$ is

$$\left(\frac{\partial^2}{\partial r_1^2} \delta h \right) + \frac{5}{r_1} \left(\frac{\partial}{\partial r_1} \delta h \right) = 0. \quad (\text{B.31})$$

which has the solution

$$\delta h(r_1) = \tilde{C}_2 + \frac{\tilde{C}_1}{4r_1^4}. \quad (\text{B.32})$$

The new constants \tilde{C}_1 and \tilde{C}_2 can be related to the former C_1 and C_2 in equation (B.14) by noting that the difference between the previous scenario and the present case comes from adding one D3 brane. One may therefore intuitively guess that [22]

$$\tilde{C}_i = \frac{C_i}{\mathcal{N}}, \quad \text{for } i = 1, 2. \quad (\text{B.33})$$

The perturbed background metric $\tilde{h}(r, r_1)$ is obtained from equations (B.14) and (B.32) and, without loss of generality, one can set $C_2 = \tilde{C}_2 = 0$ to get

$$\tilde{h}(r, r_1) = \frac{C_1}{4r^4} \left(1 + \frac{1}{\mathcal{N}} \frac{r^4}{r_1^4} \right). \quad (\text{B.34})$$

Note that as a consequence of the presence of the D3 brane (which is a localised RR charge source), the $C_{(4)}$ field is also perturbed, as can easily be seen from (B.19).

Appendix B.4. Test anti-brane in the perturbed geometry

Let us denote by $y_0^4 = r_0$ the radial position at which we insert the anti-D3 brane, while for all other extra coordinates we take $y_0^A = y_1^A$, $A = 5 \dots 9$. The anti-brane has the same tension but opposite charge as the brane and its contribution to the action in the string frame reads

$$\mathcal{S}_{\bar{\text{D3}}} = -T_3 \int_{M'_3} d^4 \xi \sqrt{-G'} - \mu_3 \int_{M'_3} C_{(4)}, \quad (\text{B.35})$$

G' being the induced four-dimensional metric on the anti-brane. We assume that the anti-brane is “light” in the sense that it does not affect the already perturbed geometry. While we keep the y_0^i static (i varying from 0 to 5), we assume that the radial anti-brane coordinate $y_0^4 = r_0$ *does* depend on the time x^0 (but not on the x^i). Deriving G' explicitly leads to the expression

$$\det G'_{\alpha\beta} = G' = -\frac{1}{\tilde{h}^2(r_0, r_1)} \left[1 - \tilde{h}(r_0, r_1) \left(\frac{\partial r_0}{\partial t} \right)^2 \right]. \quad (\text{B.36})$$

Inserted into the perturbed geometry of the previous subsection, i.e. where the warp factor is $\tilde{h}(r, r_1)$ and the 4-form $C_{(4)}$ is also perturbed, the mobile anti-brane contributes to the action the terms

$$\mathcal{S}_{\bar{\text{D3}}} = - \int d^4 \xi \frac{T_3}{\tilde{h}(r_0, r_1)} \left\{ 1 + \left[1 - \tilde{h}(r_0, r_1) \left(\frac{\partial r_0}{\partial t} \right)^2 \right]^{1/2} \right\}, \quad (\text{B.37})$$

where we have used equation (B.19). Expanding this expression for small velocities yields

$$\mathcal{S}_{\bar{\text{D3}}} = \int d^4 \xi \left[\frac{T_3}{2} \left(\frac{\partial r_0}{\partial t} \right)^2 - \frac{2T_3}{\tilde{h}(r)} \right]. \quad (\text{B.38})$$

By applying the canonic renormalisation $\phi = \sqrt{T_3} r$, the first term in (B.38) becomes a standard kinetic term for a scalar field ϕ . The second term in equation (B.38) can then be understood as the field potential and has to be evaluated at the position of the anti-brane. By means of equation (B.34), one gets

$$V(r_0, r_1) = \frac{2T_3}{\tilde{h}(r_0, r_1)} = \frac{2T_3}{\frac{C_1}{4r_0^4} \left(1 + \frac{1}{\mathcal{N}} \frac{r_0^4}{r_1^4}\right)}. \quad (\text{B.39})$$

In the limit where the branes are far apart, namely $r_1 \ll r_0$, one has

$$V(r_0, r_1) \approx 2T_3 \frac{4r_0^4}{C_1} \left(1 - \frac{1}{\mathcal{N}} \frac{r_0^4}{r_1^4}\right). \quad (\text{B.40})$$

It can moreover be shown that C_1 is related to \mathcal{N} and v through

$$C_1 = 16\pi \frac{\mathcal{N}}{v} g_s \alpha'^2 = 4r_{\text{UV}}^4, \quad (\text{B.41})$$

where r_{UV} is the “edge” of the KS throat (see section 2.5).

In this Appendix, we have recalled the derivation of the interaction potential between the brane and the anti-brane in a ten-dimensional background warped by fluxes. The resulting potential would be the same if one chose to insert the anti-brane first into the background, and then study the motion of the brane. The only difference is that a D3 brane, inserted into the warped background, does not feel any force because of the compensation between the Chern-Simons coupling and the gravitation due to its tension [note the opposite signs of the two terms in equation (B.29)]. This is not the case for an anti-brane inserted first, for which the two forces add up due the same signs in (B.35). Seeking to minimise its energy, the anti-brane therefore sinks to the bottom of the KS throat. Let us recall that the above treatment remains valid only if $r_1 \gg r_0$ and breaks down as soon as the two branes become too close (see section 2.6).

References

- [1] A. A. Starobinsky, *A new type of isotropic cosmological models without singularity*, *Phys. Lett.* **B91** (1980) 99–102.
- [2] A. H. Guth, *The inflationary universe: A possible solution to the horizon and flatness problems*, *Phys. Rev.* **D23** (1981) 347–356.
- [3] A. D. Linde, *A new inflationary universe scenario: A possible solution of the horizon, flatness, homogeneity, isotropy and primordial monopole problems*, *Phys. Lett.* **B108** (1982) 389–393.
- [4] A. A. Starobinsky, *Dynamics of phase transition in the new inflationary universe scenario and generation of perturbations*, *Phys. Lett.* **B117** (1982) 175–178.
- [5] A. Albrecht and P. J. Steinhardt, *Cosmology for grand unified theories with radiatively induced symmetry breaking*, *Phys. Rev. Lett.* **48** (1982) 1220–1223.
- [6] A. D. Linde, *Particle physics and inflationary cosmology*, *Contemp. Concepts Phys.* **5** (2005) 1–362, [hep-th/0503203].
- [7] V. F. Mukhanov and G. V. Chibisov, *Quantum fluctuation and ‘nonsingular’ universe. (in russian)*, *JETP Lett.* **33** (1981) 532–535.
- [8] S. W. Hawking, *The development of irregularities in a single bubble inflationary universe*, *Phys. Lett.* **B115** (1982) 295.

- [9] A. H. Guth and S. Y. Pi, *Fluctuations in the new inflationary universe*, *Phys. Rev. Lett.* **49** (1982) 1110–1113.
- [10] J. M. Bardeen, P. J. Steinhardt, and M. S. Turner, *Spontaneous creation of almost scale - free density perturbations in an inflationary universe*, *Phys. Rev.* **D28** (1983) 679.
- [11] J. Martin, *Inflation and precision cosmology*, *Braz. J. Phys.* **34** (2004) 1307–1321, [[astro-ph/0312492](#)].
- [12] J. Martin, *Inflationary cosmological perturbations of quantum- mechanical origin*, *Lect. Notes Phys.* **669** (2005) 199–244, [[hep-th/0406011](#)].
- [13] J. Martin, *Inflationary perturbations: The cosmological Schwinger effect*, *Lect. Notes Phys.* **738** (2008) 193–241, [[arXiv:0704.3540](#)].
- [14] G. R. Dvali, Q. Shafi, and S. Solganik, *D-brane inflation*, [hep-th/0105203](#).
- [15] C. P. Burgess *et. al.*, *The inflationary brane-antibrane universe*, *JHEP* **07** (2001) 047, [[hep-th/0105204](#)].
- [16] J. M. Cline, *String cosmology*, [hep-th/0612129](#).
- [17] S. H. Henry Tye, *Brane inflation: String theory viewed from the cosmos*, *Lect. Notes Phys.* **737** (2008) 949–974, [[hep-th/0610221](#)].
- [18] R. Kallosh, *On Inflation in String Theory*, *Lect. Notes Phys.* **738** (2008) 119–156, [[hep-th/0702059](#)].
- [19] C. P. Burgess, *Lectures on Cosmic Inflation and its Potential Stringy Realizations*, *PoS P2GC* (2006) 008, [[arXiv:0708.2865](#)].
- [20] G. R. Dvali and S. H. H. Tye, *Brane inflation*, *Phys. Lett.* **B450** (1999) 72–82, [[hep-ph/9812483](#)].
- [21] S. H. S. Alexander, *Inflation from d - anti-d brane annihilation*, *Phys. Rev.* **D65** (2002) 023507, [[hep-th/0105032](#)].
- [22] S. Kachru *et. al.*, *Towards inflation in string theory*, *JCAP* **0310** (2003) 013, [[hep-th/0308055](#)].
- [23] H. Firouzjahi and S. H. H. Tye, *Brane inflation and cosmic string tension in superstring theory*, *JCAP* **0503** (2005) 009, [[hep-th/0501099](#)].
- [24] D. Baumann and L. McAllister, *A microscopic limit on gravitational waves from D-brane inflation*, *Phys. Rev.* **D75** (2007) 123508, [[hep-th/0610285](#)].
- [25] D. Baumann *et. al.*, *On d3-brane potentials in compactifications with fluxes and wrapped d-branes*, *JHEP* **11** (2006) 031, [[hep-th/0607050](#)].
- [26] D. Baumann, A. Dymarsky, I. R. Klebanov, and L. McAllister, *Towards an Explicit Model of D-brane Inflation*, *JCAP* **0801** (2008) 024, [[arXiv:0706.0360](#)].
- [27] D. Baumann, A. Dymarsky, I. R. Klebanov, L. McAllister, and P. J. Steinhardt, *A Delicate Universe*, *Phys. Rev. Lett.* **99** (2007) 141601, [[arXiv:0705.3837](#)].
- [28] A. Krause and E. Pajer, *Chasing brane inflation in string-theory*, [0705.4682](#).
- [29] S. Panda, M. Sami, and S. Tsujikawa, *Prospects of inflation in delicate D-brane cosmology*, *Phys. Rev.* **D76** (2007) 103512, [[arXiv:0707.2848](#)].
- [30] H. Peiris and R. Easther, *Slow roll reconstruction: Constraints on inflation from the 3 year wmap dataset*, *JCAP* **0610** (2006) 017, [[astro-ph/0609003](#)].
- [31] L. Alabidi and D. H. Lyth, *Inflation models after WMAP year three*, *JCAP* **0608** (2006) 013, [[astro-ph/0603539](#)].
- [32] H. J. de Vega and N. G. Sanchez, *Single field inflation models allowed and ruled out by the three years wmap data*, [astro-ph/0604136](#).
- [33] W. H. Kinney, E. W. Kolb, A. Melchiorri, and A. Riotto, *Inflation model constraints from the wilkinson microwave anisotropy probe three-year data*, *Phys. Rev.* **D74** (2006) 023502, [[astro-ph/0605338](#)].
- [34] J. Martin and C. Ringeval, *Inflation after wmap3: Confronting the slow-roll and exact power spectra to cmb data*, *JCAP* **0608** (2006) 009, [[astro-ph/0605367](#)].
- [35] C. Ringeval, *The exact numerical treatment of inflationary models*, *Lect. Notes Phys.* **738** (2008) 243–273, [[astro-ph/0703486](#)].
- [36] J. Lesgourgues and W. Valkenburg, *New constraints on the observable inflaton potential from*

- wmap and sdss*, *Phys. Rev.* **D75** (2007) 123519, [[astro-ph/0703625](#)].
- [37] J.-M. Lamarre *et. al.*, *The planck high frequency instrument, a 3rd generation cmb experiment, and a full sky submillimeter survey*, [astro-ph/0308075](#).
- [38] A. Mennella *et. al.*, *The low frequency instrument in the esa planck mission*, *AIP Conf. Proc.* **703** (2004) 401–404, [[astro-ph/0310058](#)].
- [39] **AMI** Collaboration, R. Barker *et. al.*, *High-significance sunyaev-zel’dovich measurement: Abell 1914 seen with the arcminute microkelvin imager*, [astro-ph/0509215](#).
- [40] **ACT** Collaboration, A. Kosowsky, *The atacama cosmology telescope project: A progress report*, *New Astron. Rev.* **50** (2006) 969–976, [[astro-ph/0608549](#)].
- [41] **SPT** Collaboration, J. E. Ruhl *et. al.*, *The south pole telescope*, [astro-ph/0411122](#).
- [42] D. H. Lyth and A. Riotto, *Particle physics models of inflation and the cosmological density perturbation*, *Phys. Rept.* **314** (1999) 1–146, [[hep-ph/9807278](#)].
- [43] Q.-G. Huang, M. Li, and J.-H. She, *Brane inflation after wmap three year results*, *JCAP* **0611** (2006) 010, [[hep-th/0604186](#)].
- [44] X. Zhang, *A note on noncommutative brane inflation*, *JCAP* **0612** (2006) 002, [[hep-th/0608207](#)].
- [45] R. Bean, S. E. Shandera, S. H. Henry Tye, and J. Xu, *Comparing Brane Inflation to WMAP*, *JCAP* **0705** (2007) 004, [[hep-th/0702107](#)].
- [46] H. V. Peiris, D. Baumann, B. Friedman, and A. Cooray, *Phenomenology of D-Brane Inflation with General Speed of Sound*, *Phys. Rev.* **D76** (2007) 103517, [[arXiv:0706.1240](#)].
- [47] P. Candelas and X. C. de la Ossa, *Comments on conifolds*, *Nucl. Phys.* **B342** (1990) 246–268.
- [48] I. R. Klebanov and N. A. Nekrasov, *Gravity duals of fractional branes and logarithmic rg flow*, *Nucl. Phys.* **B574** (2000) 263–274, [[hep-th/9911096](#)].
- [49] I. R. Klebanov and A. A. Tseytlin, *Gravity duals of supersymmetric $su(n) \times su(n+m)$ gauge theories*, *Nucl. Phys.* **B578** (2000) 123–138, [[hep-th/0002159](#)].
- [50] I. R. Klebanov and M. J. Strassler, *Supergravity and a confining gauge theory: Duality cascades and chiral-resolution of naked singularities*, *JHEP* **08** (2000) 052, [[hep-th/0007191](#)].
- [51] L. A. Pando Zayas and A. A. Tseytlin, *3-branes on resolved conifold*, *JHEP* **11** (2000) 028, [[hep-th/0010088](#)].
- [52] M. Alishahiha, E. Silverstein, and D. Tong, *Dbi in the sky*, *Phys. Rev.* **D70** (2004) 123505, [[hep-th/0404084](#)].
- [53] E. Silverstein and D. Tong, *Scalar speed limits and cosmology: Acceleration from d- cceleration*, *Phys. Rev.* **D70** (2004) 103505, [[hep-th/0310221](#)].
- [54] I. R. Klebanov and E. Witten, *Superconformal field theory on threebranes at a calabi-yau singularity*, *Nucl. Phys.* **B536** (1998) 199–218, [[hep-th/9807080](#)].
- [55] S. B. Giddings, S. Kachru, and J. Polchinski, *Hierarchies from fluxes in string compactifications*, *Phys. Rev.* **D66** (2002) 106006, [[hep-th/0105097](#)].
- [56] J. Polchinski, *String theory. vol. 1: An introduction to the bosonic string*, . Cambridge, UK: Univ. Pr. (1998) 402 p.
- [57] J. Polchinski, *String theory. vol. 2: Superstring theory and beyond*, . Cambridge, UK: Univ. Pr. (1998) 531 p.
- [58] A. A. Starobinsky, *Stochastic de sitter (inflationary) stage in the early universe*, . In *De Vega, H.j. (Ed.), Sanchez, N. (Ed.): *Field Theory, Quantum Gravity and Strings**, 107-126.
- [59] X. Chen, S. Sarangi, S. H. Henry Tye, and J. Xu, *Is brane inflation eternal?*, *JCAP* **0611** (2006) 015, [[hep-th/0608082](#)].
- [60] J. Martin and M. Musso, *Solving stochastic inflation for arbitrary potentials*, *Phys. Rev.* **D73** (2006) 043516, [[hep-th/0511214](#)].
- [61] J. Martin and M. Musso, *On the reliability of the langevin perturbative solution in stochastic inflation*, *Phys. Rev.* **D73** (2006) 043517, [[hep-th/0511292](#)].
- [62] D. J. Schwarz, C. A. Terrero-Escalante, and A. A. Garcia, *Higher order corrections to primordial spectra from cosmological inflation*, *Phys. Lett.* **B517** (2001) 243–249, [[astro-ph/0106020](#)].
- [63] D. J. Schwarz and C. A. Terrero-Escalante, *Primordial fluctuations and cosmological inflation*

- after *wmap* 1.0, *JCAP* **0408** (2004) 003, [[hep-ph/0403129](#)].
- [64] S. M. Leach, A. R. Liddle, J. Martin, and D. J. Schwarz, *Cosmological parameter estimation and the inflationary cosmology*, *Phys. Rev.* **D66** (2002) 023515, [[astro-ph/0202094](#)].
- [65] A. R. Liddle, P. Parsons, and J. D. Barrow, *Formalizing the slow roll approximation in inflation*, *Phys. Rev.* **D50** (1994) 7222–7232, [[astro-ph/9408015](#)].
- [66] **WMAP** Collaboration, G. Hinshaw *et. al.*, *Three-year wilkinson microwave anisotropy probe (wmap) observations: Temperature analysis*, *Astrophys. J. Suppl.* **170** (2007) 288, [[astro-ph/0603451](#)].
- [67] M. Abramowitz and I. A. Stegun, *Handbook of mathematical functions with formulas, graphs, and mathematical tables*. National Bureau of Standards, Washington, US, ninth ed., 1970.
- [68] F. Finelli, M. Rianna, and N. Mandolesi, *Constraints on the inflationary expansion from three year wmap, small scale cmb anisotropies and large scale structure data sets*, *JCAP* **0612** (2006) 006, [[astro-ph/0608277](#)].
- [69] D. H. Lyth, *What would we learn by detecting a gravitational wave signal in the cosmic microwave background anisotropy?*, *Phys. Rev. Lett.* **78** (1997) 1861–1863, [[hep-ph/9606387](#)].
- [70] A. Lewis, A. Challinor, and A. Lasenby, *Efficient computation of cmb anisotropies in closed frw models*, *Astrophys. J.* **538** (2000) 473–476, [[astro-ph/9911177](#)].
- [71] A. Lewis and S. Bridle, *Cosmological parameters from cmb and other data: a monte-carlo approach*, *Phys. Rev.* **D66** (2002) 103511, [[astro-ph/0205436](#)].
- [72] D. S. Salopek, J. R. Bond, and J. M. Bardeen, *Designing density fluctuation spectra in inflation*, *Phys. Rev.* **D40** (1989) 1753.
- [73] I. J. Grivell and A. R. Liddle, *Inflaton potential reconstruction without slow-roll*, *Phys. Rev.* **D61** (2000) 081301, [[astro-ph/9906327](#)].
- [74] J. A. Adams, B. Cresswell, and R. Easther, *Inflationary perturbations from a potential with a step*, *Phys. Rev.* **D64** (2001) 123514, [[astro-ph/0102236](#)].
- [75] S. Tsujikawa, D. Parkinson, and B. A. Bassett, *Correlation-consistency cartography of the double inflation landscape*, *Phys. Rev.* **D67** (2003) 083516, [[astro-ph/0210322](#)].
- [76] D. Parkinson, S. Tsujikawa, B. A. Bassett, and L. Amendola, *Testing for double inflation with wmap*, *Phys. Rev.* **D71** (2005) 063524, [[astro-ph/0409071](#)].
- [77] A. Makarov, *On the accuracy of slow-roll inflation given current observational constraints*, *Phys. Rev.* **D72** (2005) 083517, [[astro-ph/0506326](#)].
- [78] X. Chen, R. Easther, and E. A. Lim, *Large non-gaussianities in single field inflation*, *JCAP* **0706** (2007) 023, [[astro-ph/0611645](#)].
- [79] J. M. Bardeen, *Gauge invariant cosmological perturbations*, *Phys. Rev.* **D22** (1980) 1882–1905.
- [80] L. P. Grishchuk, *Amplification of gravitational waves in an isotropic universe*, *Sov. Phys. JETP* **40** (1975) 409–415.
- [81] L. P. Grishchuk, *The amplification of gravitational waves and creation of gravitons in the isotropic universes. (erratum)*, *Nuovo Cim. Lett.* **12** (1975) 60–64.
- [82] J. Martin and D. J. Schwarz, *The influence of cosmological transitions on the evolution of density perturbations*, *Phys. Rev.* **D57** (1998) 3302–3316, [[gr-qc/9704049](#)].
- [83] V. F. Mukhanov, H. A. Feldman, and R. H. Brandenberger, *Theory of cosmological perturbations. part 1. classical perturbations. part 2. quantum theory of perturbations. part 3. extensions*, *Phys. Rept.* **215** (1992) 203–333.
- [84] A. Sen, *Tachyon condensation on the brane antibrane system*, *JHEP* **08** (1998) 012, [[hep-th/9805170](#)].
- [85] J. H. Brodie and D. A. Easson, *Brane inflation and reheating*, *JCAP* **0312** (2003) 004, [[hep-th/0301138](#)].
- [86] N. Barnaby, C. P. Burgess, and J. M. Cline, *Warped reheating in brane-antibrane inflation*, *JCAP* **0504** (2005) 007, [[hep-th/0412040](#)].
- [87] **WMAP** Collaboration, D. N. Spergel *et. al.*, *Wilkinson microwave anisotropy probe (wmap) three year results: Implications for cosmology*, *Astrophys. J. Suppl.* **170** (2007) 377,

- [astro-ph/0603449].
- [88] A. R. Liddle and S. M. Leach, *How long before the end of inflation were observable perturbations produced?*, *Phys. Rev.* **D68** (2003) 103503, [astro-ph/0305263].
- [89] **WMAP** Collaboration, N. Jarosik *et. al.*, *Three-year Wilkinson Microwave Anisotropy Probe (WMAP) observations: Beam profiles, data processing, radiometer characterization and systematic error limits*, *Astrophys. J. Suppl.* **170** (2007) 263, [astro-ph/0603452].
- [90] **WMAP** Collaboration, L. Page *et. al.*, *Three year wilkinson microwave anisotropy probe (wmap) observations: Polarization analysis*, *Astrophys. J. Suppl.* **170** (2007) 335, [astro-ph/0603450].
- [91] W. L. Freedman *et. al.*, *Final results from the hubble space telescope key project to measure the hubble constant*, *Astrophys. J.* **553** (2001) 47–72, [astro-ph/0012376].
- [92] A. Gelman and D. Rubin, *Inference from iterative simulations using multiple sequences*, *Statistical Science* **7** (1992) 457–511.
- [93] J. Martin and C. Ringeval, *Exploring the superimposed oscillations parameter space*, *JCAP* **0501** (2005) 007, [hep-ph/0405249].
- [94] I. P. Neupane and D. L. Wiltshire, *Cosmic acceleration from m theory on twisted spaces*, *Phys. Rev.* **D72** (2005) 083509, [hep-th/0504135].
- [95] I. P. Neupane, *Accelerating universes from compactification on a warped conifold*, *Phys. Rev. Lett.* **98** (2007) 061301, [hep-th/0609086].
- [96] C. V. Johnson, *D-brane primer*, hep-th/0007170.
- [97] I. R. Klebanov and A. Murugan, *Gauge / gravity duality and warped resolved conifold*, *JHEP* **03** (2007) 042, [hep-th/0701064].